Orbital Effects of Transverse Magnetic Fields in Quasi Two-Dimensional Electron Systems

Diplomarbeit

von

Martin Raith

aus

Sarching

durchgeführt am Institut Physik I - Theoretische Physik der Universität Regensburg
unter Anleitung von Prof. Dr. Jaroslav Fabian

Juni 2009

Contents

Symbols and Abbreviations

$\vec{A}$	vector potential
$b, b^\dagger$	bosonic ladder operators
$\vec{B}$	magnetic field
$\mathfrak{B}, \mathfrak{B}_{\tilde{y}}, \mathfrak{B}_{\tilde{z}}$	auxiliary quantities
c	speed of light
$d_{\mathrm{PQW}}(E, B)$	2D density of states per energy and unit area
$-e$	electron charge
E	energy
E_c	band-edge energy of the conduction band
$E^{\pm}_{n,n'}(k)$	eigenenergy
$E^z_{n'}$	eigenenergy of the n'th subband
$E^{1^{\mathrm{st}}}_{n,k}$	first order energy correction at the band crossing
$\vec{E}$	electric field
g	effective Landé factor of the semiconductor
$\bar{g} = g\beta/2$	trivial substitution
g_1, g_2	auxiliary quantities
$G, G_{\uparrow\downarrow}$	conductances
G	eigenvalue of the IEO
$G_{mn} = \lvert E_m - E_n \rvert$	trivial substitution
$\hbar$	Planck's constant
$H, H^{\mathfrak{r}\mathrm{D}}$	Hamilton operators (in $\mathfrak{r}$ dimensions)
$H_k, H_k^{\mathfrak{r}\mathrm{D}}$	k-dependent effective mass Hamiltonians (in $\mathfrak{r}$ dimensions)
$H_{\mathrm{H}}, H(t)$	Hamilton operators in the Heisenberg picture
$H^{\textcircled{2D}}, H^{①}, H^{②}$	Hamiltonians incl. Zeeman term and BR-SOI
H_{++}, H_{+-}	matrix elements
i	imaginary unit
$\vec{j}$	current density
$k, \vec{k}, \vec{k}_0$	quasi-momenta, wave number/vectors of the EMA
$l = \sqrt{\hbar/(m\omega)}$	oscillator length of a harmonic potential with frequency ω
$l_B = \sqrt{\hbar/(eB)}$	magnetic length

m	bulk effective mass of the semiconductor
m_e	free-electron mass
$m_\mathfrak{r}$	effective mass of the $\mathfrak{r}$-coordinate
$\overline{m} = m\sqrt{\eta}$	average effective mass
M	occupied, spin-degenerate transverse modes
M_s	occupied, spin-resolved transverse modes
n, n_0, n_1	electron densities
$\vec{n} = (B_x, B_y, B_z)/B$	spin vector
$N, \mathcal{N}_\pm$	normalization factors
$\vec{p} = -\mathrm{i}\hbar\vec{\nabla}$	momentum operator in real space
$\vec{P}$	canonical momentum operator
$\vec{P}(t)$	canonical momentum operator in the Heisenberg picture
$\bar{P}$	effective position operator
$Q(t), Q_\mathrm{H}(t)$	invariant eigen-operator (Heisenberg picture)
$\vec{r}$	eigenvalue of the position operator
$\vec{R}$	position operator
$\vec{R}(t)$	position operator in the Heisenberg picture
$\bar{R}$	effective momentum operator
$\mathcal{R}$	exponent of spin rotation operator U
$\vec{S} = \hbar\vec{\sigma}/2$	spin operator
T	Dyson time-ordering operator
$U = \exp(\mathcal{R})$	spin rotation operator
$U(t, t_0)$	time evolution operator
$v(k)$	particle velocity
V	confining potential
$z_{k_y} = \hbar k_y \omega_c/(m\tilde{\omega}^2)$	spatial shift of the mag.-el. confinement
$\bar{Z}$	effective momentum operator
α	Bychkov-Rashba parameter
$\beta = m/m_\mathrm{e}$	prefactor of the effective mass in the semiconductor
γ	coupling strength
$\digamma$	quantity describing the anisotropy
ζ	trivial substitution
$\eta = \tilde{\omega}^2/\omega_z^2$	trivial substitution
θ, Θ	angles
κ	generalized wave number
$\lambda_\mathrm{f}^\mathrm{2D} = \sqrt{2\pi/n}$	Fermi wavelength of the 2DEG
μ	effective mass of transport

$\mu_{\rm B} = e\hbar/(2m_{\rm e})$	Bohr magneton
$\mu_e = e\tau/m$	electron mobility
ν	filling factor
$\xi, \xi_\pm, \xi', \Xi$	transformation parameters
$\Pi^\pm, \Pi^\pm_{\tilde{y}}, \Pi^\pm_{\tilde{z}}$	trivial substitutions
ρ	resistivity
σ	conductivity
$\vec{\sigma}$	Pauli spin matrices
σ_-, σ_+	ladder operators of the spin system
τ	scattering time
ϕ	angle
Φ, ψ	wave functions
$\omega, \omega_y, \omega_z$	frequencies of the electrostatic, harmonic confinement
$\omega_c, \omega_{cx}, \omega_{cy}, \omega_{cz}, \omega_{\rm cip}$	(partial) cyclotron frequencies
$\bar{\omega}_{cz} = \bar{g}\omega_{cz}$	trivial substitution
$\omega_{cz}(\xi) = \omega_{cz} + \xi\omega_{cy}$	function which generalizes ω_{cz}
$\tilde{\omega}, \tilde{\omega}_y$	magneto-electric frequencies (2DEG)
$\Omega_{y,cz}, \Omega_{z,cy}, \Omega_{y,cx,cz}$	magneto-electric frequencies
$\omega_\pm, \omega_{\tilde{y}}, \omega_{\tilde{z}}$	magneto-electric frequencies (DSA)

Abbreviations

$\mathfrak{r}$D	$\mathfrak{r}$-dimensional
2DEG	infinite two-dimensional electron gas
2DES	two-dimensional electron system
BIA	bulk inversion asymmetry
BR	Bychkov-Rashba
DSA	diamagnetic shift approximation
EMA	effective mass approximation
IEO	invariant eigen-operator
MEF	magneto-electric frequency
PQW	parabolic quantum well
SdH	Shubnikov-de Haas
SHO	simple harmonic oscillator
SIA	structure inversion asymmetry
SO	spin-orbit
SOI	spin-orbit interaction

1 Introduction

In the last 50 years, miniaturization of electronic devices became the most important task in the modern world. People learnt to create circuits below the macroscopic scale and entered the regime of mesoscopic physics or nanophysics. In this limit, quantum mechanics already plays an important role, thus new techniques had to be created which close the gap between the microscopic and the well-known macroscopic world. With more and more expertise in manufacturing high quality semiconductor devices, physicists all over the world gained a playground with new phenomena and also a tool to verify the existing theories in this so far unexplored limit. Nanostructures with reduced dimensionalities such as two-dimensional electron gases, quantum wires and quantum dots are not only of major interest for fundamental research but also provide candidates for new electronic or spintronic devices which may find their right to exist in a conventional computer or even hold the breakthrough in quantum computing.
A milestone in the history of mesoscopic physics was the discovery of the *integer quantum Hall effect* [4, 10, 17, 19] by K. von Klitzing in 1980. This quantum mechanical phenomenon, which keeps us busy throughout the whole thesis, was awarded with the Nobel Prize in 1985. It can be observed in a two-dimensional Hall bar with a perpendicular magnetic field of typically some Tesla. The main feature is the conductance quantization $e^2/(2\pi\hbar)$ which can be measured with extremely high precision. As a consequence, the Hall measurement can be utilized to determine the fine-structure constant with high accuracy as suggested in von Klitzing's first publication [19]. Two years later, H. Störmer and D. Tsui found that also fractions of the conductance $e^2/(2\pi\hbar)$ can be observed once the perpendicular field exceeds 5 Tesla [42]. This discovery, which was called *fractional quantum Hall effect*, and a theoretical approach by R. Laughlin [21], was honored with the Nobel Prize in 1998. Whereas the integer quantum Hall effect can be explained within the mesoscopic theories by a one-particle picture, the latter is a many-body effect which requires a profound understanding of quantum field theory and the interaction between particles. Thus, a complete description of all underlying effects, which lead to a fractional conductance, has not been given yet.
About 20 years after von Klitzing's discovery, U. Zeitler, H. Schumacher et. al. [49] exposed strong anisotropies of the longitudinal resistance in coincidence measurements

performed on a Si/GeSi Hall bar, i.e. they observed anisotropies in transport measurements on a quantum wire in the integer quantum Hall regime with an additional magnetic field in the plane of the two-dimensional system which is tuned such as the spin-polarized energy bands of neighboring Landau levels overlap due to the Zeeman splitting. The anisotropy is with respect to the orientation of the in-plane field, that is the resistance at the coincidence differs for a lateral magnetic field which is parallel or perpendicular to the direction of transport. The reason for this effect is unknown but one of the explanations pointed to the complex band structure of silicon[1]. However, this possibility was refused one year later when W. Pan, H. Störmer, D. Tsui et. al. [26] encountered very similar anisotropies in an (Al)GaAs quantum well structure, a semiconductor with a direct band gap and therefore no valley splitting. Another idea considered *spin hot spots* [11] and the influence of spin-orbit interaction which may have a noticeable, possibly anisotropic[2] contribution to the band structure at the crossing of the spin-polarized levels. Since this proposal is checked within the framework of the present thesis, we want to spend some lines to present the concepts and the outcome of the coincidence measurements in detail. For this purpose, we stick to the publication of W. Pan et. al. [26] where they had used an (Al)GaAs system which we take as example in subsequent chapters.

The two-dimensional system is a 35 nm wide GaAs quantum well sandwiched by $Al_{0.24}Ga_{0.76}As$. The conducting region is quadratic (5 mm × 5 mm) and contacted by eight indium leads placed symmetrically around the perimeter. The electron density is such that two subbands of the quantum well are occupied which is quantitatively mapped in Fig. 2.3 (p. 15) using a harmonic approximation of the confinement. The measurements were performed in the integer quantum Hall regime at filling factors of $\nu = 4, 6, 8$ which requires a perpendicular magnetic field of about 3 T. Additionally an in-plane magnetic field up to 30 T is used to increase the Zeeman splitting until the spin-polarized bands of neighboring Landau levels overlap. This process is sketched schematically in Fig. 4.4 (p. 77) for a narrow quantum wire with zero perpendicular field and also given quantitatively in Fig. 3.2 (p. 32) for the given Hall bar. The in-plane field is parallel or perpendicular to the current and all experimental results were obtained at low temperatures (< 0.1 K). The outcome of the transport measurements are shown in Fig. 1.1 for the three filling factors. As we know from the integer

[1] Note that equivalent points in the Brillouin zone of the indirect band gap semiconductor silicon are the reason for additional splitting of the Landau levels, which is called *valley splitting* [49].

[2] However, note that without external magnetic field a 2DEG in the presence of Bychkov-Rashba and Dresselhaus SOI exhibits an anisotropic, current-induced spin accumulation but the conductivity remains isotropic [41].

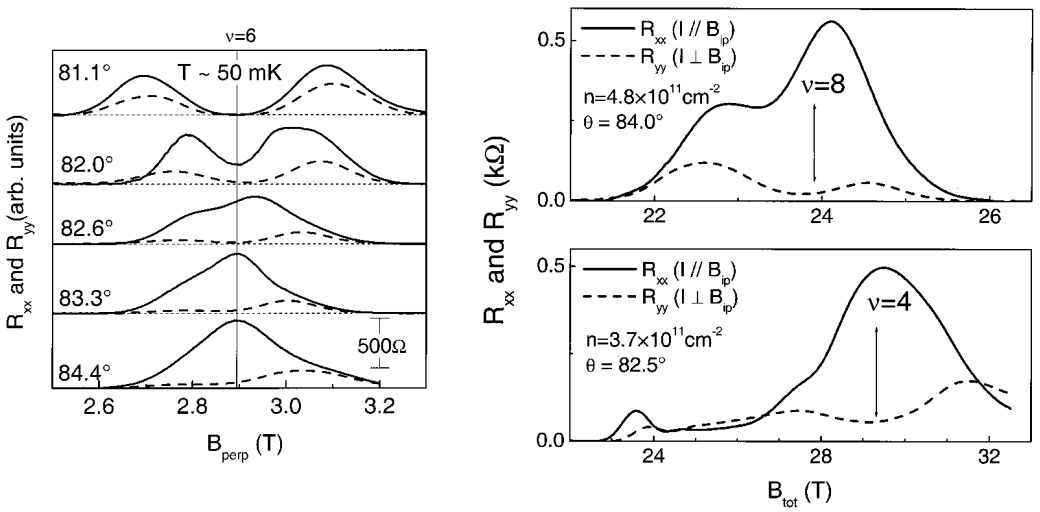

Figure 1.1: Longitudinal resistances R_{xx}, R_{yy} of the given Hall bar with an in-plane magnetic field parallel (solid lines) and perpendicular (dashed lines) to the current respectively. For the tilt angle Θ it holds $B_{\mathrm{ip}} = \tan(\Theta)B_z$ (comp. p. 32) and the measurement on the lhs was performed at an electron density of $n = 4.2 \cdot 10^{11}\,\mathrm{cm}^{-2}$. Source: Ref. [26].

quantum Hall effect, the longitudinal resistance develops peaks whenever the Fermi energy is located at an energy level of the bulk. Else, backscattering is suppressed due to the spatial separation of the states carrying current to opposite directions and the resistance drops down to nearly zero. We can identify the peaks in Fig. 1.1 with spin-polarized energy levels arising from two different Landau levels which approach for an increasing magnetic field due to the Zeeman splitting. At the level coincidence we observe a strong anisotropy of the resistance, i.e. the peaks overlap if the in-plane field is parallel to the Hall bar (R_{xx}), but the minimum persists for a magnetic field which is perpendicular to the current (R_{yy}). The difference of the longitudinal resistance for both orientations of the lateral field as displayed in Fig. 1.1 is obvious.

If this anisotropy is caused by the spin hot spots, it cannot be due to the *Dresselhaus spin-orbit interaction* [12, 18, 45, 51] of systems with bulk inversion asymmetry, because of the experiments of U. Zeitler et. al. [49], where silicon, a material with diamond structure, was used. Hence, in the present work any Dresselhaus contribution

was neglected for convenience. However, a two-dimensional approach to the influence of *Bychkov-Rashba spin-orbit interaction* [12, 18, 45, 51] at the level crossing via degenerate perturbation theory [28, 37] failed to explain the anisotropies for the dimensions of the given system. A straightforward generalization of this work implies the influence of the orbital effects of the large in-plane magnetic fields that were used in these experiments. This is a connatural, though different problem compared to the investigation of the coupling between the cyclotron motion in a perpendicular field and the spin-orbit interaction, which has recently been studied by Ref. [36, 46, 50]. One of the main tasks of this thesis was to derive a formalism which accounts for the orbital effects of lateral fields and to check the possibility of anisotropic transport due to spin-orbit interaction. Nevertheless, it turned out that also considering the third dimension and the orbital effects, the Bychkov-Rashba spin-orbit coupling was not capable to explain the measured anisotropies of Ref. [26, 49] as we can see in Chapter 4.
In opposite to the theory of spin hot spots, it was speculated about the formation of *stripe phases* [9], an energetically more advantageous state of electrons that arrange in charge-density waves rather than Landau levels. These have already been found in bilayer quantum Hall systems at odd integer filling factors [5, 27] and it sounds reasonable in this context [5] due to the large widths of the quantum wells of the given systems and also the high in-plane magnetic fields (up to 30 T) which are necessary in these experiments. A possible explanation via stripe phases has already been suggested by U. Zeitler, H. Schumacher et. al. [49].

Nevertheless, orbital effects of large lateral magnetic fields play an important role for all quantitative descriptions in this regime. For instance, taking the calculations of spin relaxation rates in quantum dots by P. Stano and J. Fabian [40], we find that the results are in good agreement for small, but deviate significantly for large in-plane magnetic fields as they did not account for these effects. For quantum dots and pure in-plane fields, an effective Hamiltonian, which includes Dresselhaus spin-orbit interaction and the orbital effects of the field, has already been given by V. Fal'ko, B. Altshuler et. al. [13]. The goal in the present work was to use similar techniques to deduce a formalism which is applicable for quantum wires considering Bychkov-Rashba spin-orbit coupling.

This thesis is organized as follows. In Chapter 2 we recapitulate the main conclusions of the *effective mass approximation* [3, 4, 45] which is commonly used in a two-dimensional form to describe heterostructures, quantum wells and other confined systems. We also discuss ways to improve the Hamiltonian considering adequate adjustments of the effective mass and the Landé factor (g-factor) and give first insight into the orbital effects of

lateral magnetic fields. Chapter 3 is dedicated to the derivation of a three-dimensional description of quantum wires which fully accounts for the orbital effects within a harmonic approximation, i.e. all confinements are approximated by harmonic potentials with appropriate parameters. In this sense, we calculate the eigenenergies of quantum wires with arbitrarily orientated magnetic fields in Chapter 3.1 using the *invariant eigen-operator method* [14, 22] and continue with a more profound investigation of the orbital effects when we look into details of the transformations that decouple two model Hamiltonians, one for an in-plane field parallel to the direction of transport, the other perpendicular to the wire (Chap. 3.2). The impact of Bychkov-Rashba spin-orbit interaction is discussed in Chapter 3.3 when we also attend to the spin hot spots as to the coincidence measurements discussed above. Chapter 3.4 is dedicated to the derivation of effective Hamiltonians which incorporate all previously discussed effects and provide a deeper understanding of spin-orbit coupling in these systems. The appearance of anisotropies and the conditions for anisotropic behavior are highlighted in Chapter 4, when we also give quantitative examples and suggestions for experimental verification. Chapter 5 completes the thesis with a short summary, closing remarks and an outlook for future efforts.

2 2D Effective Mass Approximation

It is a very common technique to describe quasi two-dimensional electron systems (quasi-2DES) with a Schrödinger equation that does not contain the full Hamiltonian of the problem but instead a rather simple one that takes care of many embedded effects of the crystal with the help of only a few altered quantities. This *effective mass Hamiltonian* (2.1) [3, 4, 45] can either be derived from the *envelope function approximation* [12, 45] or constructed from band diagrams that have been measured in experiments or calculated in computer simulations with the *tight binding model* [1, 4] or other methods. In the basic form this Hamiltonian describes non-interacting Bloch electrons of the conduction band with a quasi-momentum $\vec{k}$ close to a given point[1] in the reciprocal space $\vec{k}_0$ in terms of free electrons with an effective mass and an effective Landé g-factor. The characteristics of the lattice-periodic parts of the *Bloch functions* [1, 3, 12, 45], which are altered by spin-orbit coupling and possible external electric and magnetic fields, are hidden in the band structure and enter the formalism via the adapted quantities. The effective mass Hamiltonian for semiconductors with inversion symmetry reads

$$H^{\mathrm{3D}} = E_c + \frac{\left(\vec{P} + e\vec{A}\right)^2}{2m} + V(\vec{R}) + \frac{g}{2}\mu_{\mathrm{B}}\vec{\sigma}\vec{B} \ , \tag{2.1}$$

where E_c is the band-edge energy of the conduction band, $\vec{A}$ is the vector potential, $\vec{B} = \nabla \times \vec{A}$ is the magnetic field, $m = \beta m_{\mathrm{e}}$ is the effective mass and g is the effective Landé factor of the bulk semiconductor, m_{e} is the free-electron mass, $\mu_{\mathrm{B}} = \frac{e\hbar}{2m_{\mathrm{e}}}$ is the Bohr magneton, $-e$ is the electron charge and $V(\vec{R})$ is a potential term that may describe confinement, impurities or external electric fields. In order to account for anisotropic band structures, one can consider an anisotropic effective mass in (2.1) [1]. Note that within this approach the band-edge energy E_c is usually set to zero which is what we will do in the following.

[1] For direct band semiconductors with zinc blende structure such as GaAs, InSb, or CdTe it is usually enough to concentrate on the vicinity of the Γ point.

In a two-dimensional system (x-y plane) it holds that the potential splits up into two parts $V(\vec{R}) = V(X,Y) + V(Z)$, with $V(Z)$ describing a confinement of the electrons that is stronger than any confinement in the x- or y-direction. The shape of $V(Z)$ is usually approximated with a triangular potential for heterostructures and a harmonic potential or hard-wall potential well for quantum wells. Without a magnetic field and due to the special form of $V(\vec{R})$ the wave function can be separated [4]. In the z-direction the wave function is bound with discrete eigenenergies $E^z_{n'}$ which are denoted as *electric subbands*. The energy spacings thereof are large compared to the spacings of the remaining system. It follows that for small electron densities there are one or only a few electric subbands occupied and the system is said to be two-dimensional or quasi two-dimensional respectively. For the moment we will focus on two-dimensional systems for simplicity. A discussion on quasi two-dimensional systems will be given afterwards (p. 13).
With non-zero magnetic field the situation is somewhat more difficult. It depends on the gauge and orientation of the field whether the Hamiltonian can be written in a two-dimensional form. It is surely possible if the magnetic field is normal to the plane, since the Lorentz force acts perpendicular to the magnetic field and therefore the dynamics of the electrons along the z-direction do not change. However, a two-dimensional effective mass Hamiltonian for arbitrarily orientated magnetic fields is an approximation that neglects any orbital effects of in-plane magnetic fields. This becomes clear when we look at the vector potential in symmetric gauge:

$$\vec{A} = \frac{1}{2} \begin{pmatrix} ZB_y - YB_z \\ XB_z - ZB_x \\ YB_x - XB_y \end{pmatrix} . \tag{2.2}$$

A 2D Hamiltonain that describes the x-y plane should not depend on the z-coordinate. Moreover the explicit z-dependence should have vanished as well. What is left from (2.2) is the vector potential

$$\vec{A} = \frac{1}{2} \begin{pmatrix} -YB_z \\ XB_z \end{pmatrix} , \tag{2.3}$$

which cannot account for the in-plane magnetic fields since the corresponding components have disappeared. One can also argue that keeping the z-component and the z-dependence of (2.2), the wave function can in general not be separated any more. However, we can use (2.3) to write down naively the *two-dimensional effective mass Hamiltonian* for zero or small in-plane magnetic fields. According to (2.1) it reads

$$H^{\mathrm{2D}} = E^z_0 + \frac{(P_x + eA_x)^2}{2m} + \frac{(P_y + eA_y)^2}{2m} + V(X,Y) + \frac{g}{2}\mu_{\mathrm{B}}\vec{\sigma}\vec{B} . \tag{2.4}$$

Note that possible in-plane components of $\vec{B}$ are left only within the Zeeman term.

Since this is an approximation it is natural to ask for the validity of the formula and for possible ways to include the orbital effects of in-plane magnetic fields into the formalism. To face this question we start with a model system where an analytical solution is possible [17]. Assume we have an infinite two-dimensional electron gas (2DEG) in the x-y plane, a harmonic confining potential in z-direction and a magnetic field along the x-direction. If we use Landau gauge $\vec{A} = (0, -ZB, 0)$ and the effective mass Hamiltonian (2.1), the Schrödinger equation reads

$$\left[\frac{p_x^2}{2m} + \frac{(p_y - eBz)^2}{2m} + \frac{p_z^2}{2m} + \frac{1}{2}m\omega_z^2 z^2\right]\psi(\vec{r}) = E\psi(\vec{r}) \ , \tag{2.5}$$

where we omitted the Zeeman term for simplicity. Since there is no confinement in the plane we use a plane wave ansatz of the wave function

$$\psi(\vec{r}) = \mathrm{e}^{\mathrm{i}k_x x}\mathrm{e}^{\mathrm{i}k_y y}\ \Phi(z) \ ,$$

and after some simple algebra we obtain

$$\left[\frac{\hbar^2 k_x^2}{2m} + \frac{\hbar^2 k_y^2}{2m}\ \eta^{-1} + \frac{p_z^2}{2m} + \frac{1}{2}m\tilde{\omega}^2(z + z_{k_y})^2\right]\psi(\vec{r}) = E\psi(\vec{r}) \ , \tag{2.6}$$

where we used the substitutions

$$\tilde{\omega} := \sqrt{\omega_z^2 + \omega_c^2} \quad , \quad z_{k_y} := \frac{\hbar k_y \omega_c}{m\tilde{\omega}^2} \quad , \quad \eta := \frac{\tilde{\omega}^2}{\omega_z^2} \tag{2.7}$$

and the cyclotron frequency $\omega_c := \frac{eB}{m}$. Defining the effective mass in y-direction

$$m_y := m\eta = m\left(1 + \frac{\omega_c^2}{\omega_z^2}\right) \tag{2.8}$$

the eigenenergies of the system read

$$E_{n'}(k_x, k_y) = \frac{\hbar^2 k_x^2}{2m} + \frac{\hbar^2 k_y^2}{2m_y} + \hbar\tilde{\omega}\left(n' + \frac{1}{2}\right) \ . \tag{2.9}$$

From (2.6) we can read off the effects of the in-plane field on the system which are visualized in Fig. 2.1. We observe that the frequency of the harmonic potential has increased. This implies an increase of the energy spacings and a shift of the subbands

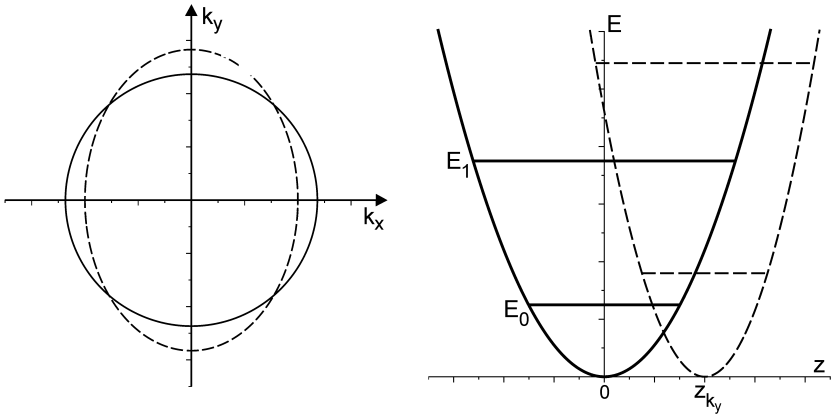

Figure 2.1: Effects of an in-plane magnetic field (x-direction) on a 2DEG (x-y plane). Left: Shape of the Fermi sphere with (dashed line) and without (solid line) magnetic field. The sphere has become elliptical because of the altered mass in y-direction. Right: Diamagnetic shift of the subbands and spatial shift of the confining potential for a finite magnetic field (dashed lines). The electrostatic potential (B=0) is given for comparison (solid lines).

$E_{n'}^{z}$ to higher energies which is called *diamagnetic shift*. We will denote the shifted subband energies as $E_{n'}^{z*}$ in the following. We also note that the parabolic confinement has moved in real space by z_{k_y} (2.7) which is proportional to B. Although this effect does not influence the eigenenergies (2.9) of the system, it will be important for the effective mass and g-factor as we will see later (p. 12). The last thing to mention is the appearance of an anisotropic mass. The effective mass perpendicular to the magnetic field has increased by the factor η (2.8) and, as a consequence, the density of states increases as well [17, 33]. With $\bar{m} = \sqrt{m\, m_y} = m\sqrt{\eta}$ being the average effective mass, the density of states per energy and unit area for this quasi two-dimensional system of a parabolic quantum well reads

$$d_{\mathrm{PQW}}(E,B) = \frac{\overline{m}}{\pi\hbar^2} \sum_{n=0}^{\infty} \Theta\!\left(E - \hbar\tilde{\omega}\left(n + \frac{1}{2}\right)\right) \ . \tag{2.10}$$

So if we used (2.4) to describe a system with finite in-plane magnetic fields, we would not include the diamagnetic shift of the eigenenergies, spatial shift of the eigenstates and the anisotropic effective mass which leads to an increased density of states. Thus

the two-dimensional effective mass Hamiltonian (2.4) is valid only as long as these effects are negligible. This is the case if $\omega_c \ll \omega_z$, hence the validity depends on the confinement and the effective mass of the semiconductor. For instance if we compared the magnetic length $l_B = \sqrt{\hbar/m\omega_c} = \sqrt{\hbar/eB}$ of an AlGaAs/GaAs/AlGaAs quantum well with the oscillator length $l = \sqrt{\hbar/m\omega_z} \approx 12\,\mathrm{nm}$, the approximation would be valid for in-plane fields up to about 1 T. For narrow quantum wells with $l \approx 3\,\mathrm{nm}$ the formula would hold up to 10 T. This specifies the meaning of "weak in-plane fields" in this context.

In the following we will discuss some methods to extend the formalism to improve the accuracy at higher fields. We have seen that an in-plane magnetic field along the x-direction results in an increased effective mass in the y-direction and shifted energy levels. One way to take these effects into account is to put the altered mass (2.8) and the diamagnetically shifted energy E_0^{z*} into the two-dimensional effective mass Hamiltonian (2.4) by hand [13]:

$$H^{\mathrm{2D}} = E_0^{z*} + \frac{(P_x + eA_x)^2}{2m} + \frac{(P_y + eA_y)^2}{2m_y} + V(X,Y) + \frac{g}{2}\mu_{\mathrm{B}}\vec{\sigma}\vec{B}\ . \tag{2.11}$$

Note that this Hamiltonian is valid only for a magnetic field with its in-plane component along the x-direction. For the moment it is not clear why (2.11) should give a reasonable description of confined systems since m_y was derived for an infinite system. To explore this issue consider a harmonic confinement in y-direction $V(X,Y) = V(X) + \frac{1}{2}m\omega_y^2 Y^2$. The wave function can be separated and its y-dependence is the solution of the harmonic oscillator. Since the mass that comes along with the momentum operator is the altered effective mass m_y, the mass within the potential must be adapted. We need to rewrite the potential as $V(Y) = \frac{1}{2}m_y(\omega_y/\sqrt{\eta})^2 Y^2$ and note that the frequency has changed. The new frequency is given by

$$\tilde{\omega}_y := \frac{\omega_y}{\sqrt{\eta}} = \frac{\omega_y\ \omega_z}{\sqrt{\omega_z^2 + \omega_c^2}} \tag{2.12}$$

which yields the effects of an in-plane magnetic field on a confined system. It turns out that this is indeed a very good approximation for pure in-plane fields as we will show later in Chapter 3 (p. 29).

Another effect of the magnetic field, which we have not mentioned yet, is a modification of the g-factor. Both an in-plane and a perpendicular field influence the Landé factor of a heterostructure or quantum well in the effective mass approximation. This has

been studied experimentally and theoretically by many authors [6, 7, 8, 16, 23, 29, 38, 39, 45, 48]. Since there is no closed analytic formula for this problem we will not go into detail. Instead we discuss the dependence on the magnetic field qualitatively to deliver insight into the nature of the alteration.
As an example consider an $Al_{0.3}Ga_{0.7}As/GaAs/Al_{0.3}Ga_{0.7}As$ quantum well where the bulk g-factors read [16]

$$g_{(\mathrm{GaAs})} = -0.44 \quad , \quad g_{(\mathrm{Al_{0.3}Ga_{0.7}As})} = +0.46 \; .$$

Note that the height of the well is finite (about 300meV) and the wave function penetrates the walls of the well. Therefore there is a finite probability to find the electron in the region of AlGaAs which increases the average g-factor of the electron. The penetration and thus the Landé factor increases for strong in-plane fields due to the spatial shift of the magnetic confinement (Fig. 2.1) and for decreasing well width. Additionally, we have to take the diamagnetic shift into account. For large energies, that is high magnetic fields, large quasi-momenta $\vec{k}$ or, in a Hall bar, high Landau level indices, the effective mass approximation lacks accuracy. This is because the dispersion relation is assumed to be parabolic which is in fact not true. Due to the non-parabolicity of the band structure the effective mass and the g-factor change as the energy levels are shifted towards higher energies. Of course the well width and the diamagnetic shift influence the eigenenergies directly and the mismatch of these quantities compared to bulk values must be considered. Since both in-plane and perpendicular fields account for diamagnetic shifts and an in-plane field increases the penetration of the wave function because the magnetic confinement is spatially shifted dependent on the strength of the field, the g-factor differs from the bulk g-factor of GaAs. For narrow quantum wells and, where required, strong magnetic fields the Landé factor of an (Al)GaAs QW may become zero or even positive. In the following we will write g^* to stress that the g-factor differs from the bulk value.

The non-parabolicity of the band structure leads to an additional effect that should be included in the effective mass equation (2.11). As mentioned above the possible energy levels of the electrostatic or magneto-electric confinement in the z-direction increase for small quantum wells and high fields. As a consequence the effective mass of the confined electron differs from the bulk value at the $\vec{k}_0$-point (comp. p. 7) and equation (2.11) should be adapted. It is ad hoc not clear how exactly the effective mass changes but one can assume that the properties of the electron on a subband with specific energy are equivalent to the properties of bulk electrons at the same energy [38]. In the following we will denote the adapted effective mass m^* and the adapted effective

mass in y-direction (2.8) m_y^*.

In a nutshell we are left with the *improved two-dimensional effective mass Hamiltonian* that describes systems with a tilted magnetic field with its in-plane component along the x-direction:

$$H^{\mathrm{2D}} = E_0^{z*} + \frac{(P_x + eA_x)^2}{2m^*} + \frac{(P_y + eA_y)^2}{2m_y^*} + V(X,Y) + \frac{g^*}{2}\mu_{\mathrm{B}}\vec{\sigma}\vec{B} \ . \tag{2.13}$$

So far we have omitted spin-orbit coupling effects that arise due to inversion asymmetry, namely the appearance of the *Bychkov-Rashba* and *Dresselhaus Hamiltonians* [12, 18, 51]. This can, in principle, be included and the effect of a magnetic field can be incorporated via *minimal coupling* in a known way [12, 45, 51]. However up to now it is not clear how exactly the contributions are altered by arbitrarily orientated and strong magnetic fields. For a system with structure inversion asymmetry we will face this question in Chapter 3.3 and 3.4 when we discuss the Bychkov-Rashba spin-orbit interaction in the diamagnetic shift approximation. This will yield a way to measure the Bychkov-Rashba parameter α for a wide range of magnetic field strengths. Effects that arise due to bulk inversion asymmetry (Dresselhaus spin-orbit interaction) are neglected here as we are mainly interested in the effects that appear in 2DEGs of any material.

Let us complete this discussion with some remarks on quasi two-dimensional systems. Typically "quasi two-dimensional" states that there are exactly two energy levels of the confining potential in z-direction occupied and in the following we will use this notation. If we neglect intersubband scattering we can treat each subband independently and the description becomes quite simple. However it is important to note that different subbands may have different scattering times (τ), different electron densities (n) and different effective masses (m), thus they are not equal and must be treated individually. For each subband we can use the improved two-dimensional effective mass Hamiltonian (2.13) with the appropriate quantities. To illustrate the important features of a quasi-2DES we will use a concrete example[2].
Consider a harmonic confinement in the growth-direction (z-axis) of an (Al)GaAs system with an electron density such as two electric subbands are populated. Experimentally the electron densities of both subbands (n_0, n_1) can be determined by analyzing Shubnikov-de Haas (SdH) oscillations [4]. Once we know the densities we can use

[2]The example is a harmonic approximation of the setup used by W. Pan et. al. in Ref. [26].

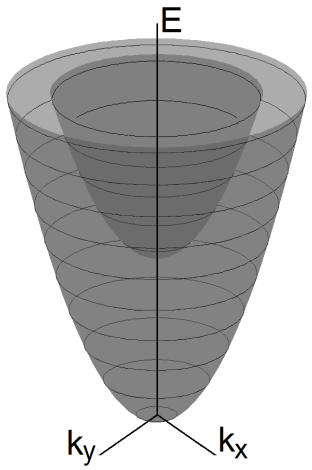

Figure 2.2: Dispersion relation of a free quasi two-dimensional electron gas. The paraboloids of revolution are shifted by the energy spacing of the electric subbands.

the Fermi wavelength of a spin-degenerate two-dimensional system ($\lambda_{\mathrm{f}}^{\mathrm{2D}} = \sqrt{2\pi/n}$) to determine the Fermi energy relative to the subbands and thus the energy spacing between the levels ($\Delta E = E_1^z - E_0^z$). This allows us to calculate the frequency of the harmonic confinement, which may be of interest for ongoing calculations (Chap. 3), via $\omega_z = \Delta E/\hbar$. The subband spacing defines the offset in the 2D dispersion relation. For a free 2DEG without magnetic field we have two paraboloids of revolution[3] shifted in energy by ΔE (Fig. 2.2). In the integer quantum Hall regime the states are localized and the paraboloids become flat energy levels independent of the wave vector. The Landau Levels are created for each electric subband by the magnetic confinement separately. Fig. 2.3 visualizes this situation and gives a quantitative description of the given example. Note that the energy of the conduction band edge was set zero.
The 2D Hamiltonians of the subbands and the dispersion relation of the system change according to the effects previously discussed when an in-plane magnetic field is applied. An appropriate treatment of the situation is based on the improved two-dimensional effective mass Hamiltonian (2.13)

$$H_{n'}^{\mathrm{2D}} = E_{n'}^{z*} + \frac{(P_x + eA_x)^2}{2m_{n'}^*} + \frac{(P_y + eA_y)^2}{2m_{n'y}^*} + V(X,Y) + \frac{g_{n'}^*}{2}\mu_{\mathrm{B}}\vec{\sigma}\vec{B}\ , \tag{2.14}$$

[3] A *paraboloid* is defined by $\frac{x^2}{a} + \frac{y^2}{b} = z$ (Cartesian coordinates; $a, b \in \mathbb{R}$). A *paraboloid of revolution* is given by the additional condition $a = b$.

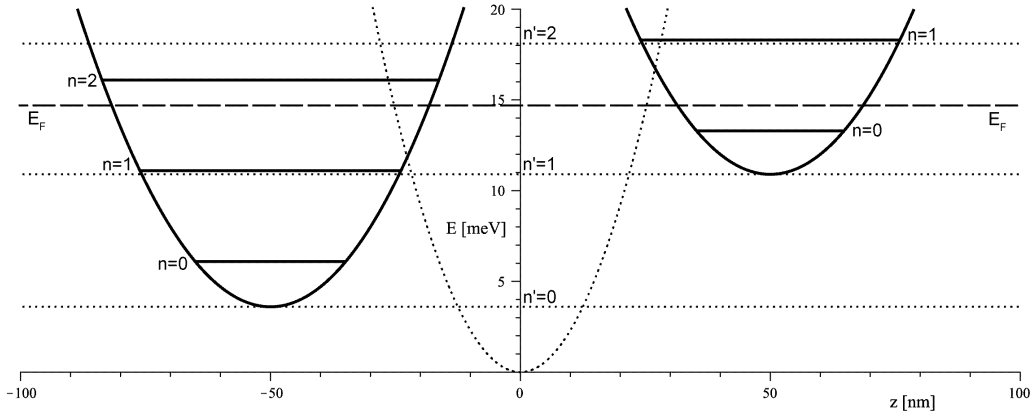

Figure 2.3: Energy levels of a quasi two-dimensional electron gas in the integer quantum Hall regime. The electrostatic confinement in z-direction ($\hbar\omega_z = 7.24\,\mathrm{meV}$; dotted curve) of the (Al)GaAs system creates equidistant electric subbands (dotted lines) and for each the magnetic confinement ($\omega_c = eB/m$, $B_z = 2.9\,\mathrm{T}$; solid curves, shifted for clarity) creates Landau Levels (solid lines). The Fermi energy (dashed line) indicates a filling factor of $\nu = 6$. Note that the graph does not show the Zeeman splitting which would additionally shift the spin-polarized levels by $\pm 0.04\,\mathrm{meV}$. The electron density of the system is $n = 4.2 \cdot 10^{11}\,\mathrm{cm}^{-2}$ which splits up into $n_0 = 3.1 \cdot 10^{11}\,\mathrm{cm}^{-2}$ and $n_1 = 1.1 \cdot 10^{11}\,\mathrm{cm}^{-2}$ for the states originating from the lowest and first excited electric subband respectively.

where $n' = 0, 1$ denotes the subband index. Note that since the g-factor depends on the non-parabolicity of the band structure and therefore on the position in the energy scale, it may differ significantly from one subband to the other and needs to be indexed as well. We have seen that an in-plane field increases the energy spacing of the subbands (Fig. 2.1) which may lead to depopulation of the upper level once the Fermi energy becomes less than $E_1^{z*} + \frac{1}{2}\hbar\omega_c$ [17]. In this case the quasi-2DES becomes two-dimensional and we do not need to worry about other subbands any more. However, from this point of view we cannot give a detailed prediction of the conditions for this effect to happen since we do not have analytic expressions for the adapted effective mass m^* or the diamagnetic shift.

3 Diamagnetic Shift Approximation

In this chapter we deal with the consequences of a tilted magnetic field on a quasi-2DES within a simple model. It is a one-particle picture based on the effective mass Hamiltonian in three dimensions (2.1) where the confining potentials are assumed to be harmonic. We have already discussed the effects of a magnetic field on the two-dimensional effective mass Hamiltonian qualitatively (2.13), now we want to investigate the diamagnetic shift (Fig. 2.1) and the anisotropic effective mass (2.8) quantitatively within a harmonic approximation, the *diamagnetic shift approximation* (DSA), where an analytic solution is possible.

Our starting point is a Hamilton operator describing a quantum wire that is aligned along the x-direction. It reads

$$H^{\mathrm{3D}} = \frac{\left(\vec{P} + e\vec{A}\right)^2}{2m} + V_y(Y) + V_z(Z) \ , \tag{3.1}$$

where $-e$ is the electron charge, m is the effective mass of the conduction band electrons and

$$V_y(Y) = \frac{1}{2}\, m\, \omega_y^2\, Y^2 \quad , \quad V_z(Z) = \frac{1}{2}\, m\, \omega_z^2\, Z^2$$

are the confinements in y- and z-direction respectively. Note that for now we omit the Zeeman splitting and spin-orbit coupling for convenience. The role of spin will be discussed separately in Chapter 3.3. The 2DES is supposed to be in the x-y plane, thus we have the condition $\omega_y \ll \omega_z$. An infinite 2DEG can be constructed using the limit $\omega_y \to 0$.

For further analysis we use a plane wave ansatz in x-direction $\langle x|k\rangle = \frac{1}{\sqrt{2\pi}} \mathrm{e}^{\mathrm{i}kx}$ which is possible for adequate gauges. The time independent Schrödinger equation reads

$$H^{\mathrm{3D}} \ |k\rangle \otimes |\psi\rangle = E \ |k\rangle \otimes |\psi\rangle$$

and since H^{3D} does not have any constraint in x-direction, we can formally write $\langle k|H^{3D}|k\rangle = H_k$, i.e. doing the substitution "$P_x \to \hbar k$", and thus

$$H_k \ |\psi\rangle = E_k \ |\psi\rangle \ . \tag{3.2}$$

Note that the Hamiltonian H_k depends explicitly on the wave number k, indicated by the superscript, from which follows the k-dependence of the eigenenergy. In this picture, the wave number needs to be seen as parameter since any new value gives rise to a different Hamiltonian and thus to a new system.
In the following we restrict ourselves to the two most important situations which we call "system ①" and "system ②". A general treatment for arbitrarily orientated magnetic fields can, in principle, be constructed using the same methods. However, we focus especially on the difference between the systems ① and ② by using both cases separately. They are defined as follows:

① $\mathbf{B_x = 0}$: The magnetic field lies in the y-z plane, that is perpendicular to the direction of transport. Using the vector potential $\vec{A}^{①} = (ZB_y - YB_z, 0, 0)$ in the Landau gauge the Hamiltonian reads

$$H_k^{①} = \frac{\left(\hbar k + e\left(ZB_y - YB_z\right)\right)^2}{2m} + \frac{P_y^2}{2m} + \frac{P_z^2}{2m} + \frac{1}{2}\, m\, \omega_y^2\, Y^2 + \frac{1}{2}\, m\, \omega_z^2\, Z^2 \ ,$$

which can be written as

$$\begin{aligned} H_k^{①} \ =& \frac{P_y^2}{2m} + \frac{1}{2} m \Omega_{y,cz}^2 Y^2 - \hbar k \omega_{cz} Y + \\ &+ \frac{P_z^2}{2m} + \frac{1}{2} m \Omega_{z,cy}^2 Z^2 + \hbar k \omega_y Z - m \omega_{cy} \omega_{cz} Y Z + \frac{\hbar^2 k^2}{2m} \ , \end{aligned} \tag{3.3}$$

where we have defined

$$\Omega_{y,cz} := \sqrt{\omega_y^2 + \omega_{cz}^2} \quad , \quad \Omega_{z,cy} := \sqrt{\omega_z^2 + \omega_{cy}^2} \ , \tag{3.4}$$

and the partial cyclotron frequencies $\omega_{cy} := \frac{eB_y}{m}$ and $\omega_{cz} := \frac{eB_z}{m}$.

② $\mathbf{B_y = 0}$: The magnetic field lies in the x-z plane, that is the in-plane component of $\vec{B}$ is parallel to the direction of transport. Using the Landau gauge the vector potential reads $\vec{A}^{②} = (-YB_z, 0, YB_x)$ and the Hamiltonian is given by

$$H_k^{②} = \frac{\left(\hbar k - eYB_z\right)^2}{2m} + \frac{P_y^2}{2m} + \frac{\left(P_z + eYB_x\right)^2}{2m} + \frac{1}{2}\, m\, \omega_y^2\, Y^2 + \frac{1}{2}\, m\, \omega_z^2\, Z^2 \ ,$$

which can be rewritten as

$$H_k^{②} = \frac{P_y^2}{2m} + \frac{1}{2} m \Omega_{y,cx,cz}^2 Y^2 - \hbar k \omega_{cz} Y + \frac{P_z^2}{2m} + \frac{1}{2} m \omega_z^2 Z^2 + \omega_{cx} Y P_z + \frac{\hbar^2 k^2}{2m} \ , \tag{3.5}$$

where we have defined

$$\Omega_{y,cx,cz} := \sqrt{\omega_y^2 + \omega_{cx}^2 + \omega_{cz}^2} \tag{3.6}$$

and the partial cyclotron frequencies $\omega_{cx} := \frac{eB_x}{m}$ and $\omega_{cz} := \frac{eB_z}{m}$ in analogy to system ①.

For these cases, we study the Schrödinger equation (3.2) within the DSA in subsequent chapters. They are structured as follows: In Chapter 3.1 we determine the eigenenergies of the model systems with the *invariant eigen-operator method* (IEO method) and compare the results with well known common approximations. In Chapter 3.2 we derive explicit transformations that decouple both systems and end up with exact Hamiltonians which also account for anisotropic effective masses due to the magnetic field. Using these transformations on can include the effect of *Bychkov-Rashba spin-orbit interaction* (BR-SOI) into the theory (Chap. 3.3) and investigate SOI induced anisotropies. Chapter 3.4 is dedicated to the derivation of effective Hamiltonians for these systems which are useful to compare the different approximations.

3.1 Invariant Eigen-Operator Method

In this chapter we will use the *invariant eigen-operator method* (IEO method) [14, 22] to derive the k-independent part of the eigenenergies of the two Hamiltonians (3.3) and (3.5). The IEO yields information about the energy spacings of the system, and since we assume the (k-independent part of the) transformed Hamiltonians to be of the form

$$\tilde{H} = \frac{P_{\tilde{y}}^2}{2m_{\tilde{y}}} + \frac{1}{2}\, m_{\tilde{y}}\, \omega_{\tilde{y}}^2\, \tilde{Y}^2 + \frac{P_{\tilde{z}}^2}{2m_{\tilde{z}}} + \frac{1}{2}\, m_{\tilde{z}}\, \omega_{\tilde{z}}^2\, \tilde{Z}^2$$

we will obtain the frequencies $\omega_{\tilde{y}}$ and $\omega_{\tilde{z}}$ through this method. However we will neither gain any information about the explicit transformation $H \leftrightarrow \tilde{H}$ nor will we be able to account for possible anisotropic masses $m_{\tilde{y}}$, $m_{\tilde{z}}$. We will face these questions in Chapter 3.2 when we discuss in detail how the systems ① and ② are decoupled.
The IEO method takes place in the Heisenberg picture. Hence we will start with a short reminder on the pictures of quantum mechanics, namely the Schrödinger and Heisenberg picture, and continue with a general introduction to the method afterwards. Once we got the gist of IEO, we will derive the decoupled frequencies and close the chapter with a general discussion on validity and limits of $\omega_{\tilde{y}}$ and $\omega_{\tilde{z}}$ compared to other approximations.

Parenthesis: Schrödinger and Heisenberg Picture

In the ***Schrödinger picture***, the time dependence is carried by the states and the equation of motion is the well-known time-dependent Schrödinger equation

$$\mathrm{i}\hbar \frac{d}{dt} |\psi(t)\rangle = H_t\, |\psi(t)\rangle \ ,$$

where the subscript indicates a possibly explicit time dependence of the Hamiltonian. One can define a unitary *time evolution operator* $U(t, t')$ for which it holds

$$|\psi(t)\rangle = U(t, t_0)\, |\psi(t_0)\rangle \ .$$

Hence the equation of motion for the time evolution operator reads

$$\mathrm{i}\hbar \frac{d}{dt} U(t, t_0) = H_t\ U(t, t_0)$$

and the solution is given by the *von Neumann series*

$$U(t, t_0) = T\mathrm{e}^{-\frac{\mathrm{i}}{\hbar}\int_{t_0}^{t} dt' H_{t'}}$$

which simplifies to

$$U(t,t_0) = \mathrm{e}^{-\frac{\mathrm{i}}{\hbar}(t-t_0)H}$$

for a time-independent Hamiltonian. T denotes the *Dyson time-ordering operator*, which is defined by

$$TA_{t_1}B_{t_2} = \begin{cases} A_{t_1}B_{t_2}, & t_1 > t_2 \\ B_{t_2}A_{t_1}, & t_2 < t_1 \end{cases} .$$

In the ***Heisenberg picture*** the states

$$|\psi_\mathrm{H}\rangle := |\psi(t_0)\rangle = U^\dagger(t,t_0)\,|\psi(t)\rangle$$

are time independent and, as a consequence, the dynamics is inclosed by the operators. They transform according to

$$A_\mathrm{H}(t) = U^\dagger(t,t_0)\ A_t\ U(t,t_0)\ ,$$

for an operator A_t in the Schrödinger picture, which may have an explicit time dependence. The equation of motion reads

$$\mathrm{i}\hbar\frac{d}{dt}A_\mathrm{H}(t) = [A_\mathrm{H}(t), H_\mathrm{H}] + \mathrm{i}\hbar\ U^\dagger(t,t_0)\left(\frac{\partial}{\partial t}A_t\right)U(t,t_0)\ . \tag{3.7}$$

3.1.1 Introducing the IEO Method

The IEO method uses the equation of motion (3.7) of an operator $Q_\mathrm{H}(t)$ in the Heisenberg picture without explicit time dependence in the Schrödinger picture to deduce the energy gap between certain levels. This is possible as, for two eigenstates $|m\rangle$, $|n\rangle$ of a system described by H_0 with eigenenergies E_m and E_n respectively, it holds

$$\begin{aligned} \langle m|\left(\mathrm{i}\hbar\frac{d}{dt}\right)^2 Q_\mathrm{H}(t)\,|n\rangle &= \langle m|\,[[Q_\mathrm{H}(t),H_0]\,,H_0]\,|n\rangle = \\ &= \langle m|\left(Q_\mathrm{H}(t)H_0^2 - 2H_0Q_\mathrm{H}(t)H_0 + H_0^2Q_\mathrm{H}(t)\right)|n\rangle = \\ &= (E_m-E_n)^2\,\langle m|\,Q_\mathrm{H}(t)\,|n\rangle = \\ &= G_{mn}^2\,\langle m|\,Q_\mathrm{H}(t)\,|n\rangle \end{aligned} \tag{3.8}$$

where

$$G_{mn} := |E_m - E_n|\ .$$

The formula indicates that it is possible to construct information about the eigenenergies of H_0, however an intelligent choice of $Q_{\mathrm{H}}(t)$ is necessary.
Assume that the operator $Q_{\mathrm{H}}(t)$, which has at least one non-zero matrix element

$$\langle m|\, Q_{\mathrm{H}}(t)\, |n\rangle \neq 0 \tag{3.9}$$

where $|m\rangle$ and $|n\rangle$ are eigenstates with different eigenenergies, satisfies the operator identity[1]

$$\left(\mathrm{i}\hbar\frac{d}{dt}\right)^2 Q_{\mathrm{H}}(t) \equiv G^2\, Q_{\mathrm{H}}(t) \quad , \quad \text{with } G \in \mathbb{R} \text{ fixed.} \tag{3.10}$$

It follows that $G = G_{mn}$, i.e. we found the energy difference between $|m\rangle$ and $|n\rangle$ by solving (3.10). Of course G depends on the choice of $Q_{\mathrm{H}}(t)$ which is not unique. Moreover $Q_{\mathrm{H}}(t)$ may be "degenerate", that is there are two or more invariant eigenoperators satisfying (3.10) with the same G.

Although the problem reduces to equation (3.10), it can still be challenging to find the IEOs. A solution of (3.10) cannot be derived analytically but rather be guessed as we will see later. In order to approach this task, it proves useful to mention the crucial commutation relations [32]

$$\begin{aligned}\left[X_i, F(\vec{P})\right] &= +\mathrm{i}\hbar\,\frac{\partial F}{\partial P_i}\ ,\\ \left[P_i, F(\vec{X})\right] &= -\mathrm{i}\hbar\,\frac{\partial F}{\partial X_i}\end{aligned} \tag{3.11}$$

for any function F that can be expressed as power series in its arguments. The derivative of an operator is defined via

$$\frac{\partial}{\partial A}A^n = n\,A^{n-1}\ .$$

3.1.2 Determining the Eigenenergies of ① and ②

We will now use the IEO method to derive the k-independent eigenenergies of the systems ① and ②, that is we will determine IEOs for the relevant Hamiltonian and calculate the corresponding G respectively. They will be proportional to the frequencies ω_- and ω_+ which will define the energy levels of the decoupled harmonic oscillators.

[1] The operator identity "$\equiv$" states that the relation holds for all states of the given Hilbert space.

① In order to find an IEO of the Hamiltonian

$$\begin{aligned} H_k^{①} =& \frac{P_y^2}{2m} + \frac{1}{2} m\Omega_{y,cz}^2 Y^2 - \hbar k \omega_{cz} Y + \\ &+ \frac{P_z^2}{2m} + \frac{1}{2} m\Omega_{z,cy}^2 Z^2 + \hbar k \omega_{cy} Z - m\omega_{cy}\omega_{cz} YZ + \frac{\hbar^2 k^2}{2m} \end{aligned} \qquad \text{(same as 3.3)}$$

we calculate some basic commutation relations. We get[2]

$$\begin{aligned} \left[Y(t), H_k^{①}\right] &= +\mathrm{i}\hbar\, \frac{1}{m} P_y(t) \ , \\ \left[Z(t), H_k^{①}\right] &= +\mathrm{i}\hbar\, \frac{1}{m} P_z(t) \ , \\ \left[P_y(t), H_k^{①}\right] &= -\mathrm{i}\hbar \left(m\,\Omega_{y,cz}^2\, Y(t) - \hbar k \omega_{cz} - m\omega_{cy}\omega_{cz}\, Z(t)\right) \ , \\ \left[P_z(t), H_k^{①}\right] &= -\mathrm{i}\hbar \left(m\,\Omega_{z,cy}^2\, Z(t) + \hbar k \omega_{cy} - m\omega_{cy}\omega_{cz}\, Y(t)\right) \ , \end{aligned}$$

and therefore we assume an IEO to be of the form

$$Q(t) = Y(t) + g_1 Z(t) + g_2 \ , \qquad (3.12)$$

which we will use in the following. Note that we could also choose the IEO based on the momentum operators, i.e.

$$Q'(t) = P_y(t) + g_1' P_z(t) + g_2' \ ,$$

which would indeed be an adequate alternative. However it turns out that $Q'(t)$ in (3.10) leads to the same energy spacings G, thus it is equivalent to $Q(t)$. For our calculation we stick to (3.12).
Substituting $Q(t)$ into (3.10) we get

$$\left(\mathrm{i}\hbar \frac{d}{dt}\right)^2 Q(t) = \left[\left[Q(t), H_k^{①}\right], H_k^{①}\right] =$$

$$= \hbar^2 \left[\left(\Omega_{y,cz}^2 - g_1\omega_{cy}\omega_{cz}\right) Y(t) + \left(-\omega_{cy}\omega_{cz} + g_1\Omega_{z,cy}^2\right) Z(t) + \frac{\hbar k}{m}\left(g_1\omega_y - \omega_{cz}\right)\right] =$$

$$= \hbar^2 \left(\Omega_{y,cz}^2 - g_1\omega_{cy}\omega_{cz}\right) \left[Y(t) + \left(\frac{-\omega_{cy}\omega_{cz} + g_1\Omega_{z,cy}^2}{\Omega_{y,cz}^2 - g_1\omega_{cy}\omega_{cz}}\right) Z(t) + \left(\frac{\hbar k}{m}\frac{g_1\omega_y - \omega_{cz}}{\Omega_{y,cz}^2 - g_1\omega_{cy}\omega_{cz}}\right)\right] =$$

$$\stackrel{!}{=} G^2 \left[Y(t) + g_1 Z(t) + g_2\right] \ .$$

[2] Note that in this chapter we will suppress the subscript "H" for convenience. An operator is said to be in the Heisenberg picture if it is presented as a function of time, e.g. $A(t)$.

This implies a quadratic equation for g_1 with its solutions

$$g_1 = \frac{\Omega_{y,cz}^2 - \Omega_{z,cy}^2}{2\omega_{cy}\omega_{cz}} \pm \sqrt{1 + \left(\frac{\Omega_{y,cz}^2 - \Omega_{z,cy}^2}{2\omega_{cy}\omega_{cz}}\right)^2} \ .$$

Hence we have

$$G^2 = \hbar^2\left(\Omega_{y,cz}^2 - g_1\omega_{cy}\omega_{cz}\right) = \frac{\hbar^2}{2}\left(\Omega_{y,cz}^2 + \Omega_{z,cy}^2 \pm \sqrt{\left(\Omega_{y,cz}^2 - \Omega_{z,cy}^2\right)^2 + 4\,\omega_{cy}^2\omega_{cz}^2}\right) \ .$$

To put it in a nutshell, the ansatz (3.12) gave rise to two different IEOs with two energy spacings G_+ and G_-. We argued above (p. 20) that the decoupled system will consist of harmonic oscillators again, thus the k-independent eigenenergy levels of system ① read

$$E_{n,n'} = \hbar\omega_-^{①}\left(n + \frac{1}{2}\right) + \hbar\omega_+^{①}\left(n' + \frac{1}{2}\right) \ ,$$

where

$$\begin{aligned} \omega_-^{①} &= \frac{1}{\hbar}G_- = \sqrt{\frac{1}{2}\left(\Omega_{y,cz}^2 + \Omega_{z,cy}^2\right) - \frac{1}{2}\sqrt{\left(\Omega_{y,cz}^2 - \Omega_{z,cy}^2\right)^2 + 4\,\omega_{cy}^2\omega_{cz}^2}} \ , \\ \omega_+^{①} &= \frac{1}{\hbar}G_+ = \sqrt{\frac{1}{2}\left(\Omega_{y,cz}^2 + \Omega_{z,cy}^2\right) + \frac{1}{2}\sqrt{\left(\Omega_{y,cz}^2 - \Omega_{z,cy}^2\right)^2 + 4\,\omega_{cy}^2\omega_{cz}^2}} \ . \end{aligned} \tag{3.13}$$

These frequencies yield information about the diamagnetic shift $\omega_z \to \omega_+^{①}$ and first evidence about in-plane orbital effects $\omega_y \to \omega_-^{①}$ of a magnetic field perpendicular to the direction of transport in an electron waveguide or Hall bar.

② In this system, where the in-plane component of the magnetic field is parallel to the direction of transport (x-direction), the Hamiltonian is given by

$$\begin{aligned} H_k^{②} = &\frac{P_y^2}{2m} + \frac{1}{2}m\Omega_{y,cx,cz}^2 Y^2 - \hbar k\omega_{cz}Y + \\ &+ \frac{P_z^2}{2m} + \frac{1}{2}m\omega_z^2 Z^2 + \omega_{cx}YP_z + \frac{\hbar^2k^2}{2m} \end{aligned} \qquad \text{(same as 3.5)}$$

which is somewhat more complicated to handle due to the momentum-position coupling as we will see later. However it is as simple to find the k-independent energy eigenvalues as it is for system ① if we make use of the IEO method. This is what we will do in the following.

To get an idea how an IEO of $H_k^{②}$ could look like, we start calculating basic commutation relations as we did in the previous case. We get

$$\begin{aligned}
\left[Y(t), H_k^{②}\right] &= +\mathrm{i}\hbar\,\frac{1}{m}P_y(t)\ , \\
\left[Z(t), H_k^{②}\right] &= +\mathrm{i}\hbar\left(\frac{1}{m}P_z(t) + \omega_{cx}Y(t)\right)\ , \\
\left[P_y(t), H_k^{②}\right] &= -\mathrm{i}\hbar\left(m\,\Omega_{y,cx,cz}^2\,Y(t) - \hbar k\omega_{cz} + \omega_{cx}\,P_z(t)\right)\ , \\
\left[P_z(t), H_k^{②}\right] &= -\mathrm{i}\hbar\, m\omega_z^2 Z(t)\ .
\end{aligned}$$

Hence we assume that an IEO should look like

$$Q(t) = Y(t) + g_1 P_z(t) + g_2\ , \tag{3.14}$$

or like

$$Q'(t) = P_y(t) + g_1' Z(t) + g_2'\ .$$

It can be shown that both IEOs lead to the same energy spacings and we will use (3.14) for ongoing calculations.
Substituting $Q(t)$ into (3.10) we get

$$\left(\mathrm{i}\hbar\frac{d}{dt}\right)^2 Q(t) = \left[\left[Q(t), H_k^{②}\right], H_k^{②}\right] =$$

$$= \hbar^2\left[\left(\Omega_{y,cx,cz}^2 + g_1 m\omega_z^2\omega_{xc}\right)Y(t) + \left(\frac{1}{m}\omega_{cx} + g_1\Omega_{y,cx,cz}^2\right)P_z(t) - \frac{\hbar k}{m}\,\omega_{cz}\right] =$$

$$= \hbar^2\left(\Omega_{y,cx,cz}^2 + g_1 m\omega_z^2\omega_{xc}\right)\left[Y(t) + \left(\frac{\omega_{cx} + g_1 m\Omega_{y,cx,cz}^2}{m\Omega_{y,cx,cz}^2 + g_1 m^2\omega_z^2\omega_{xc}}\right)P_z(t) + \right.$$

$$\left. + \left(\frac{\hbar k}{m}\,\frac{-\omega_{cz}}{\Omega_{y,cx,cz}^2 + g_1 m\omega_z^2\omega_{xc}}\right)\right] \stackrel{!}{=} G^2\left[Y(t) + g_1 P_z(t) + g_2\right]\ .$$

By comparing the coefficients we get a quadratic equation for g_1, thus

$$g_1 = \frac{\Omega_{y,cx,cz}^2 - \omega_z^2}{2m\omega_{cx}\omega_z^2} \pm \sqrt{\frac{1}{m^2\omega_z^2} + \left(\frac{\Omega_{y,cx,cz}^2 - \omega_z^2}{2m\omega_{cx}\omega_z^2}\right)^2}$$

and therefore

$$G^2 = \hbar^2\left(\Omega_{y,cx,cz}^2 + g_1 m\omega_z^2\omega_{cx}\right) = \frac{\hbar^2}{2}\left(\Omega_{y,cx,cz}^2 + \omega_z^2 \pm \sqrt{\left(\Omega_{y,cx,cz}^2 - \omega_z^2\right)^2 + 4\omega_{cx}^2\omega_z^2}\right)\ .$$

We conclude that by choosing the ansatz (3.14) we also get two IEOs with energy differences G_+ and G_- respectively. We assumed the k-independent eigenenergies of system ② to be harmonic oscillator levels, therefore they read

$$E_{n,n'} = \hbar\omega_-^{②}\left(n+\frac{1}{2}\right) + \hbar\omega_+^{②}\left(n'+\frac{1}{2}\right) \ ,$$

with the frequencies given by

$$\begin{aligned} \omega_-^{②} &= \frac{1}{\hbar}G_- = \sqrt{\frac{1}{2}\left(\Omega_{y,cx,cz}^2+\omega_z^2\right) - \frac{1}{2}\sqrt{\left(\Omega_{y,cx,cz}^2-\omega_z^2\right)^2+4\,\omega_{cx}^2\omega_z^2}} \ , \\ \omega_+^{②} &= \frac{1}{\hbar}G_+ = \sqrt{\frac{1}{2}\left(\Omega_{y,cx,cz}^2+\omega_z^2\right) + \frac{1}{2}\sqrt{\left(\Omega_{y,cx,cz}^2-\omega_z^2\right)^2+4\,\omega_{cx}^2\omega_z^2}} \ . \end{aligned} \tag{3.15}$$

These are the formulas that possess information about the diamagnetic shift $\omega_z \to \omega_+^{②}$ and some in-plane orbital effects $\omega_y \to \omega_-^{②}$ that a magnetic field with its in-plane component along the direction of transport generates.

Parenthesis: General Solution for Arbitrary Orientations As mentioned before, one can also derive the eigenenergy levels of a quantum wire in an arbitrarily orientated magnetic field with the help of the IEO method. Once we merge system ① and ② and follow the same procedure as above, we find that the IEO must depend on all operators. Thus, we insert the ansatz

$$Q(t) = Y + g_1P_y + g_2Z + g_3P_z + g_4$$

into equation (3.10) and obtain the MEFs

$$\omega_\pm = \sqrt{\frac{1}{2}\sum_{\substack{i=y,z,\\ cx,cy,cz}}\omega_i^2 \pm \frac{1}{2}\sqrt{\sum_{\substack{i,j=y,z,\\ cx,cy,cz}}\omega_i^2\omega_j^2 - 4\left(\omega_y^2\omega_{cy}^2+\omega_z^2\omega_{cz}^2+\omega_y^2\omega_z^2\right)}}$$

in their most general form. Nevertheless, we stick in the following to the physically most important cases described by ① and ② which yield best insight into all important features of the orbital effects due to transverse magnetic fields.

Why "k-independent" eigenenergies? Let us dedicate a few lines to face the question why we have always stressed that the IEO method did not give us any k-dependence of the eigenenergies of the systems ① and ②. First, since we have used the formal transformation (3.2) of the Hamiltonian H^{3D} (3.1), k lost its operator

character. As a scalar, it commutes with any operator, particularly with all terms in H_k, so it cannot satisfy the Heisenberg equation of motion (3.7) which is essential for the IEO method. The term $\frac{\hbar^2 k^2}{2m}$ drops out automatically. Second, the k-dependent linear terms in $H_k^{①}$ and $H_k^{②}$ shift the parabolas in real space but do not alter the frequencies $\Omega_{y,cz}$, $\Omega_{z,cy}$ or $\Omega_{y,cx,cz}$, ω_z. It follows that the k-dependencies of these terms result in a constant term proportional to k^2 which drops out as well. Third, since the conductor is assumed to be infinite in x-direction, the energy eigenvalues lack discretization and IEO would not be applicable for this coordinate anyway.
As a consequence, the eigenenergies calculated by the IEO method cannot account for any k-dependence. Nevertheless it is present and will be derived in Chapter 3.2 when we discuss the transformations to decouple the systems in detail. We will find that the eigenenergies of both systems can be written as

$$E_{n,n'}(k) = \hbar\omega_- \left(n + \frac{1}{2}\right) + \hbar\omega_+ \left(n' + \frac{1}{2}\right) + \frac{\hbar^2 k^2}{2\mu} \ ,$$

with corresponding frequencies and effective masses μ for the two systems respectively.

3.1.3 Discussion and Summary

On the previous pages we have used

$$H^{3\mathrm{D}} = \frac{\left(\vec{P} + e\vec{A}\right)^2}{2m} + V_y(Y) + V_z(Z) \ , \qquad \text{(same as 3.1)}$$

with the electrostatic confinements

$$V_y(Y) = \frac{1}{2}\, m\, \omega_y^2\, Y^2 \quad , \quad V_z(Z) = \frac{1}{2}\, m\, \omega_z^2\, Z^2$$

to calculate the energy eigenvalues for a non-zero magnetic field with its in-plane component perpendicular (①) or parallel (②) to the direction of transport. Whereas for vanishing magnetic field we get the energy levels

$$E_{n,n'}(k) = \hbar\omega_y \left(n + \frac{1}{2}\right) + \hbar\omega_z \left(n' + \frac{1}{2}\right) + \frac{\hbar^2 k^2}{2m} \ ,$$

we found the eigenenergies for a finite field to be

$$E_{n,n'}(k) = \hbar\omega_- \left(n + \frac{1}{2}\right) + \hbar\omega_+ \left(n' + \frac{1}{2}\right) + \frac{\hbar^2 k^2}{2\mu} \ ,$$

with the *magneto-electric frequencies* (MEFs)

$$\omega_{-}^{①} = \sqrt{\frac{1}{2}\left(\Omega_{y,cz}^2 + \Omega_{z,cy}^2\right) - \frac{1}{2}\sqrt{\left(\Omega_{y,cz}^2 - \Omega_{z,cy}^2\right)^2 + 4\,\omega_{cy}^2\omega_{cz}^2}}\ ,$$
$$\omega_{+}^{①} = \sqrt{\frac{1}{2}\left(\Omega_{y,cz}^2 + \Omega_{z,cy}^2\right) + \frac{1}{2}\sqrt{\left(\Omega_{y,cz}^2 - \Omega_{z,cy}^2\right)^2 + 4\,\omega_{cy}^2\omega_{cz}^2}}\ , \qquad \text{(same as 3.13)}$$

$$\Omega_{y,cz} = \sqrt{\omega_y^2 + \omega_{cz}^2} \quad , \quad \Omega_{z,cy} = \sqrt{\omega_z^2 + \omega_{cy}^2} \qquad \text{(same as 3.4)}$$

for system ①, and

$$\omega_{-}^{②} = \sqrt{\frac{1}{2}\left(\Omega_{y,cx,cz}^2 + \omega_z^2\right) - \frac{1}{2}\sqrt{\left(\Omega_{y,cx,cz}^2 - \omega_z^2\right)^2 + 4\,\omega_{cx}^2\omega_z^2}}\ ,$$
$$\omega_{+}^{②} = \sqrt{\frac{1}{2}\left(\Omega_{y,cx,cz}^2 + \omega_z^2\right) + \frac{1}{2}\sqrt{\left(\Omega_{y,cx,cz}^2 - \omega_z^2\right)^2 + 4\,\omega_{cx}^2\omega_z^2}}\ , \qquad \text{(same as 3.15)}$$

$$\Omega_{y,cx,cz} = \sqrt{\omega_y^2 + \omega_{cx}^2 + \omega_{cz}^2} \qquad \text{(same as 3.6)}$$

for system ② respectively. It is obvious that the transition $\omega_z \to \omega_+$ describes the diamagnetic shift (2.7) and $\omega_y \to \omega_-$ reflects in a sense the anisotropic effective mass (2.8) which was introduced in Chapter 2. Thus the altered frequencies ω_- and ω_+ yield a quantitative generalization of the improved 2D effective mass Hamiltonian (2.13).

In this section we will show that the results of the model system in Chapter 2 can be obtained from the MEFs $\omega_\pm$ and check the validity of the anisotropic effective mass, i.e. equation (2.12). We will end this chapter with a discussion on possible anisotropies and deliver insight into the complication of calculating energy levels at very high magnetic fields.

Let us verify the MEFs by checking their limits with well-known situations, starting with the Quantum Hall Effect (QHE). The QHE of a Hall bar described by the effective mass Hamiltonian (3.1) in Landau gauge [4, 17] leads to the magneto-electric frequency $\sqrt{\omega_y^2 + \omega_{cz}^2}$ of the in-plane confinement while ω_z remains unchanged. Thus the MEFs for both systems need to converge with this result as there should not be any difference between ① and ② for zero in-plane fields.

In system ① the frequencies are given by (3.13). In the quantum Hall regime the partial cyclotron frequency ω_{cy} vanishes and the MEFs reduce to

$$\omega_{-}^{①} = \sqrt{\frac{1}{2}\left(\omega_y^2 + \omega_{cz}^2 + \omega_z^2\right) - \frac{1}{2}\sqrt{\left(\omega_y^2 + \omega_{cz}^2 - \omega_z^2\right)^2}} = \sqrt{\omega_y^2 + \omega_{cz}^2}\ ,$$
$$\omega_{+}^{①} = \sqrt{\frac{1}{2}\left(\omega_y^2 + \omega_{cz}^2 + \omega_z^2\right) + \frac{1}{2}\sqrt{\left(\omega_y^2 + \omega_{cz}^2 - \omega_z^2\right)^2}} = \omega_z$$

as expected.
In system ② the frequencies of (3.15) for $\omega_{cx} = 0$ reduce to

$$\omega_-^{②} = \sqrt{\frac{1}{2}\left(\omega_y^2 + \omega_{cz}^2 + \omega_z^2\right) - \frac{1}{2}\sqrt{\left(\omega_y^2 + \omega_{cz}^2 - \omega_z^2\right)^2}} = \sqrt{\omega_y^2 + \omega_{cz}^2}\ ,$$
$$\omega_+^{②} = \sqrt{\frac{1}{2}\left(\omega_y^2 + \omega_{cz}^2 + \omega_z^2\right) + \frac{1}{2}\sqrt{\left(\omega_y^2 + \omega_{cz}^2 - \omega_z^2\right)^2}} = \omega_z\ ,$$

which coincides with the previous result. We notice that the MEFs derived by the IEO method match for zero in-plane fields and confirm the known results from the QHE, thus fulfill validity in the limit of zero in-plane field.

Now we approach the situation of (2.5) discussed in Chapter 2, that is a pure in-plane magnetic field $\vec{B} = (B, 0, 0)$. Within the model of an infinite 2DEG we got a diamagnetic shift $\omega_z \to \sqrt{\omega_z^2 + \omega_{cx}^2}$ and an effective mass perpendicular to the $\vec{B}$-field (2.8) which gave rise to the modified frequency

$$\tilde{\omega}_y = \frac{\omega_y}{\sqrt{\eta}} = \frac{\omega_y\,\omega_z}{\sqrt{\omega_z^2 + \omega_{cx}^2}}\ . \qquad \text{(same as 2.12)}$$

Of course we need to use system ② to verify these statements.
The MEFs (3.15), with the partial cyclotron frequency $\omega_{cz} = 0$, read

$$\omega_-^{②} = \sqrt{\frac{1}{2}\left(\omega_y^2 + \omega_{cx}^2 + \omega_z^2\right) - \frac{1}{2}\sqrt{\left(\omega_y^2 + \omega_{cx}^2 - \omega_z^2\right)^2 + 4\,\omega_{cx}^2\omega_z^2}}\ ,$$
$$\omega_+^{②} = \sqrt{\frac{1}{2}\left(\omega_y^2 + \omega_{cx}^2 + \omega_z^2\right) + \frac{1}{2}\sqrt{\left(\omega_y^2 + \omega_{cx}^2 - \omega_z^2\right)^2 + 4\,\omega_{cx}^2\omega_z^2}}\ .$$

As it holds $\omega_y \ll \omega_z$ we can do a Taylor expansion in ω_y and get

$$\omega_-^{②} = \frac{\omega_y\,\omega_z}{\sqrt{{\omega_z}^2 + {\omega_{cx}}^2}} - \frac{\omega_z\,{\omega_{cx}}^2}{2\left({\omega_z}^2 + {\omega_{cx}}^2\right)^{5/2}}\,{\omega_y}^3 + O\left({\omega_y}^5\right)\ ,$$
$$\omega_+^{②} = \sqrt{{\omega_z}^2 + {\omega_{cx}}^2} + \frac{{\omega_{cx}}^2}{2\left({\omega_z}^2 + {\omega_{cx}}^2\right)^{3/2}}\,{\omega_y}^2 + O\left({\omega_y}^4\right)\ ,$$

which verifies the statement above up to higher orders in ω_y. It is obvious that the MEFs derived by the IEO method provide a better description of the diamagnetic shift and of the effects on the in-plane magneto-electric confinement in a quantum wire than the model system (2.5) of Chapter 2 which assumes an infinite 2DEG.

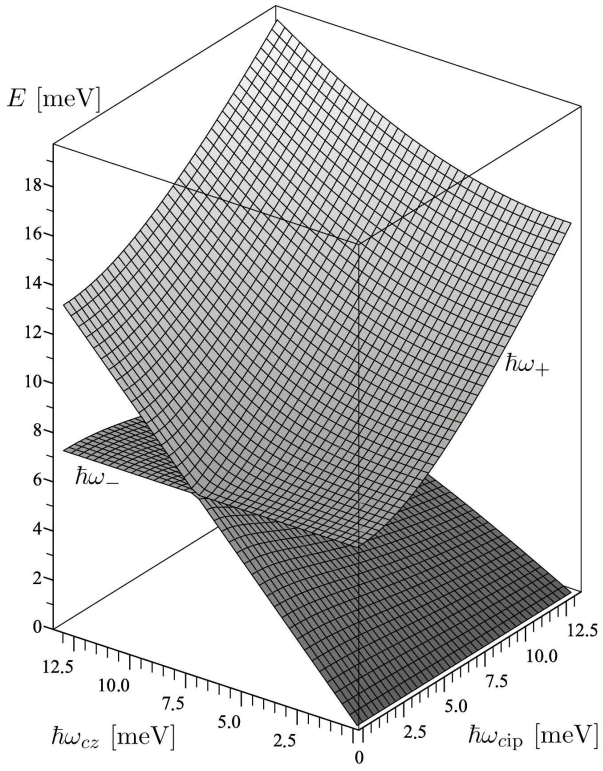

Figure 3.1: Magneto-electric frequencies of both system ① and ② for $\omega_y = 0$ and $\hbar\omega_z = 7.24\,\mathrm{meV}$. The upper area is given by $\hbar\omega_+$ and the lower lying one demonstrates $\hbar\omega_-$. Note that the planes touch only for a vanishing in-plane field.

Let us now focus on general behavior and possible anisotropies of the magneto-electric frequencies. For the limit $\omega_y \to 0$, i.e. an infinite 2DEG, the MEFs are indeed isotropic.[3] They can be rewritten as

$$\omega_\pm = \sqrt{\frac{1}{2}\left(\omega_{\mathrm{cip}}^2 + \omega_{cz}^2 + \omega_z^2\right) \pm \frac{1}{2}\sqrt{\omega_{\mathrm{cip}}^4 + \omega_{cz}^4 + \omega_z^4 + 2\left(\omega_{\mathrm{cip}}^2\omega_{cz}^2 + \omega_{\mathrm{cip}}^2\omega_z^2 - \omega_{cz}^2\omega_z^2\right)}}\,,$$

for both systems, where $\omega_{\mathrm{cip}} = \omega_{cy}$ and $\omega_{\mathrm{cip}} = \omega_{cx}$ for system ① and ② respectively. The general behavior of the MEFs in this case are visualized in Fig. 3.1. Hence for any

[3] So is the total system. Although the effective masses μ that couple with the parameter k and define the curvature of the dispersion relation, are different for system ① and system ②, they diverge for vanishing ω_y and, as a consequence, the kinetic term disappears. Explicit expressions for μ will be derived in the next chapter.

anisotropy to occur the condition $\omega_y \neq 0$ is mandatory - it is a boundary effect. This implies that for very wide electron waveguides, i.e. bulk states, the MEF and therefore the energy levels of the system are isotropic.

For narrow wires, $\omega_y \neq 0$, the system is anisotropic, i.e. the MEFs differ for an in-plane magnetic field perpendicular or parallel to the direction of transport. However since we have started with a two-dimensional electron system, we still have the condition $\omega_y \ll \omega_z$ which implies that anisotropic effects due to the confinement remain small. Nevertheless, they are discussed in Chapter 4 in detail.

The magneto-electric frequencies (3.13) (①), (3.15) (②) for the model system described by (3.1) are, in principle, valid for arbitrarily strong magnetic fields. On the other hand the calculation is based on the effective mass Hamiltonian, which is an approximation itself. We remind that for both large energies and high magnetic fields we have to take non-parabolicity of the band structure and spatial shift of the states into account, that is we have the same problems as described in Chapter 2. The MEFs provide an approximation for diamagnetic shift and in-plane magneto-electric confinement, but in order to calculate energy levels for very high magnetic fields particularly with a dominant Zeeman term, one would need expressions that describe the energy and field dependence of the effective mass and Landé factor. We have already stated that they are hard to find and we would rather refer to [6, 7, 8, 16, 23, 29, 38, 39, 48] for further details. Nevertheless we will close this chapter with a model calculation of the energy levels that correspond to the setup used by W. Pan et. al. in Ref. [26], a system with a very high in-plane field.

The system of interest is a 5 mm wide Hall bar which is based on an $Al_{0.24}Ga_{0.76}As$ / GaAs / $Al_{0.24}Ga_{0.76}As$ quantum well. Due to the large width of the system, we expect boundary effects to be negligible and use $\omega_y = 0$, i.e. the system is isotropic and we can use either ① or ②. We will describe the magnetic field in terms of the tilt angle $\Theta = \measuredangle(\hat{z}, \vec{B})$, thus we have the relations

$$|\vec{B}| = \frac{B_z}{\cos(\Theta)} = \frac{B_{\mathrm{ip}}}{\sin(\Theta)} \ .$$

The setup was used to investigate transport in the integer quantum Hall regime ($B_z \sim 2.9\,\mathrm{T}$) with a very strong in-plane field ($B_{\mathrm{ip}} \sim 25\,\mathrm{T}$). In our calculations the quantum well is approximated by a harmonic confinement with $\hbar\omega_z = 7.24\,\mathrm{meV}$. The bulk

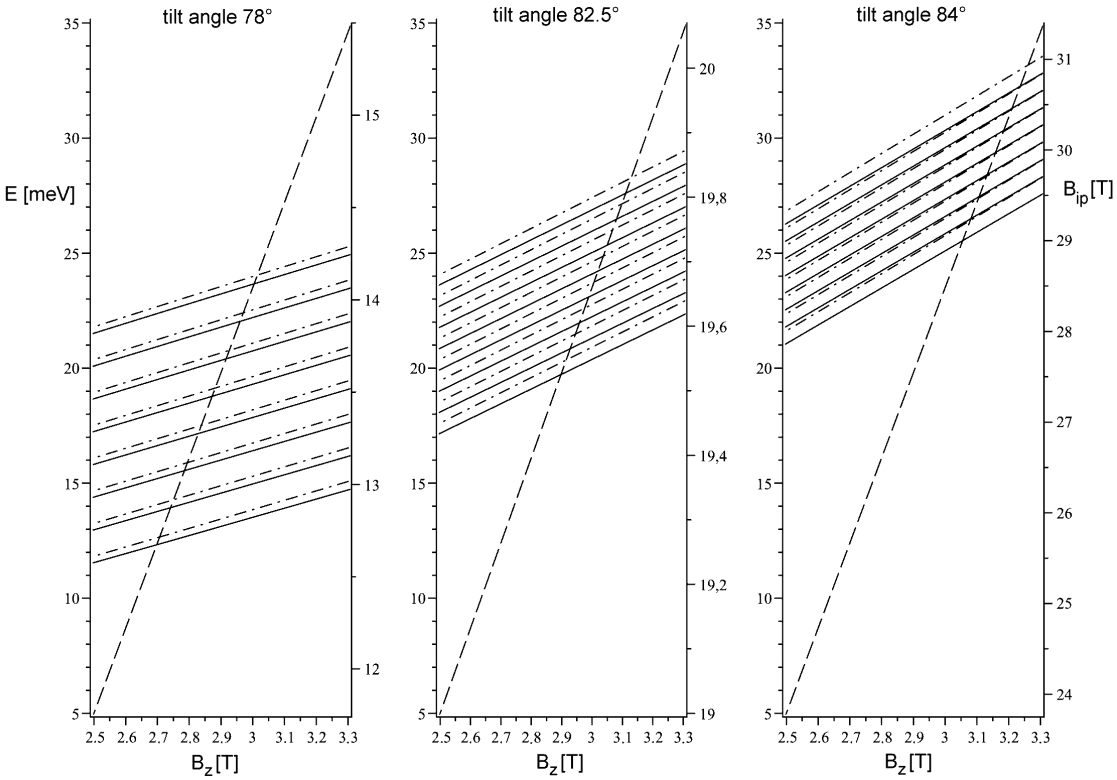

Figure 3.2: Energy levels of an infinitely wide (Al)GaAs Hall bar with $g^* = -0.4$ and $m^* = 0.067\,m_\mathrm{e}$. The spin-polarized levels (solid and dash-dot lines) cross for $B_z \approx 2.9\,\mathrm{T}$ and $B_\mathrm{ip} \approx 23\,\mathrm{T}$ (i.e. $\Theta > 83°$). The dashed lines indicate the in-plane magnetic field dependent on the perpendicular field for the three tilt angles.

values of g-factor and effective mass for GaAs read

$$g_{(\mathrm{GaAs})} = -0.44 \quad , \quad m_{(\mathrm{GaAs})} = 0.067\,m_\mathrm{e} \; .$$

For the g-factor and effective mass in the current situation we assume to have

$$g^* = -0.4 \quad , \quad m^* = 0.067\,m_\mathrm{e} \; ,$$

with a slightly different Landé factor due to the effects discussed in Chapter 2 [7, 29, 38]. The author stated that in this regime the spin-polarized bands of neighboring Landau levels may cross and also eigenenergies of different subbands may coincide. With the parameters given above we can verify a possible crossing of spin-polarized levels (Fig.

3.2) for the given magnetic field and tilt angle, but a coincidence of eigenenergies originating from different subbands seems to be impossible[4] due to a large diamagnetic shift. Therefore it seems conceivable that transport anisotropies, as reported in Ref. [26], may have the origin in band crossing of neighboring Zeeman split Landau levels. We will pick up this idea again in Chapter 3.3 when we discuss the effect of BR-SOI at the crossing, but we will find that this contribution is isotropic in the given setup since $\omega_y = 0$, thus this experiment cannot be explained by our results.
For now, let us investigate Fig. 3.2 in more detail. The k-independent eigenenergies

$$E_{n,n'} = \hbar\omega_- \left(n + \frac{1}{2}\right) + \hbar\omega_+ \left(n' + \frac{1}{2}\right) \pm \frac{g^*}{2}\mu_\mathrm{B}|\vec{B}|$$

are displayed for different tilt angles dependent on the perpendicular field. Since, for fixed Θ, changing B_z also changes the in-plane component linearly, we can also plot B_ip which is given by the dashed lines and belongs to the scalings of the right axes each. Note that the plots only show the first eight Landau levels of the lowest subband. Since we have $\omega_- \ll \omega_+$, the levels of the second subband are beyond the scaling of these graphs. This means that this initial quasi-2DEG (comp. Fig. 2.3) becomes two-dimensional due to the diamagnetic shift $\omega_z \to \omega_+$ of the in-plane magnetic field. With increasing tilt angle the Zeeman split Landau levels start to overlap and the crossing at a perpendicular field of $B_z \approx 2.9\,\mathrm{T}$ happens for $\Theta = 83°$, that is an in-plane field of $B_\mathrm{ip} \approx 23\,\mathrm{T}$. Higher order mixing may occur beyond this for larger tilt angles. Note, however, that the parameters g^* and m^* were held constant for all plots of Fig. 3.2 and one would need to consider different values for fields significantly different to 25 T.

[4] Recall that we are working with an one-particle picture that neglects electron-electron interaction.

3.2 Orbital Effects

In this chapter we are interested in the explicit transformations that decouple the systems ① and ②. Once we know how the eigenstates change due to the tilted magnetic field, we get insight into the orbital effects. The derived transformations can then also be applied to spin-orbit coupling terms to get an idea of magnetic impact on these.
In the first section we will deal with system ① and derive the MEFs and the explicit transformation for a magnetic field perpendicular to the direction of transport with the help of archetype 2 (Appendix A). In Section 3.2.2 we will repeat this but with system ② using archetype 3 (Appendix A). Subsequent to this we will dedicate one section to show that the derived MEFs match with the MEFs obtained by the IEO method and close this chapter with a discussion on the transformations.

3.2.1 Decoupling System ①

Our starting point is the Hamiltonian

$$\begin{aligned} H_k^{①} &= \frac{P_y^2}{2m} + \frac{1}{2}m\Omega_{y,cz}^2 Y^2 - \hbar k\omega_{cz} Y + \\ &+ \frac{P_z^2}{2m} + \frac{1}{2}m\Omega_{z,cy}^2 Z^2 + \hbar k\omega_y Z - m\omega_{cy}\omega_{cz} Y Z + \frac{\hbar^2 k^2}{2m} \end{aligned} \qquad \text{(same as 3.3)}$$

which needs to be transformed in two steps using the methods given in Appendix A. The first substitution implies a shift of the x-axis which is dependent on the wave vector k. The new position operators read

$$\begin{aligned} Y' &:= Y - \frac{\omega_{cz}\,\omega_z^2}{\omega_{cy}^2\,\omega_y^2 + \omega_{cz}^2\,\omega_z^2 + \omega_y^2\,\omega_z^2}\,\frac{\hbar k}{m}\,, \\ Z' &:= Z + \frac{\omega_{cy}\,\omega_y^2}{\omega_{cy}^2\,\omega_y^2 + \omega_{cz}^2\,\omega_z^2 + \omega_y^2\,\omega_z^2}\,\frac{\hbar k}{m}\,, \end{aligned} \qquad (3.16)$$

and the Hamiltonian $H_k^{①}$ in the shifted coordinate system can be written as

$$H_k^{①} = \frac{P_{y'}^2}{2m} + \frac{1}{2}\,m\,\Omega_{y,cz}^2\,Y'^2 + \frac{P_{z'}^2}{2m} + \frac{1}{2}\,m\,\Omega_{z,cy}^2\,Z'^2 + \gamma\,Y'Z' + \frac{\hbar^2 k^2}{2\mu}\,,$$

where we used the transformed frequencies defined in (3.4). The coupling strength is given by $\gamma = -m\,\omega_{cy}\,\omega_{cz}$ and the effective mass μ, which describes the effect of the magnetic field on transport properties of the system, is

$$\mu := m\left(1 + \frac{\omega_{cz}^2}{\omega_y^2} + \frac{\omega_{cy}^2}{\omega_z^2}\right)\,. \qquad (3.17)$$

The operators Y' and Z' are still coupled, thus the second step will be to perform the transformation of archetype 1. This is a rotation of the angle $\theta = arctan(-\xi)$ around the shifted x-axis, with ξ being an essential, although k-independent parameter of the transformation. It holds

$$\xi = \Xi \pm \sqrt{1+\Xi^2} \qquad \text{with} \qquad \Xi = \frac{\Omega_{y,cz}^2 - \Omega_{z,cy}^2}{2\,\omega_{cy}\,\omega_{cz}} \tag{3.18}$$

and the rotated operators are given by

$$\tilde{Y} = N\left(Y' + \xi Z'\right) \quad , \quad \tilde{Z} = N\left(-\xi Y' + Z'\right) \quad , \quad N = \frac{1}{\sqrt{1+\xi^2}}\ . \tag{3.19}$$

This leaves us with the final form of the Hamiltonian (3.3)

$$H_k^{①} = \frac{P_{\tilde{y}}^2}{2m} + \frac{1}{2}\,m\,\omega_{\tilde{y}}^{①\,2}\,\tilde{Y}^2 + \frac{P_{\tilde{z}}^2}{2m} + \frac{1}{2}\,m\,\omega_{\tilde{z}}^{①\,2}\,\tilde{Z}^2 + \frac{\hbar^2 k^2}{2\mu}\ , \tag{3.20}$$

which consists out of two independent harmonic oscillators and a k-dependent term describing the dispersion relation of free electrons with an effective mass μ (3.17).
The eigenenergies of the system read

$$E_{n,n'}(k) = \hbar\omega_{\tilde{y}}^{①}\left(n+\frac{1}{2}\right) + \hbar\omega_{\tilde{z}}^{①}\left(n'+\frac{1}{2}\right) + \frac{\hbar^2 k^2}{2\mu}\ , \tag{3.21}$$

which verifies the statement on page 27. The MEFs are found to be

$$\begin{aligned} \omega_{\tilde{y}}^{①} &= \sqrt{N^2\left(\xi^2\Omega_{z,cy}^2 + \Omega_{y,cz}^2 + \frac{2\gamma\xi}{m}\right)}\ , \\ \omega_{\tilde{z}}^{①} &= \sqrt{N^2\left(\Omega_{z,cy}^2 + \xi^2\Omega_{y,cz}^2 - \frac{2\gamma\xi}{m}\right)}\ . \end{aligned} \tag{3.22}$$

We will prove later that (3.22) is indeed equivalent to the MEFs $\omega_\pm$ derived by the IEO method (3.13).

3.2.2 Decoupling System ②

The Hamiltonian of interest in this case reads

$$H_k^{②} = \frac{P_y^2}{2m} + \frac{1}{2}m\Omega_{y,cx,cz}^2 Y^2 - \hbar k\omega_{cz} Y + \frac{P_z^2}{2m} + \frac{1}{2}m\omega_z^2 Z^2 + \omega_{cx} Y P_z + \frac{\hbar^2 k^2}{2m} \quad \text{(same as 3.5)}$$

with the characteristic momentum-position coupling. To deal with this problem one needs to perform the transformation of archetype 3 given in Appendix A, that is we rewrite (3.5) in terms of the effective momentum $\bar{Z}$ and effective position $\bar{P}_z$ operators which we define

$$\bar{P}_z := \frac{P_z}{m\omega_z} \quad , \quad \bar{Z} := -m\omega_z\, Z \ . \tag{3.23}$$

Note that we could also choose the sign convention

$$\bar{P}_z := -\frac{P_z}{m\omega_z} \quad , \quad \bar{Z} := m\omega_z\, Z$$

and would obtain the same result. In the following we will stick to the definitions of (3.23).
The Hamiltonian reads

$$H_k^{②} = \frac{P_y^2}{2m} + \frac{1}{2}m\Omega_{y,cx,cz}^2 Y^2 - \hbar k\omega_{cz} Y + \frac{\bar{Z}^2}{2m} + \frac{1}{2}m\omega_z^2\bar{P}_z^2 + m\omega_z\omega_{cx} Y\bar{P}_z + \frac{\hbar^2k^2}{2m} \tag{3.24}$$

and can be transformed in the same way as we handled $H_k^{①}$ in Section 3.2.1 using the method of archetype 2. The (effective) position operators are first shifted by a k-dependent summand. They read[5]

$$\begin{aligned} Y' &= Y - \frac{\omega_{cz}}{\omega_y^2 + \omega_{cz}^2}\frac{\hbar k}{m} \ , \\ \bar{P}_{z'} &= \bar{P}_z + \frac{\omega_{cx}\,\omega_{cz}}{\omega_{cz}^2\,\omega_z + \omega_y^2\,\omega_z}\frac{\hbar k}{m} \ , \end{aligned} \tag{3.25}$$

and the Hamiltonian (3.24) becomes

$$H_k^{②} = \frac{P_{y'}^2}{2m} + \frac{1}{2}m\Omega_{y,cx,cz}^2 Y'^2 + \frac{\bar{Z}'^2}{2m} + \frac{1}{2}m\omega_z^2\bar{P}_{z'}^2 + m\omega_z\omega_{cx} Y'\bar{P}_{z'} + \frac{\hbar^2k^2}{2\mu} \ ,$$

where $\Omega_{y,cx,cz} = \sqrt{\omega_y^2 + \omega_{cx}^2 + \omega_{cz}^2}$ was defined in (3.6). The effective mass μ is given by

$$\mu := m\left(1 + \frac{\omega_{cz}^2}{\omega_y^2}\right) \ . \tag{3.26}$$

The operators are still coupled, thus the next step will be to perform the transformation of archetype 1 (Appendix A). This is a rotation of the angle $\theta = arctan(-\xi)$ around the shifted x-axis, with the k-independent parameter ξ. We have

$$\xi = \Xi \pm \sqrt{1 + \Xi^2} \qquad \text{with} \qquad \Xi = -\frac{\Omega_{y,cx,cz}^2 - \omega_z^2}{2\,\omega_{cx}\,\omega_z} \tag{3.27}$$

[5] Note that it holds $P_{y'} = P_y$ and $\bar{Z}' = \bar{Z}$.

and the rotated operators are given by

$$\begin{aligned} \text{(Effective) position operators: } \bar{P}_{\tilde{z}} &= N\left(\bar{P}_{z'} - \xi Y'\right) \ , \ \tilde{Y} = N\left(\xi \bar{P}_{z'} + Y'\right) \\ \text{(Effective) momentum operators: } \tilde{\bar{Z}} &= N\left(\bar{Z}' - \xi P_{y'}\right) \ , \ P_{\tilde{y}} = N\left(\xi \bar{Z}' + P_{y'}\right) \\ \text{with } N &= \frac{1}{\sqrt{1+\xi^2}} \ . \end{aligned} \tag{3.28}$$

This leaves us with the decoupled version of Hamiltonian (3.24)

$$\begin{aligned} H_k^{②} &= \frac{P_{\tilde{y}}^2}{2m} + \frac{1}{2}\, m\, \omega_{\tilde{y}}^{②\,2}\, \tilde{Y}^2 + \frac{\tilde{\bar{Z}}^2}{2\, m} + \frac{1}{2}\, m\, \omega_{\tilde{z}}^{②\,2}\, \bar{P}_{\tilde{z}}^2 + \frac{\hbar^2 k^2}{2\mu} = \\ &= \frac{P_{\tilde{y}}^2}{2m} + \frac{1}{2}\, m\, \omega_{\tilde{y}}^{②\,2}\, \tilde{Y}^2 + \frac{P_{\tilde{z}}^2}{2m_{\tilde{z}}} + \frac{1}{2} m_{\tilde{z}} \omega_{\tilde{z}}^{②\,2}\, \tilde{Z}^2 + \frac{\hbar^2 k^2}{2\mu} \end{aligned} \tag{3.29}$$

which consists out of two independent harmonic oscillators and a k-dependent term describing the dispersion relation of free electrons with an effective mass μ (3.26). Note the appearance of an effective mass for the $\tilde{z}$-coordinate

$$m_{\tilde{z}} := m\, \frac{\omega_z^2}{\omega_{\tilde{z}}^{②\,2}} \tag{3.30}$$

which, however, does not become manifest in the energy levels

$$E_{n,n'}(k) = \hbar\omega_{\tilde{y}}^{②}\left(n + \frac{1}{2}\right) + \hbar\omega_{\tilde{z}}^{②}\left(n' + \frac{1}{2}\right) + \frac{\hbar^2 k^2}{2\mu} \ , \tag{3.31}$$

since the mass of the harmonic oscillator does not appear explicitly. The MEFs are given by

$$\begin{aligned} \omega_{\tilde{y}}^{②} &= \sqrt{N^2\left(\xi^2\omega_z^2 + \Omega_{y,cx,cz}^2 + \frac{2\gamma\xi}{m}\right)} \ , \\ \omega_{\tilde{z}}^{②} &= \sqrt{N^2\left(\omega_z^2 + \xi^2\Omega_{y,cx,cz}^2 - \frac{2\gamma\xi}{m}\right)} \ , \end{aligned} \tag{3.32}$$

where $\gamma = m\omega_{cx}\omega_z$ is the coupling strength (comp. (3.24)).

3.2.3 Comparing with IEO Results

We still owe the connection between the MEFs (3.13) and (3.22) of system ① and (3.15) and (3.32) of system ②. The problem that we have to face arises due to the fact that the MEFs derived by the explicit transformation do not necessarily need to fulfill

the condition $\omega_{\tilde{y}} \leqq \omega_{\tilde{z}}$. This is because we define the rotation such as the system is decoupled without knowing which frequency is smaller whereas the IEO method gave us constant energy spacings which we can name ω_- for the smaller and ω_+ for the larger frequency without knowing the transformation. We would need to make the choice of the explicit transformation dependent on the magnetic field orientation to have the frequencies ordered with respect to their magnitude, i.e. $\omega_{\tilde{y}} \leqq \omega_{\tilde{z}}$, in order to have the general allocation $\omega_{\tilde{y}} = \omega_-$ and $\omega_{\tilde{z}} = \omega_+$. Alternatively we could abandon this fixed allocation and use $\omega_{\tilde{y}}$ and $\omega_{\tilde{z}}$ as they appear through the transformation, i.e. we cannot say for all magnetic field orientations whether $\omega_{\tilde{y}}$ or $\omega_{\tilde{z}}$ is bigger because this can flip. In the following we will need the explicit transformation, thus we have to distinguish the cases $\omega_{\tilde{y}} < \omega_{\tilde{z}}$ from what follows $\omega_{\tilde{y}} = \omega_-$ and $\omega_{\tilde{z}} = \omega_+$, and $\omega_{\tilde{y}} > \omega_{\tilde{z}}$ from what follows $\omega_{\tilde{y}} = \omega_+$ and $\omega_{\tilde{z}} = \omega_-$. The question is: Under what conditions which one of the MEFs $\omega_{\tilde{y}}$, $\omega_{\tilde{z}}$ is bigger?

For the following considerations, we need to choose a transformation, that is we need to pick the sign in ξ (3.18), (3.27). It can be shown that both possibilities lead to the same physical results, thus the choice is a matter of taste. We use the minus sign and write

$$\xi_- := \xi = \Xi - \sqrt{1+\Xi^2}$$

which will be fixed for all calculations. Note that it holds

$$\xi_- = -\xi_+^{-1} \qquad \text{and} \qquad \xi_- < 0 \quad \forall\, \Xi$$

with $\xi_+ := \Xi + \sqrt{1+\Xi^2}$.

① We have

$$\begin{aligned}
\omega_{\tilde{y}}^{①} &= \sqrt{N^2\left(\xi^2\Omega_{z,cy}^2 + \Omega_{y,cz}^2 + \frac{2\gamma\xi}{m}\right)} = \\
&= \sqrt{\frac{1}{\xi_- + \xi_-^{-1}}\left(\xi_-\Omega_{z,cy}^2 + \xi_-^{-1}\Omega_{y,cz}^2 + \frac{2\gamma}{m}\right)} = \\
&= \sqrt{\frac{1}{2\sqrt{1+\Xi^2}}\left(-\xi_-\Omega_{z,cy}^2 + \xi_+\Omega_{y,cz}^2 + 2\omega_{cy}\omega_{cz}\right)} = \\
&= \sqrt{\frac{1}{2}\left(\Omega_{y,cz}^2 + \Omega_{z,cy}^2\right) + \frac{1}{2}\left(\Omega_{y,cz}^2 - \Omega_{z,cy}^2\right)\frac{\Xi}{\sqrt{1+\Xi^2}} + \frac{\omega_{cy}\omega_{cz}}{\sqrt{1+\Xi^2}}} = \\
&= \sqrt{\frac{1}{2}\left(\Omega_{y,cz}^2 + \Omega_{z,cy}^2\right) + \left(\Xi^2\,\omega_{cy}\omega_{cz} + \omega_{cy}\omega_{cz}\right)\frac{1}{\sqrt{1+\Xi^2}}} =
\end{aligned} \tag{3.33}$$

$$= \sqrt{\frac{1}{2}\left(\Omega_{y,cz}^2 + \Omega_{z,cy}^2\right) + \frac{1}{2}\sqrt{\left(\Omega_{y,cz}^2 - \Omega_{z,cy}^2\right)^2 + 4\omega_{cy}^2\omega_{cz}^2}\ \frac{\omega_{cy}\omega_{cz}}{\sqrt{\omega_{cy}^2\omega_{cz}^2}}} =$$

$$= \sqrt{\frac{1}{2}\left(\Omega_{y,cz}^2 + \Omega_{z,cy}^2\right) + \mathrm{sign}(\omega_{cy}\omega_{cz})\ \frac{1}{2}\sqrt{\left(\Omega_{y,cz}^2 - \Omega_{z,cy}^2\right)^2 + 4\omega_{cy}^2\omega_{cz}^2}} =$$

$$= \begin{cases} \omega_-^{①} & \text{if} \quad \mathrm{sign}(\omega_{cy}\omega_{cz}) = -1 \\ \omega_+^{①} & \text{if} \quad \mathrm{sign}(\omega_{cy}\omega_{cz}) = +1 \end{cases}.$$

Similarly we get

$$\omega_{\tilde{z}}^{①} = \sqrt{\frac{1}{2}\left(\Omega_{y,cz}^2 + \Omega_{z,cy}^2\right) - \mathrm{sign}(\omega_{cy}\omega_{cz})\ \frac{1}{2}\sqrt{\left(\Omega_{y,cz}^2 - \Omega_{z,cy}^2\right)^2 + 4\omega_{cy}^2\omega_{cz}^2}} =$$

$$= \begin{cases} \omega_+^{①} & \text{if} \quad \mathrm{sign}(\omega_{cy}\omega_{cz}) = -1 \\ \omega_-^{①} & \text{if} \quad \mathrm{sign}(\omega_{cy}\omega_{cz}) = +1 \end{cases}, \tag{3.34}$$

where $\Omega_{y,cz}$ and $\Omega_{z,cy}$ are given in (3.4).

② For this system, using an analog derivation, we find

$$\omega_{\tilde{y}}^{②} = \sqrt{\frac{1}{2}\left(\Omega_{y,cx,cz}^2 + \omega_z^2\right) - \mathrm{sign}(\omega_{cx})\ \frac{1}{2}\sqrt{\left(\Omega_{y,cx,cz}^2 - \omega_z^2\right)^2 + 4\omega_{cx}^2\omega_z^2}} =$$

$$= \begin{cases} \omega_-^{②} & \text{if} \quad \mathrm{sign}(\omega_{cx}) = +1 \\ \omega_+^{②} & \text{if} \quad \mathrm{sign}(\omega_{cx}) = -1 \end{cases} \tag{3.35}$$

and

$$\omega_{\tilde{z}}^{②} = \sqrt{\frac{1}{2}\left(\Omega_{y,cx,cz}^2 + \omega_z^2\right) + \mathrm{sign}(\omega_{cx})\ \frac{1}{2}\sqrt{\left(\Omega_{y,cx,cz}^2 - \omega_z^2\right)^2 + 4\omega_{cx}^2\omega_z^2}} =$$

$$= \begin{cases} \omega_+^{②} & \text{if} \quad \mathrm{sign}(\omega_{cx}) = +1 \\ \omega_-^{②} & \text{if} \quad \mathrm{sign}(\omega_{cx}) = -1 \end{cases}, \tag{3.36}$$

where $\Omega_{y,cx,cz}$ is given in (3.6).

This gives us the connection between the MEFs of the IEO method $\omega_\pm$ and the MEFs of the explicit transformation $\omega_{\tilde{y}/\tilde{z}}$ and generalizes the previous results. This will prove useful when analyzing the magnetic effects on BR-SOI as we will see later.

3.2.4 Discussion

We know the eigenenergies of both systems and also the transformations that decouple the Hamiltonians. In order to get an intuitive insight into the effetcs of magnetic field

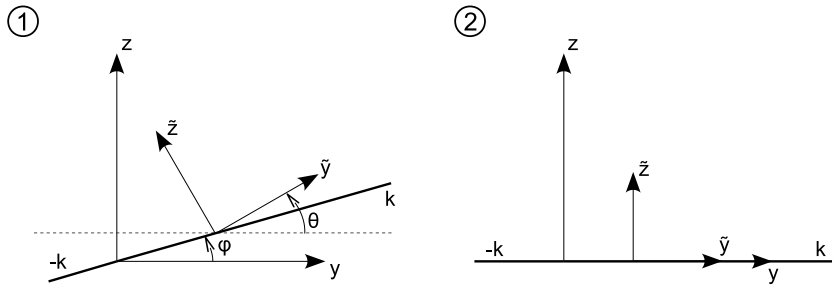

Figure 3.3: Schematic coordinate transformations of system ① and ② in real space. ①: The origin is first shifted along the tilted k-axes (thick, solid line) and then rotated by θ, which is independent of the wave number. Note that the tilt angle φ does not depend on k either. ②: The system is moved along the y-axis and rescaled. Note that the coordinates $\tilde{R}$ are virtual variables that also contain momenta. In this picture only the space dependence of the transformed system is plotted.

influence, we visualize what has happened during the substitutions of Section 3.2.1 and 3.2.2.

In system ① (Sect. 3.2.1) we started with a linear shift in real space $R \to R'$ (3.16). The coordinate system offset depends, besides system specific parameters, only on the magnetic field $\vec{B}$ and the wave number k, where the former defines the tilt angle, the latter the position on the tilted axis where the new origin must be located (Fig. 3.3). Once you allow a variation of the wave number you find that all the shifted coordinate systems R'_k must be located on this tilted axis and due to its linear dependency we can label it with k. This resembles the k-dependent spatial shift across a Hall bar of extended states in the quantum Hall regime (no in-plane field), but is generalized taking the third dimension and effects of the lateral field into account. The tilt angle φ is given by

$$\varphi = \arctan\left(-\frac{\omega_{cy}\,\omega_y^2}{\omega_{cz}\,\omega_z^2}\right) \ .$$

One can easily see that the angle becomes negligibly small in the two-dimensional limit ($\omega_y \ll \omega_z$) or for vanishing in-plane field.
Additional to the characteristic shift we get another effect which is new compared to

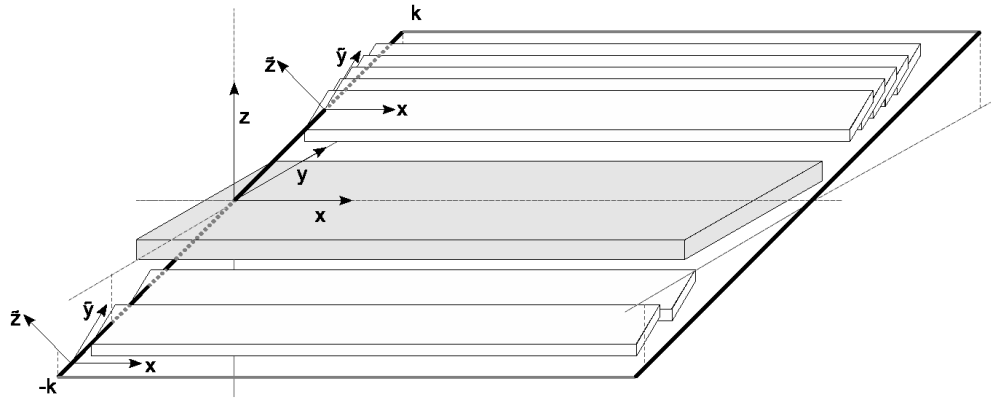

Figure 3.4: System ①: Channels of electron transport for different values of k. Although all confinements in the model system are harmonic, the channels are plotted as cuboids for convenience. Note that all magneto-electric confinements are aligned parallel since the tilt angle does not depend on k.

the 2D quantum Hall effect: the rotation $R' \to \tilde{R}$ (3.18), (3.19). The rotation angle θ is given by

$$\theta = \arctan(-\xi) \ ,$$

where

$$\xi = \Xi \pm \sqrt{1+\Xi^2} \qquad \text{with} \qquad \Xi = \frac{\Omega_{y,cz}^2 - \Omega_{z,cy}^2}{2\,\omega_{cy}\,\omega_{cz}} \ , \qquad \text{(same as (3.18))}$$

and is independent of k, i.e. the decoupled harmonic oscillators are parallel for all wave vectors and aligned along the k-axis. This is visualized in Fig. 3.4, where the cuboids represent the magneto-electric confinement channels in which the electrons move. The gray, large cuboid shows the electrostatic, initial Hall bar. Electrons close to the Fermi energy but with opposite velocity are spatially separated and backscattering is suppressed. Although the situation is more general, the same arguments as for the quantum Hall regime hold [4, 17] and can be used to describe transport phenomena in this setup.
Note that this out-of-plane rotation of the magneto-electric confinement has also been observed by the analysis of classical trajectories. Fig. 3.5 (lhs) was obtained by solving

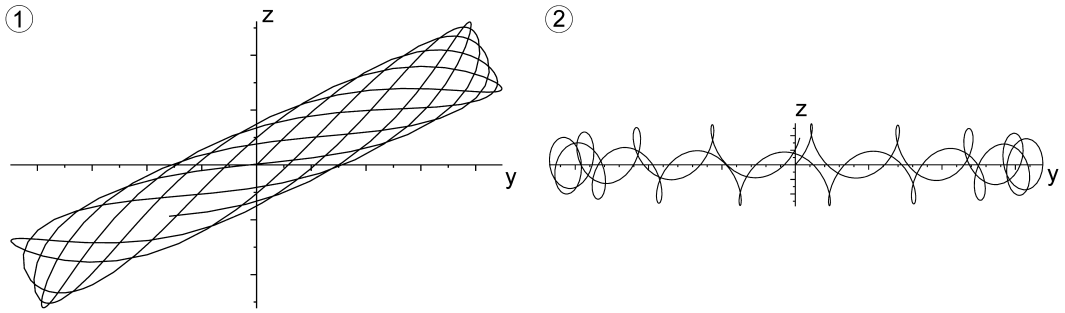

Figure 3.5: Classical trajectories of confined electrons in a magnetic field projected onto the y-z plane in arbitrary units. ①: The electron in the magnetic field $\vec{B} = (0, B_y, B_z)$ is trapped within the tilted rectangle. The motion resembles the trajectory of a confined electron in zero magnetic field (not shown here) but rotated and rescaled. ②: In the case of $\vec{B} = (B_x, 0, B_z)$ the shape of the trajectory has changed significantly. The electron is trapped within an effective confinement which is oriented like the initial, electrostatic potential, but its motion demonstrates additional dynamics. The magnetic field causes *skipping orbits* within the y-z plane, i.e. the electron circles around the origin along the potential's edge. This is the classical version of the position-momentum coupling of $H_k^{②}$ (3.5) and gives intuitive insight into the rotation of (effective) operators performed in (3.28).

the equation of motion

$$m\ddot{\vec{r}} = -m\begin{pmatrix} 0 \\ \omega_y^2\, y \\ \omega_z^2\, z \end{pmatrix} - e\begin{pmatrix} B_z\,\dot{y} - B_y\,\dot{z} \\ -B_z\,\dot{x} \\ B_y\,\dot{x} \end{pmatrix}$$

and projecting the result of a certain time interval onto the y-z plane. The analogy is obvious.

System ② (Sect. 3.2.1) is somewhat more complicated to map. The first transformation $R \to R'$ (3.25) consists of a linear shift along the y-axis and a linear shift in the momentum basis along the P_z-axis not visible in real space (Fig. 3.3). The offset of the coordinate system's origin is linear to the wave number and therefore we can label the axis of all possible translations with k. Note that the dynamics of the system along the z-axis has changed, but the origin of the z-axis has stayed the same.
The second substitution is a mixing of momentum and position operators $R' \to \tilde{R}$

(3.27), (3.28) and the resulting coordinates do not have a trivial real space representation. However, we assume that the projection of the coordinate system on the real space does not shift, i.e. the states are somehow located at the origin of system R'. This means that states with opposite wave numbers are spatially separated and we can use the same arguments as in the quantum Hall regime [4, 17] and as we did above for system ①.
To get an idea of the effective confinement and the relative orientation of the states, we solve the classical equation of motion

$$m\ddot{\vec{r}} = -m\begin{pmatrix} 0 \\ \omega_y^2\, y \\ \omega_z^2\, z \end{pmatrix} - e\begin{pmatrix} B_z\,\dot{y} \\ B_x\,\dot{z} - B_z\,\dot{x} \\ -B_x\,\dot{y} \end{pmatrix}$$

and plot the trajectory for some time interval (Fig. 3.5 (rhs)). One can clearly see that although the coupling causes some "internal" dynamics, the electron is trapped in a well defined region which is not tilted as in system ①. Therefore we expect the electron transport channels to be in the plane of the initial, electrostatic Hall bar for all values of k.

In summary we find that the out-of-plane shift and tilt are special features of system ①, where the magnetic field is perpendicular to the direction of transport. In system ②, the states become more complicated, but stay in the x-y plane of the initial 2DES. Nevertheless, for both systems quantum Hall effect arguments can still be used to describe transport phenomena since the states of opposite k-vectors are spatially separated.

3.3 Bychkov-Rashba Spin-Orbit Interaction

The theory of relativity predicts that whenever a charged particle moves in an electric field, it observes a magnetic field in its rest frame. The electrons in a solid state move in the ionic field and since they hold an intrinsic magnetic moment called *spin* [32], they interact with the resulting magnetic field. The interaction is called *spin-orbit coupling* (SO coupling) [12, 18, 45, 51] and is described by

$$H_{\mathrm{SO}} = \frac{\hbar}{4m_{\mathrm{e}}^2c^2}\left(\vec{P} + e\vec{A}\right)\cdot\left(\vec{\sigma}\times\vec{\nabla}V\right)$$

which appears through a non-relativistic approximation to the Dirac equation. The electric field of the crystal potential alters the energy levels and we assume for our considerations that this embedded effect has already been incorporated into the material dependent band structure parameters. On the other hand additional contributions have to be taken into account if there are additional electric fields in the system such as built-in fields of heterostructures or external fields. However, for a system that is inversion symmetric in time, which yields the relation $E_\uparrow(k) = E_\downarrow(-k)$ called *Kramers degeneracy*, and space, from what follows $E_\uparrow(k) = E_\uparrow(-k)$, we can conclude that the spin states must be degenerate, i.e. $E_\uparrow(k) = E_\downarrow(k)$ [12, 45]. The time inversion symmetry can simply be broken by an external magnetic field which results in the well-known Zeeman splitting. For a violation of the space inversion symmetry one usually distinguishes two cases: the structure inversion asymmetry (SIA) which gives rise to the so called *Bychkov-Rashba Hamiltonian*, and the bulk inversion asymmetry (BIA) from what the *Dresselhaus Hamiltonian* follows. Although we will use for model calculations an (Al)GaAs system which has zinc blende structure and therefore lacks bulk inversion symmetry, we will neglect the Dresselhaus contribution since we are interested in effects that are present in all kinds of 2DEGs. Thus we focus on the effects of a tilted magnetic field on Bychkov-Rashba spin-orbit coupling.

The model system H^{3D} (3.1) consists of harmonic potentials. This means that there is no structure inversion asymmetry and therefore there should be no BR-SO contribution to the eigenenergies. Nevertheless, the model Hamiltonian is an approximation which could have been done for an asymmetric system, e.g. a 2DEG which was created by a triangular potential along the growth-axis, sometimes referred to as *Rashba potential*. Moreover it has been shown [2] that even in a perfectly symmetric system one may sill observe SO interaction effects if there are two or more energy levels occupied. Hence we calculate the BR Hamiltonian in the transformed coordinates for the systems ①

and ②. The result will be appropriate for finding the energy correction where spin-polarized Landau levels cross as we will see later in this chapter, and for the derivation of effective spin Hamiltonians, which is done in Chapter 3.4. However, a possible effect on the eigenenergies due to the lateral confinement $V_y(Y)$ as described in Ref. [24] will be neglected for simplicity.

3.3.1 Calculating BR-SOI in the 2D EMA

Before we approach the effects of the lateral magnetic field on *Bychkov-Rashba spin-orbit interaction* (BR-SOI), we discuss the same situation within a common approximation, the 2D effective mass approximation which has already been introduced in Chapter 2. Based on H^{2D} (2.4) we can write down the Hamiltonian for a quantum wire along the x-direction with an arbitrarily orientated but small magnetic field in the Landau gauge

$$\begin{aligned} H^{\mathrm{2D}} &= \frac{(P_x - eB_z Y)^2}{2m} + \frac{P_y^2}{2m} + \frac{1}{2}\, m\, \omega_y^2\, Y^2 + \frac{g}{2}\mu_{\mathrm{B}} \vec{\sigma} \vec{B} \\ \rightarrow H_k^{\mathrm{2D}} &= \frac{P_y^2}{2m} + \frac{1}{2}\, m\, \Omega_{y,cz}^2 \Bigg[\underbrace{Y - \frac{\omega_{cz}}{\Omega_{y,cz}^2} \frac{\hbar k}{m}}_{=:Y'} \Bigg]^2 + \frac{\hbar^2 k^2}{2\mu} + \frac{g}{2}\mu_{\mathrm{B}} \vec{\sigma} \vec{B} \end{aligned} \tag{3.37}$$

where σ_i is the i-th Pauli matrix, $\Omega_{y,cz}^2 := \omega_y^2 + \omega_{cz}^2$ is the magneto-electric frequency and $\mu = m\left(1 + \frac{\omega_{cz}^2}{\omega_y^2}\right)$ is the effective mass of the dispersion relation. Note that the subband offset E_0^z was set to zero. The solution of the stationary Schrödinger equation reads

$$\left|\psi_n^{\pm}\right\rangle = |n\rangle \otimes |\pm\rangle =: |n, \pm\rangle$$

with $|n\rangle$ being the solution of the harmonic oscillator with frequency $\Omega_{y,cz}$, and $|\pm\rangle$ being the spin part of the wave function. In the basis of $\{|\uparrow\rangle, |\downarrow\rangle\}$, the eigenstates of the spin operator S_z, they read

$$\langle \uparrow | \pm \rangle = \frac{1}{\sqrt{\mathcal{N}_{\pm}}} \quad , \quad \langle \downarrow | \pm \rangle = \frac{1}{\sqrt{\mathcal{N}_{\pm}}} \frac{\pm B - B_z}{B_x - \mathrm{i}B_y} \, , \tag{3.38}$$

where

$$\mathcal{N}_{\pm} := \frac{\pm 2B\,(\pm B - B_z)}{B_x^2 + B_y^2}$$

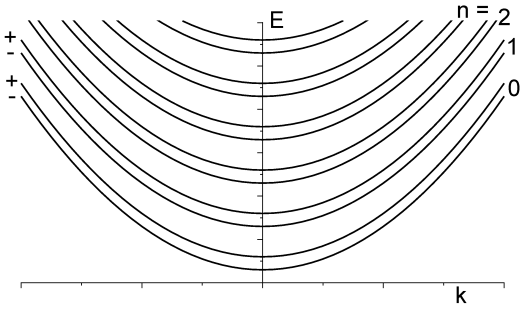

Figure 3.6: Band structure of the Zeeman split magneto-electric Landau levels for a two-dimensional Hall bar.

is the normalization factor and $B = |\vec{B}|$. The eigenvalues[6]

$$E_n^{\pm}(k) = \hbar\Omega_{y,cz}\left(n + \frac{1}{2}\right) + \frac{\hbar^2 k^2}{2\mu} \pm \frac{g}{2}\mu_{\mathrm{B}} B \tag{3.39}$$

are displayed schematically in Fig. 3.6. Note that the in-plane components of the magnetic field only appear in the Zeeman term. Any orbital effects are suppressed. In this model it is obvious that the in-plane field is only used to adjust the Zeeman splitting as desired.

Assume the in-plane field is such as the spin-polarized levels of the $|-\rangle$ states coincide with the adjacent $|+\rangle$ states, that is $E_n^+(k) = E_{n+1}^-(k)$ which is the case if

$$B_{\mathrm{ip}} = \sqrt{B_x^2 + B_y^2} = \pm\frac{m}{\bar{g}e}\sqrt{\omega_y^2 + (1-\bar{g}^2)\,\omega_{cz}^2}\ , \tag{3.40}$$

where

$$\bar{g} := \frac{g}{2}\beta \quad , \quad \beta := \frac{m}{m_{\mathrm{e}}} \tag{3.41}$$

for a given perpendicular field. We expect the BR-SO coupling to have an important effect on the eigenenergies [28, 37] at the band crossing and calculate the correction via degenerate perturbation theory. The total Hamiltonian reads

$$H^{\textcircled{2D}} = H_k^{\mathrm{2D}} + \alpha H_{\mathrm{BR}}^{\mathrm{2D}} \quad , \quad H_{\mathrm{BR}}^{\mathrm{2D}} = \frac{1}{\hbar}\left(\sigma_x P_y - \sigma_y\left(\hbar k - eB_z Y\right)\right)\ ,$$

[6] The notation was chosen such that $E_n^+(k) > E_n^-(k)$ for $g > 0$ what we will use in the following. A negative g-factor would just flip the spin states but would not change the energy spectrum what we are interested in.

where α is the Bychkov-Rashba parameter[7] and expansion coefficient. We solve this problem with the *operator method* [31], that is we use the bosonic ladder operators $b, b^\dagger$ to find the first order energy correction $E^{1^{\text{st}}}_{n,k}$ at the crossing. We need to take special care of the spatial shift of the harmonic oscillator when defining the operators. Let

$$b_y = \left(\frac{m\Omega_{y,cz}}{2\hbar}\right)^{1/2} Y + \mathrm{i}\left(\frac{1}{2m\Omega_{y,cz}\hbar}\right)^{1/2} P_y$$

be the annihilator of the unshifted potential, then the appropriate operator for the shifted system reads

$$b_{y'} := b_y - \hbar k \frac{\omega_{cz}}{\Omega_{y,cz}} \left(\frac{1}{2m\Omega_{y,cz}\hbar}\right)^{1/2}$$

and we can write

$$\begin{aligned} H^{2\mathrm{D}}_{\mathrm{BR}} = \frac{1}{\hbar}\Bigg[& \left(+\sigma_x \mathrm{i} \left(\frac{m\Omega_{y,cz}\hbar}{2}\right)^{1/2} + \sigma_y e B_z \left(\frac{\hbar}{2m\Omega_{y,cz}}\right)^{1/2} \right) b^\dagger_{y'} + \\ & + \left(-\sigma_x \mathrm{i} \left(\frac{m\Omega_{y,cz}\hbar}{2}\right)^{1/2} + \sigma_y e B_z \left(\frac{\hbar}{2m\Omega_{y,cz}}\right)^{1/2} \right) b_{y'} - \sigma_y \hbar k \frac{\omega_y^2}{\Omega^2_{y,cz}} \Bigg] = \\ = \frac{\mathrm{i}}{\hbar}\Bigg[& \left(\Pi^- \sigma_+ + \Pi^+ \sigma_-\right) b^\dagger_{y'} - \left(\Pi^+ \sigma_+ + \Pi^- \sigma_-\right) b_{y'} + \hbar k \frac{\omega_y^2}{\Omega^2_{y,cz}} \left(\sigma_+ - \sigma_-\right) \Bigg] \ , \end{aligned}$$

where we defined

$$\Pi^\pm := \left(\frac{m\Omega_{y,cz}\hbar}{2}\right)^{1/2} \pm e B_z \left(\frac{\hbar}{2m\Omega_{y,cz}}\right)^{1/2}$$

and used the ladder operators for the spin system

$$\sigma_x = \sigma_+ + \sigma_- \qquad , \qquad \mathrm{i}\sigma_y = \sigma_+ - \sigma_- \ .$$

With this form of $H^{2\mathrm{D}}_{\mathrm{BR}}$ the matrix elements are easily calculated. The secular equation leads to the first order energy correction which is given by

$$E^{1^{\text{st}}}_{n,k} = \pm\alpha\sqrt{H^2_{++} + |H_{+-}|^2}$$

with the matrix elements

$$\begin{aligned} H_{++} &= \langle n,+|\, H^{2\mathrm{D}}_{\mathrm{BR}}\, |n,+\rangle = -\langle n+1,-|\, H^{2\mathrm{D}}_{\mathrm{BR}}\, |n+1,-\rangle = -H_{--} \ , \\ H_{+-} &= \langle n,+|\, H^{2\mathrm{D}}_{\mathrm{BR}}\, |n+1,-\rangle = \langle n+1,-|\, H^{2\mathrm{D}}_{\mathrm{BR}}\, |n,+\rangle^* = H^*_{-+} \ , \end{aligned}$$

[7] Typical values for several semiconductors can be taken from Ref. [12].

and we get the solutions

$$H_{++}^2 = \left(\frac{B_y}{B}\,k\right)^2 \left(\frac{\omega_y^2}{\omega_y^2+\omega_{cz}^2}\right)^2 \quad , \tag{3.42a}$$

$$|H_{+-}|^2 = \frac{n+1}{\hbar\Omega_{y,cz}}\left[\frac{1}{2m}\left(\frac{m\Omega_{y,cz}}{B}+e\right)^2 B_z^2 + \frac{1}{2}m\omega_y^2\frac{B_y^2}{B^2}\right] \quad . \tag{3.42b}$$

The direct term (3.42a) is the square of the first order non-degenerate perturbation theory correction to the energy and is present for all states. The second term (3.42b), which arises due to band mixing, is the characteristic one for the degenerate case. We will discuss this result, and the generalization of it which will be derived in the following, in Section 3.3.3.

3.3.2 Calculating BR-SOI in the DSA

In this section we will use the outcome of Chapter 3 to calculate the correction due to BR-SOI at the crossing of spin-polarized energy levels. Whereas Section 3.3.1 was capable to deal with arbitrarily orientated magnetic fields, we need to restrict ourselves to the systems ① and ② in this case. The condition for the crossing in the limit $\omega_y \to 0$ reads[8]

$$|B_{\mathrm{ip}}| = \frac{m}{e}\sqrt{\frac{\omega_z}{2\left(\bar{g}^2-1\right)}\left(\omega_z - \sqrt{\omega_z^2+\frac{1}{4}\left(\frac{1}{\bar{g}^2}-1\right)\omega_{cz}^2}\right)-\omega_{cz}^2}\ , \tag{3.43}$$

what we will use for both systems. However, note that B_{ip} can be significantly different in narrow quantum wires for the systems ① and ② as we will show in Chap. 4. Nevertheless, it is hard to calculate B_{ip} for any value of B_z globally since, for strong fields, the effective mass and the Landé factor themselves depend on $\vec{B}$ (Chapter 2). A complex rhs in (3.43) states that no crossing is possible.

① The total system is described by

$$H^{①} = H_k^{①} + \frac{g}{2}\mu_{\mathrm{B}}\vec{\sigma}\vec{B} + \alpha H_{\mathrm{BR}}^{①} \quad , \quad H_{\mathrm{BR}}^{①} = \frac{1}{\hbar}\left[\sigma_x P_y - \sigma_y\left(\hbar k + e\left(B_y Z - B_z Y\right)\right)\right]$$

with the *Bychkov-Rashba parameter* [12, 45, 51] and expansion coefficient α. We will perform the same transformations as used in Section 3.2.1 and calculate the

[8] The condition for narrow quantum wires is given by equation (4.4).

energy correction with degenerate perturbation theory afterwards.
The BR Hamiltonian after the spatial shift (3.16) reads

$$H_{\mathrm{BR}}^{①} = \frac{1}{\hbar}\left[\sigma_x P_{y'} - \sigma_y\left(\hbar k + e\left(B_y Z' - B_z Y'\right)\right) + \sigma_y \hbar k \,\frac{\omega_{cy}^2\omega_y^2 + \omega_{cz}^2\omega_z^2}{\omega_{cy}^2\omega_y^2 + \omega_{cz}^2\omega_z^2 + \omega_y^2\omega_z^2}\right]$$

and after the rotation (3.19) we get

$$\begin{aligned} H_{\mathrm{BR}}^{①} =& \frac{N}{\hbar}\left[\sigma_x P_{\tilde{y}} - \sigma_x \xi P_{\tilde{z}} - \sigma_y e\left(\xi B_y - B_z\right)\tilde{Y} - \sigma_y e\left(B_y + \xi B_z\right)\tilde{Z}\right] - \\ & - \sigma_y k \,\frac{\omega_y^2\omega_z^2}{\omega_{cy}^2\omega_y^2 + \omega_{cz}^2\omega_z^2 + \omega_y^2\omega_z^2}\ . \end{aligned}$$

Introducing the ladder operators of the transformed coordinate system $b_{\tilde{y}}$, $b_{\tilde{y}}^\dagger$ and $b_{\tilde{z}}$, $b_{\tilde{z}}^\dagger$, where

$$\tilde{Y} = \left(\frac{\hbar}{2m\omega_{\tilde{y}}}\right)^{1/2}\left(b_{\tilde{y}}^\dagger + b_{\tilde{y}}\right) \quad , \quad \tilde{P}_{\tilde{y}} = \mathrm{i}\left(\frac{m\omega_{\tilde{y}}\hbar}{2}\right)^{1/2}\left(b_{\tilde{y}}^\dagger - b_{\tilde{y}}\right)\ ,$$

$$\tilde{Z} = \left(\frac{\hbar}{2m\omega_{\tilde{z}}}\right)^{1/2}\left(b_{\tilde{z}}^\dagger + b_{\tilde{z}}\right) \quad , \quad \tilde{P}_{\tilde{z}} = \mathrm{i}\left(\frac{m\omega_{\tilde{z}}\hbar}{2}\right)^{1/2}\left(b_{\tilde{z}}^\dagger - b_{\tilde{z}}\right)\ ,$$

we can write

$$\begin{aligned} H_{\mathrm{BR}}^{①} = \frac{N}{\hbar}\Bigg[& \left(+\sigma_x \mathrm{i}\left(\frac{m\omega_{\tilde{y}}\hbar}{2}\right)^{1/2} + \sigma_y e\,(\,B_z - \xi\,B_y\,)\left(\frac{\hbar}{2m\omega_{\tilde{y}}}\right)^{1/2}\right) b_{\tilde{y}}^\dagger + \\ & + \left(-\sigma_x \mathrm{i}\left(\frac{m\omega_{\tilde{y}}\hbar}{2}\right)^{1/2} + \sigma_y e\,(\,B_z - \xi\,B_y\,)\left(\frac{\hbar}{2m\omega_{\tilde{y}}}\right)^{1/2}\right) b_{\tilde{y}} - \\ & - \xi\left(+\sigma_x \mathrm{i}\left(\frac{m\omega_{\tilde{z}}\hbar}{2}\right)^{1/2} + \sigma_y e\left(B_z + \frac{1}{\xi}B_y\right)\left(\frac{\hbar}{2m\omega_{\tilde{z}}}\right)^{1/2}\right) b_{\tilde{z}}^\dagger - \\ & - \xi\left(-\sigma_x \mathrm{i}\left(\frac{m\omega_{\tilde{z}}\hbar}{2}\right)^{1/2} + \sigma_y e\left(B_z + \frac{1}{\xi}B_y\right)\left(\frac{\hbar}{2m\omega_{\tilde{z}}}\right)^{1/2}\right) b_{\tilde{z}}\Bigg] - \\ & - \sigma_y k \,\frac{\omega_y^2\omega_z^2}{\omega_{cy}^2\omega_y^2 + \omega_{cz}^2\omega_z^2 + \omega_y^2\omega_z^2} = \end{aligned}$$

$$\begin{aligned} = N\frac{\mathrm{i}}{\hbar}\Big[& \left(\Pi_{\tilde{y}}^{①-}\sigma_+ + \Pi_{\tilde{y}}^{①+}\sigma_-\right) b_{\tilde{y}}^\dagger - \left(\Pi_{\tilde{y}}^{①+}\sigma_+ + \Pi_{\tilde{y}}^{①-}\sigma_-\right) b_{\tilde{y}} - \\ & - \xi\left(\left(\Pi_{\tilde{z}}^{①-}\sigma_+ + \Pi_{\tilde{z}}^{①+}\sigma_-\right) b_{\tilde{z}}^\dagger - \left(\Pi_{\tilde{z}}^{①+}\sigma_+ + \Pi_{\tilde{z}}^{①-}\sigma_-\right) b_{\tilde{z}}\right)\Big] + \\ & + \mathrm{i}k\,\frac{\omega_y^2\omega_z^2}{\omega_{cy}^2\omega_y^2 + \omega_{cz}^2\omega_z^2 + \omega_y^2\omega_z^2}\left(\sigma_+ - \sigma_-\right)\ , \end{aligned} \tag{3.44}$$

where we defined

$$\Pi_{\tilde{y}}^{①\pm} := \left(\frac{m\omega_{\tilde{y}}\hbar}{2}\right)^{1/2} \pm e\,(\,B_z - \xi\,B_y\,)\left(\frac{\hbar}{2m\omega_{\tilde{y}}}\right)^{1/2}\,,$$
$$\Pi_{\tilde{z}}^{①\pm} := \left(\frac{m\omega_{\tilde{z}}\hbar}{2}\right)^{1/2} \pm e\left(B_z + \frac{1}{\xi}B_y\right)\left(\frac{\hbar}{2m\omega_{\tilde{z}}}\right)^{1/2}\,.$$

To calculate the energy correction we need to select one specific transformation which will be fixed for all following considerations. Analogous to Section 3.2.3, we choose $\xi = \xi_-$ and recall the identity

$$\xi_- = -\xi_+^{-1}\,.$$

The eigenstates of the unperturbed system read

$$\left|\psi_{n,n'}^{\pm}\right\rangle = |n\rangle \otimes \left|n'\right\rangle \otimes |\pm\rangle =: \left|n, n', \pm\right\rangle$$

with $|n\rangle$ being the solution of the harmonic oscillator with frequency $\omega_{\tilde{y}}$, $|n'\rangle$ being the solution of the harmonic oscillator with frequency $\omega_{\tilde{z}}$, and $|\pm\rangle$ being the spin part of the wave function which is identical to (3.38). The problem we have to face is that we do not know which magneto-electric frequency is bigger, thus we need to look at both cases separately. Another problem arises when $\omega_{\tilde{y}} \approx \omega_{\tilde{z}}$, because, whereas in Section 3.3.1 we had to deal with a two-fold degenerate eigenenergy, we would have to deal with higher degeneracies. Since this condition only holds in a small region compared to the whole spectrum of the MEFs (comp. Fig. 3.1), we will just look at the cases

a) $\omega_{\tilde{y}} \gg \omega_{\tilde{z}}$

b) $\omega_{\tilde{y}} \ll \omega_{\tilde{z}}$

and use the same two-fold degenerate perturbation theory technique as in Section 3.3.1.
The secular equation gives us

$$E_{n,k}^{①,1^{\text{st}}} = \pm\alpha\sqrt{H_{++}^2 + |H_{+-}|^2}$$

and with the matrix element

$$H_{++} = \langle +|\; H_{\text{BR}}^{①}\; |+\rangle = -\,\langle -|\; H_{\text{BR}}^{①}\; |-\rangle = -H_{--}$$

we get for both (a) and (b)

$$H_{++}^2 = \left(\frac{B_y}{B}\,k\right)^2 \left(\frac{\omega_y^2\omega_z^2}{\omega_{cy}^2\omega_y^2 + \omega_{cz}^2\omega_z^2 + \omega_y^2\omega_z^2}\right)^2 . \tag{3.45a}$$

It is obvious that this is a generalization to (3.42a) which can be obtained from (3.45a) in the limits $\omega_y \ll \omega_z$ and $\omega_{cy} \ll \omega_z$.
For the matrix element H_{+-} we need to distinguish the two cases:

a) ($\omega_{\tilde{y}} \gg \omega_{\tilde{z}}$): The system is effectively two-dimensional with only the lowest state of the $\omega_{\tilde{y}}$-oscillator being occupied. The matrix element reads

$$H_{+-} = \langle 0, n', +|\ H_{\mathrm{BR}}^{①}\ |0, n'+1, -\rangle = \langle 0, n'+1, -|\ H_{\mathrm{BR}}^{①}\ |0, n', +\rangle^* = H_{-+}^*$$

with the solution

$$|H_{+-}|^2 = \frac{n'+1}{\hbar\omega_{\tilde{z}}} N^2\xi^2 \left[\frac{1}{2}m\left(\frac{e\left(B_z + \xi^{-1}B_y\right)}{m}\frac{B_z}{B} + \omega_{\tilde{z}}\right)^2\right] .$$

b) ($\omega_{\tilde{y}} \ll \omega_{\tilde{z}}$): In this situation the system is two-dimensional with occupancy of only the lowest state of the $\omega_{\tilde{z}}$-oscillator. The matrix element in this case reads

$$H_{+-} = \langle n, 0, +|\ H_{\mathrm{BR}}^{①}\ |n+1, 0, -\rangle = \langle n+1, 0, -|\ H_{\mathrm{BR}}^{①}\ |n, 0, +\rangle^* = H_{-+}^*$$

and the solution is given by

$$|H_{+-}|^2 = \frac{n+1}{\hbar\omega_{\tilde{y}}} N^2 \left[\frac{1}{2}m\left(\frac{e\left(B_z - \xi B_y\right)}{m}\frac{B_z}{B} + \omega_{\tilde{y}}\right)^2\right] .$$

Since the formula for case (a) can be obtained from the formula of case (b) by substituting $\xi \to -\xi^{-1}$, they can be combined in the short hand notation:

$$\begin{aligned} |H_{+-}|^2 &= \frac{n+1}{\hbar\omega_-^{①}} \frac{1}{1+\xi'^2} \left[\frac{1}{2}m\left(\left(\omega_{cz} - \xi'\omega_{cy}\right)\frac{B_z}{B} + \omega_-^{①}\right)^2\right] \\ \text{with}\quad \xi' &= \begin{cases} \xi_+ & \text{if} \quad \mathrm{sign}(\omega_{cy}\omega_{cz}) = +1 \\ \xi_- & \text{if} \quad \mathrm{sign}(\omega_{cy}\omega_{cz}) = -1 \end{cases} \end{aligned} \tag{3.45b}$$

and $\omega_-^{①}$ given in (3.13). It can be shown that this result is equal to (3.42b) in the limit $\xi \to 0$, thus $E_{n,k}^{①,1^{\mathrm{st}}}$ is a generalization of the two-dimensional approximation $E_{n,k}^{1^{\mathrm{st}}}$ for an in-plane magnetic field perpendicular to the direction of transport.

② The total Hamiltonian of the system reads

$$H^{②} = H_k^{②} + \frac{ge\hbar}{4m}\,\vec{\sigma}\vec{B} + \alpha H_{\mathrm{BR}}^{②} \quad , \quad H_{\mathrm{BR}}^{②} = \frac{1}{\hbar}\left[\sigma_x P_y - \sigma_y\left(\hbar k - eB_z Y\right)\right]$$

with α being the same parameter as in case ①. We will use the transformations derived in 3.2.2, rewrite $H_{\mathrm{BR}}^{②}$ in terms of ladder operators and calculate the energy correction with degenerate perturbation theory.
Applying the spatial shift (3.25) we get

$$H_{\mathrm{BR}}^{②} = \frac{1}{\hbar}\left[\sigma_x P_{y'} - \sigma_y\left(\hbar k - eB_z Y'\right) + \sigma_y \hbar k\,\frac{\omega_{cz}^2}{\omega_y^2 + \omega_{cz}^2}\right]$$

and after the rotation (3.28) with the sign convention (3.23) we obtain

$$H_{\mathrm{BR}}^{②} = \frac{N}{\hbar}\left[\sigma_x P_{\tilde{y}} - \sigma_y \xi \frac{eB_z}{m\omega_z} P_{\tilde{z}} + \sigma_y e B_z \tilde{Y} + \sigma_x \xi m \omega_z \tilde{Z}\right] - \sigma_y k\,\frac{\omega_y^2}{\omega_y^2 + \omega_{cz}^2} \ .$$

If we want to define ladder operators for the decoupled Hamiltonian (3.29), we need to take special care of the effective mass $m_{\tilde{z}}$ in $\tilde{z}$-direction (3.30). It holds

$$\tilde{Y} = \left(\frac{\hbar}{2m\omega_{\tilde{y}}}\right)^{1/2}\left(b_{\tilde{y}}^\dagger + b_{\tilde{y}}\right) \quad , \quad P_{\tilde{y}} = \mathrm{i}\left(\frac{m\omega_{\tilde{y}}\hbar}{2}\right)^{1/2}\left(b_{\tilde{y}}^\dagger - b_{\tilde{y}}\right) \ ,$$

$$\tilde{Z} = \left(\frac{\hbar}{2m_{\tilde{z}}\omega_{\tilde{z}}}\right)^{1/2}\left(b_{\tilde{z}}^\dagger + b_{\tilde{z}}\right) \quad , \quad P_{\tilde{z}} = \mathrm{i}\left(\frac{m_{\tilde{z}}\omega_{\tilde{z}}\hbar}{2}\right)^{1/2}\left(b_{\tilde{z}}^\dagger - b_{\tilde{z}}\right) \ ,$$

and it follows

$$\begin{aligned} H_{\mathrm{BR}}^{②} = \frac{N}{\hbar}\Bigg[& \left(+\sigma_x \mathrm{i}\left(\frac{m\omega_{\tilde{y}}\hbar}{2}\right)^{1/2} + \sigma_y e B_z \left(\frac{\hbar}{2m\omega_{\tilde{y}}}\right)^{1/2}\right) b_{\tilde{y}}^\dagger + \\ & + \left(-\sigma_x \mathrm{i}\left(\frac{m\omega_{\tilde{y}}\hbar}{2}\right)^{1/2} + \sigma_y e B_z \left(\frac{\hbar}{2m\omega_{\tilde{y}}}\right)^{1/2}\right) b_{\tilde{y}} - \\ & - \mathrm{i}\xi\left(+\sigma_x \mathrm{i}\left(\frac{m\omega_{\tilde{z}}\hbar}{2}\right)^{1/2} + \sigma_y e B_z \left(\frac{\hbar}{2m\omega_{\tilde{z}}}\right)^{1/2}\right) b_{\tilde{z}}^\dagger + \\ & + \mathrm{i}\xi\left(-\sigma_x \mathrm{i}\left(\frac{m\omega_{\tilde{z}}\hbar}{2}\right)^{1/2} + \sigma_y e B_z \left(\frac{\hbar}{2m\omega_{\tilde{z}}}\right)^{1/2}\right) b_{\tilde{z}}\Bigg] - \\ & - \sigma_y k\,\frac{\omega_y^2}{\omega_y^2 + \omega_{cz}^2} = \end{aligned}$$

$$
\begin{aligned}
&= N\frac{\mathrm{i}}{\hbar}\left[\left(\Pi_{\tilde{y}}^{②-}\sigma_+ + \Pi_{\tilde{y}}^{②+}\sigma_-\right) b_{\tilde{y}}^\dagger - \left(\Pi_{\tilde{y}}^{②+}\sigma_+ + \Pi_{\tilde{y}}^{②-}\sigma_-\right) b_{\tilde{y}} - \right. \\
&\quad \left. -\mathrm{i}\xi\left(\left(\Pi_{\tilde{z}}^{②-}\sigma_+ + \Pi_{\tilde{z}}^{②+}\sigma_-\right) b_{\tilde{z}}^\dagger + \left(\Pi_{\tilde{z}}^{②+}\sigma_+ + \Pi_{\tilde{z}}^{②-}\sigma_-\right) b_{\tilde{z}}\right)\right] + \\
&\quad + \mathrm{i}k\,\frac{\omega_y^2}{\omega_y^2+\omega_{cz}^2}\left(\sigma_+ - \sigma_-\right)
\end{aligned}
\tag{3.46}
$$

where we defined

$$
\begin{aligned}
\Pi_{\tilde{y}}^{②\pm} &:= \left(\frac{m\omega_{\tilde{y}}\hbar}{2}\right)^{1/2} \pm eB_z\left(\frac{\hbar}{2m\omega_{\tilde{y}}}\right)^{1/2}, \\
\Pi_{\tilde{z}}^{②\pm} &:= \left(\frac{m\omega_{\tilde{z}}\hbar}{2}\right)^{1/2} \pm eB_z\left(\frac{\hbar}{2m\omega_{\tilde{z}}}\right)^{1/2}.
\end{aligned}
$$

Again we need to pick one transformation, which will be $\xi = \xi_-$, and keep it for the rest of our calculation. In analogy to the previous case, we denote the eigenstates of the unperturbed system

$$
\left|\psi_{n,n'}^{\pm}\right\rangle = |n\rangle \otimes \left|n'\right\rangle \otimes |\pm\rangle =: \left|n, n', \pm\right\rangle
$$

with $|n\rangle$ and $|n'\rangle$ being the solution of the harmonic oscillator with frequency $\omega_{\tilde{y}}$ and $\omega_{\tilde{z}}$ respectively. The spin part of the wave function $|\pm\rangle$ is the same as in (3.38). We distinguish two cases

a) $\omega_{\tilde{y}} \gg \omega_{\tilde{z}}$

b) $\omega_{\tilde{y}} \ll \omega_{\tilde{z}}$

in order to justify a treatment with the two-fold degenerate perturbation theory as in Section 3.3.1.
The secular equation gives us for the first order energy correction

$$
E_{n,k}^{②,1^{\mathrm{st}}} = \pm\alpha\sqrt{H_{++}^2 + |H_{+-}|^2}
$$

with the matrix element

$$
H_{++} = \langle +|\, H_{\mathrm{BR}}^{②}\, |+\rangle = -\langle -|\, H_{\mathrm{BR}}^{②}\, |-\rangle = -H_{--}\ .
$$

For both (a) and (b) we find

$$
H_{++}^2 = 0 \tag{3.47a}
$$

which coincides with (3.42a) for $B_y = 0$. This also means that the first order correction for non-degenerate states vanishes.
The case differentiation is necessary to calculate the matrix element H_{+-}:

a) ($\omega_{\tilde{y}} \gg \omega_{\tilde{z}}$): Here we have an effective two-dimensional system with lowest subband occupancy of the $\omega_{\tilde{y}}$-oscillator. The matrix element reads

$$H_{+-} = \langle 0, n', + |\ H^{②}_{\mathrm{BR}}\ | 0, n'+1, - \rangle = \langle 0, n'+1, - |\ H^{②}_{\mathrm{BR}}\ | 0, n', + \rangle^* = H^*_{-+}$$

with the solution

$$|H_{+-}|^2 = \frac{n'+1}{\hbar\omega_{\tilde{z}}} N^2 \xi^2 \left[\frac{1}{2} m \left(\frac{eB_z}{m} + \omega_{\tilde{z}} \frac{B_z}{B} \right)^2 \right] .$$

b) ($\omega_{\tilde{y}} \ll \omega_{\tilde{z}}$): Because only the lowest energy level of the $\omega_{\tilde{z}}$-oscillator is occupied, the matrix element in this case reads

$$H_{+-} = \langle n, 0, + |\ H^{②}_{\mathrm{BR}}\ | n+1, 0, - \rangle = \langle n+1, 0, - |\ H^{②}_{\mathrm{BR}}\ | n, 0, + \rangle^* = H^*_{-+}$$

and the solution is given by

$$|H_{+-}|^2 = \frac{n+1}{\hbar\omega_{\tilde{y}}} N^2 \left[\frac{1}{2} m \left(\frac{eB_z}{m} + \omega_{\tilde{y}} \frac{B_z}{B} \right)^2 \right] .$$

We have the same relation between the formulas of case (a) and (b) as we had in system ①, i.e. we get one matrix element from the other one by substituting $\xi \to -\xi^{-1}$. It allows us to write $|H_{+-}|^2$ in the compact form:

$$\begin{aligned} |H_{+-}|^2 &= \frac{n+1}{\hbar\omega^{②}_{-}} \frac{1}{1+\xi'^2} \left[\frac{1}{2} m \left(\omega_{cz} + \omega^{②}_{-} \frac{B_z}{B} \right)^2 \right] \\ \text{with} \quad \xi' &= \begin{cases} \xi_- & \text{if} \quad \mathrm{sign}(\omega_{cx}) = +1 \\ \xi_+ & \text{if} \quad \mathrm{sign}(\omega_{cx}) = -1 \end{cases} \end{aligned} \tag{3.47b}$$

and $\omega^{②}_{-}$ given in (3.15). This is a generalization to the two-dimensional approximation $E^{1^{\mathrm{st}}}_{n,k}$ for an in-plane magnetic field parallel to the direction of transport.

3.3.3 Discussion and Summary

In conclusion we found the energy eigenvalues of a quantum wire described by $H^{3\mathrm{D}}$ (3.1) for the case $\omega_- \ll \omega_+$ to be

$$E_n(k) = \hbar\omega_- \left(n + \frac{1}{2} \right) + \frac{1}{2}\hbar\omega_+ + \frac{\hbar^2 k^2}{2\mu} \pm \frac{g}{2}\mu_{\mathrm{B}} B + E^{1^{\mathrm{st}}}_{n,k} ,$$

where

$$\mu = \begin{cases} m\left(1+\dfrac{\omega_{cz}^2}{\omega_y^2}+\dfrac{\omega_{cy}^2}{\omega_z^2}\right) & \text{for system ① (comp. (3.17))} \\ m\left(1+\dfrac{\omega_{cz}^2}{\omega_y^2}\right) & \text{for system ② (comp. (3.26))} \end{cases}$$

and $E_{n,k}^{1^{\text{st}}}$ being the first order correction due to Bychkov-Rashba spin-orbit coupling. The MEFs for both systems can be found in (3.13) and (3.15) respectively. We calculated $E_{n,k}^{1^{\text{st}}}$ for the special case that the in-plane magnetic field is such as the spin-polarized magneto-electric bands $|n,+\rangle$ and $|n+1,-\rangle$ overlap. It can be written as

$$E_{n,k}^{1^{\text{st}}} = \pm\alpha\sqrt{H_{++}^2+|H_{+-}|^2}\ ,$$

with the expressions for the matrix elements H_{++} and H_{+-} as follows:

In the two-dimensional approximation, neglecting the orbital effects of the in-plane field, we get

$$H_{++}^2 = \left(\frac{B_y}{B}\,k\right)^2\left(\frac{\omega_y^2}{\omega_y^2+\omega_{cz}^2}\right)^2\ , \qquad \text{(same as (3.42a))}$$

$$|H_{+-}|^2 = \frac{n+1}{\hbar\Omega_{y,cz}}\left[\frac{1}{2m}\left(\frac{m\Omega_{y,cz}}{B}+e\right)^2 B_z^2+\frac{1}{2}m\omega_y^2\frac{B_y^2}{B^2}\right]\ , \qquad \text{(same as (3.42b))}$$

whereas a more general approach led to the expressions

$$H_{++}^2 = \left(\frac{B_y}{B}\,k\right)^2\left(\frac{\omega_y^2\omega_z^2}{\omega_{cy}^2\omega_y^2+\omega_{cz}^2\omega_z^2+\omega_y^2\omega_z^2}\right)^2\ , \qquad \text{(same as (3.45a))}$$

$$|H_{+-}|^2 = \frac{n+1}{\hbar\omega_-^{①}}\,\frac{1}{1+\xi'^2}\left[\frac{1}{2}m\left(\left(\omega_{cz}-\xi'\omega_{cy}\right)\frac{B_z}{B}+\omega_-^{①}\right)^2\right] \qquad \text{(same as (3.45b))}$$

$$\text{with}\quad \xi' = \begin{cases}\xi_+ & \text{if}\quad \operatorname{sign}(\omega_{cy}\omega_{cz})=+1\\ \xi_- & \text{if}\quad \operatorname{sign}(\omega_{cy}\omega_{cz})=-1\end{cases}$$

for system ①, and

$$H_{++}^2 = 0\ , \qquad \text{(same as (3.47a))}$$

$$|H_{+-}|^2 = \frac{n+1}{\hbar\omega_-^{②}}\,\frac{1}{1+\xi'^2}\left[\frac{1}{2}m\left(\omega_{cz}+\omega_-^{②}\frac{B_z}{B}\right)^2\right] \qquad \text{(same as (3.47b))}$$

$$\text{with}\quad \xi' = \begin{cases}\xi_- & \text{if}\quad \operatorname{sign}(\omega_{cx})=+1\\ \xi_+ & \text{if}\quad \operatorname{sign}(\omega_{cx})=-1\end{cases}$$

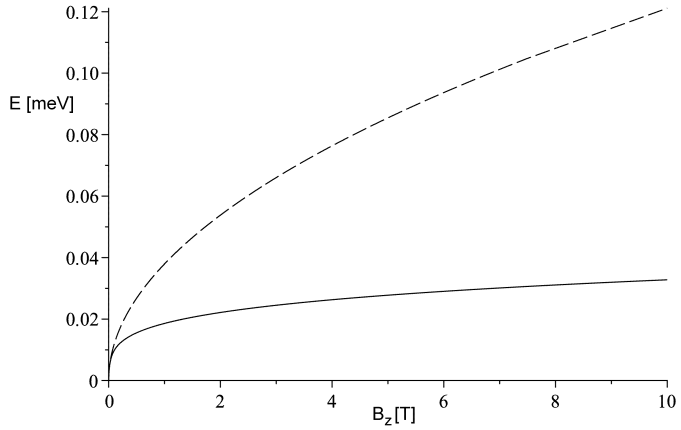

Figure 3.7: BR-SOI induced energy gap $2E^{1\text{st}}_{0,0}$ as a function of B_z with $g = -0.4$ and $\beta = 0.067$ for the isotropic case ($\omega_y = 0$). The two-dimensional approximation (dashed line) satisfies the condition (3.40) whereas the DSA solution (solid line) satisfies (3.43). The graph maps the situation for a wide (Al)GaAs Hall bar with $\hbar\omega_z = 7.24\,\text{meV}$.

for system ②. The MEFs $\omega_-^{①}$ and $\omega_-^{②}$ in the corresponding form are given in (B.1a) and (B.2a) and the $\xi_\pm$ were introduced in (3.18) for system ① and (3.27) for system ② respectively.

Finally we apply these formulas to a model system - the setup used by W. Pan et. al. in Ref. [26]. In Section 3.1.3 we have shown that for $B_z \sim 2.9\,\text{T}$ and $B_{\text{ip}} \sim 25\,\text{T}$ a crossing of the spin-polarized levels is conceivable. We have already stated that for this very wide Hall bar it is suitable to assume $\omega_y = 0$, thus we have $\omega_-^{①} = \omega_-^{②} = \omega_-$, i.e. no anisotropy in the MEFs. Fig. 3.7 shows the energy gap $2E^{1\text{st}}_{0,0}$ of the two-dimensional and three-dimensional approach. It is quite remarkable that although (3.45b) and (3.47b) look very different, they are equal for $\omega_y = 0$, thus the system is isotropic for wide waveguides. It can only become anisotropic for a noticeable confinement in the two-dimensional plane and, similar to the MEFs, also anisotropies of Bychkov-Rashba energy level anticrossings are just due to boundary effects.[9] Moreover we notice that the preciser solution is smaller which is even a global attribute. Since we do not

[9] For wide Hall bars with $\omega_y \to 0$, we assume that the potential increases slowly, with respect to the cyclotron radius, towards the edges of the sample. Thus we can convert the bulk states to the edge states adiabatically and expect the same behavior as for the bulk [4, 25, 30].

know the exact values and behavior of g and m, we cannot solve the conditions (3.40) and (3.43) exactly. However, we can give an approximation for fixed values using $g = -0.4$ and $\beta = 0.067$. The variation of the energy correction for a given B_z in the three-dimensional approximation is small and we can summarize that the energy band anticrossing is about $2E_{0,0}^{1^{\text{st}}} \approx 20\,\mu\text{eV}$. Thus, without taking the orbital effects of high magnetic fields into account, the effect of BR-SOI is overestimated. However, note that we assumed that the Bychkov-Rashba parameter α stayed constant for all considerations. In principle one could think of a deviation from the listed value at high fields which was neglected in Fig. 3.7. Since the general behavior of $E_{0,0}^{1^{\text{st}}}$ is the same for both approximations, it seems possible that the difference is (partially) compensated by a Bychkov-Rashba parameter that also depends on $\vec{B}$. A systematic investigation of this possibility has not been performed.

For a quantum wire with finite width the anticrossing becomes anisotropic and increases with shrinking size of the system. This important feature and its consequences will be discussed in Chapter 4.

3.4 Effective Hamiltonians

The Hamiltonians discussed in the previous chapters are exact within the effective mass approximation using only harmonic confinements. However, it is not always advantageous or even necessary to use these general forms. Sometimes the important physics can also be captured by an approximated Hamiltonian which is much easier to handle. In this sense one can create Hamiltonians which are valid only for high magnetic fields and small spin-orbit coupling (Sect. 3.4.1) or use a unitary transformation to embed SOI up to a given order of the Bychkov-Rashba parameter (Sect. 3.4.2). In this chapter we will derive these *effective Hamiltonians* for the two-dimensional and for both cases of the three-dimensional system. But first, let us recall for completeness the full and exact Hamiltonians that we derived in former sections and that we will need in the following.

(2D) In the two-dimensional approximation the full Hamiltonian, which was introduced in Section 3.3.1, is given by

$$H^{(2D)} = \hbar\Omega_{y,cz}\left(b_{y'}^{\dagger}b_{y'} + \frac{1}{2}\right) + \frac{\hbar^2k^2}{2\mu} + \frac{g}{2}\mu_{\mathrm{B}}\vec{\sigma}\vec{B} + H_{\mathrm{BR}}^{\mathrm{2D}}\ , \tag{3.48}$$

where

$$H_{\mathrm{BR}}^{\mathrm{2D}} = \alpha\frac{1}{\hbar}\left(\sigma_x P_y - \sigma_y\left(\hbar k - eB_z Y\right)\right) =$$

$$= \alpha\frac{\mathrm{i}}{\hbar}\left[\left(\Pi^{-}\sigma_{+} + \Pi^{+}\sigma_{-}\right)b_{y'}^{\dagger} - \left(\Pi^{+}\sigma_{+} + \Pi^{-}\sigma_{-}\right)b_{y'}\right] - \alpha k\,\frac{\omega_y^2}{\Omega_{y,cz}^2}\sigma_y$$

and

$$\Pi^{\pm} = \left(\frac{m\Omega_{y,cz}\hbar}{2}\right)^{1/2} \pm eB_z\left(\frac{\hbar}{2m\Omega_{y,cz}}\right)^{1/2}\ .$$

Note that it holds $\Omega_{y,cz}^2 = \omega_y^2 + \omega_{cz}^2$ and $\mu = m\left(1 + \frac{\omega_{cz}^2}{\omega_y^2}\right)$.

① Using the assumptions of model system ① we derived the decoupled Hamiltonian (Sect. 3.2.1) and its corresponding Bychkov-Rashba term (Sect. 3.3.2), which read

$$H^{①} = \hbar\omega_{\tilde{y}}^{①}\left(b_{\tilde{y}}^{\dagger}b_{\tilde{y}} + \frac{1}{2}\right) + \hbar\omega_{\tilde{z}}^{①}\left(b_{\tilde{z}}^{\dagger}b_{\tilde{z}} + \frac{1}{2}\right) + \frac{\hbar^2k^2}{2\mu} + \frac{g}{2}\mu_{\mathrm{B}}\vec{\sigma}\vec{B} + H_{\mathrm{BR}}^{①}\ , \tag{3.49}$$

where

$$\begin{aligned}H^{①}_{\mathrm{BR}} &= \alpha\frac{1}{\hbar}\left[\sigma_x P_y - \sigma_y\left(\hbar k + e\left(B_y Z - B_z Y\right)\right)\right] = \\ &= \alpha N\frac{\mathrm{i}}{\hbar}\left[\left(\Pi^{①-}_{\tilde{y}}\sigma_+ + \Pi^{①+}_{\tilde{y}}\sigma_-\right)b^\dagger_{\tilde{y}} - \left(\Pi^{①+}_{\tilde{y}}\sigma_+ + \Pi^{①-}_{\tilde{y}}\sigma_-\right)b_{\tilde{y}} - \right. \\ &\quad \left. - \xi\left(\left(\Pi^{①-}_{\tilde{z}}\sigma_+ + \Pi^{①+}_{\tilde{z}}\sigma_-\right)b^\dagger_{\tilde{z}} - \left(\Pi^{①+}_{\tilde{z}}\sigma_+ + \Pi^{①-}_{\tilde{z}}\sigma_-\right)b_{\tilde{z}}\right)\right] + \\ &\quad - \alpha k\,\frac{\omega_y^2\omega_z^2}{\omega_{cy}^2\omega_y^2 + \omega_{cz}^2\omega_z^2 + \omega_y^2\omega_z^2}\sigma_y\end{aligned}$$

and

$$\begin{aligned}\Pi^{①\pm}_{\tilde{y}} &= \left(\frac{m\omega_{\tilde{y}}\hbar}{2}\right)^{1/2} \pm e\left(B_z - \xi B_y\right)\left(\frac{\hbar}{2m\omega_{\tilde{y}}}\right)^{1/2}, \\ \Pi^{①\pm}_{\tilde{z}} &= \left(\frac{m\omega_{\tilde{z}}\hbar}{2}\right)^{1/2} \pm e\left(B_z + \frac{1}{\xi}B_y\right)\left(\frac{\hbar}{2m\omega_{\tilde{z}}}\right)^{1/2}.\end{aligned}$$

The MEFs and the effective mass μ are given in (3.22) and (3.17) respectively.

② The Hamiltonian of system ② was deduced in Section 3.2.2 and the Bychkov-Rashba contribution was studied in Section 3.3.2. We found

$$H^{②} = \hbar\omega^{②}_{\tilde{y}}\left(b^\dagger_{\tilde{y}}b_{\tilde{y}} + \frac{1}{2}\right) + \hbar\omega^{②}_{\tilde{z}}\left(b^\dagger_{\tilde{z}}b_{\tilde{z}} + \frac{1}{2}\right) + \frac{\hbar^2k^2}{2\mu} + \frac{g}{2}\mu_{\mathrm{B}}\vec{\sigma}\vec{B} + H^{②}_{\mathrm{BR}}\,, \quad (3.50)$$

where

$$\begin{aligned}H^{②}_{\mathrm{BR}} &= \alpha\frac{1}{\hbar}\left[\sigma_x P_y - \sigma_y\left(\hbar k - eB_z Y\right)\right] = \\ &= \alpha N\frac{\mathrm{i}}{\hbar}\left[\left(\Pi^{②-}_{\tilde{y}}\sigma_+ + \Pi^{②+}_{\tilde{y}}\sigma_-\right)b^\dagger_{\tilde{y}} - \left(\Pi^{②+}_{\tilde{y}}\sigma_+ + \Pi^{②-}_{\tilde{y}}\sigma_-\right)b_{\tilde{y}} - \right. \\ &\quad \left. - \mathrm{i}\xi\left(\left(\Pi^{②-}_{\tilde{z}}\sigma_+ + \Pi^{②+}_{\tilde{z}}\sigma_-\right)b^\dagger_{\tilde{z}} + \left(\Pi^{②+}_{\tilde{z}}\sigma_+ + \Pi^{②-}_{\tilde{z}}\sigma_-\right)b_{\tilde{z}}\right)\right] + \\ &\quad - \alpha k\,\frac{\omega_y^2}{\omega_y^2 + \omega_{cz}^2}\sigma_y\end{aligned}$$

and

$$\begin{aligned}\Pi^{②\pm}_{\tilde{y}} &= \left(\frac{m\omega_{\tilde{y}}\hbar}{2}\right)^{1/2} \pm eB_z\left(\frac{\hbar}{2m\omega_{\tilde{y}}}\right)^{1/2}, \\ \Pi^{②\pm}_{\tilde{z}} &= \left(\frac{m\omega_{\tilde{z}}\hbar}{2}\right)^{1/2} \pm eB_z\left(\frac{\hbar}{2m\omega_{\tilde{z}}}\right)^{1/2}.\end{aligned}$$

The MEFs and the effective mass μ can be found in (3.32) and (3.26) respectively.

3.4.1 Using the High Field Approximation

For a strong external magnetic field and weak SOI, we can assume that the spins are aligned parallel or antiparallel to the field lines. Hence, one can make the substitution

$$\vec{\sigma} \to (n_x, n_y, n_z) \ ,$$

where the n_i are no operators, but scalars. This vector, which we will denote $\vec{n}$ in the following, must be normalized and we can write

$$\vec{\sigma} \to \vec{n} = \pm \left(\frac{B_x}{B}, \frac{B_y}{B}, \frac{B_z}{B} \right) \tag{3.51}$$

to ensure alignment along the field. The variable sign takes care of the two spin orientations which we may call $|+\rangle$ and $|-\rangle$ in analogy to the notation used in Chapter 3.3. Once we have done this substitution in one of the Hamiltonians (3.48), (3.49) or (3.50), we are able to solve the systems exactly without doing any other approximation. The limitation to this technique is that SOI rotates the spins out of the alignment. This may be negligible, but for strong SO coupling we cannot define a global and fixed spin orientation,[10] thus we cannot substitute $\vec{\sigma}$ with a fixed vector. Particularly this method does not work for the degenerate case (Chap. 3.3), where SOI is very dominant. In the following we discuss this approximation method for the Hamiltonians of the two- and three-dimensional systems separately. A summary and short discussion will conclude this section.

(2D) Looking at the Hamiltonian (3.48), we see that within the high field approximation we can diagonalize the system by using a constant shift of the ladder operator

$$b'_{y'} := b_{y'} + \alpha \sqrt{\frac{m}{2\hbar^3 \Omega_{y,cz}}} \left(\frac{\omega_{cz}}{\Omega_{y,cz}} n_y + \mathrm{i} n_x \right) \ .$$

The final Hamiltonian then reads

$$\begin{aligned} H^{(2D)} = & \hbar\Omega_{y,cz} \left(b'^{\dagger}_{y'} b'_{y'} + \frac{1}{2} \right) + \frac{\hbar^2 k^2}{2\mu} + \frac{g}{2} \mu_{\mathrm{B}} \vec{n} \vec{B} - \\ & - \alpha k \frac{\omega_y^2}{\Omega_{y,cz}^2} n_y - \alpha^2 \frac{m}{2\hbar^2} \left(n_x^2 + \frac{\omega_{cz}^2}{\Omega_{y,cz}^2} n_y^2 \right) \end{aligned} \tag{3.52}$$

with $\Omega_{y,cz}^2 = \omega_y^2 + \omega_{cz}^2$ and $\mu = m \left(1 + \frac{\omega_{cz}^2}{\omega_y^2} \right)$ (comp. p. 58). The term linear in the Bychkov-Rashba parameter is the equivalent to the direct term (3.42a) that we

[10] Recall that the spin-orbit field B_{SO} depends on the quasi-momentum $\vec{k}$ [12, 45, 51].

obtained via degenerate perturbation theory in Section 3.3.1 and is proportional to the normalized magnetic field component in y-direction. The term quadratic in α is new and gives a second order correction to the Hamiltonian. Note that the only operator that is left, is the number operator $b'^{\dagger}_{y'} b'_{y'}$ of the harmonic oscillator. Thus the solution is trivial.

① In this system, where $n_x = 0$ since $B_x = 0$, the Hamiltonian (3.49) is diagonalized in the same spirit as in ②D. This means that shifting the operators according to

$$b'_{\tilde{y}} := b_{\tilde{y}} + \alpha N \sqrt{\frac{m}{2\hbar^3 \omega_{\tilde{y}}^3}}\, \omega_{cz}(-\xi)\, n_y \ ,$$
$$b'_{\tilde{z}} := b_{\tilde{z}} - \alpha N \xi \sqrt{\frac{m}{2\hbar^3 \omega_{\tilde{z}}^3}}\, \omega_{cz}(\xi^{-1})\, n_y \ ,$$

we end up with

$$\begin{aligned} H^{①} = &\hbar\omega_{\tilde{y}} \left(b'^{\dagger}_{\tilde{y}} b'_{\tilde{y}} + \frac{1}{2} \right) + \hbar\omega_{\tilde{z}} \left(b'^{\dagger}_{\tilde{z}} b'_{\tilde{z}} + \frac{1}{2} \right) + \frac{\hbar^2 k^2}{2\mu} + \frac{g}{2} \mu_{\mathrm{B}} \vec{n} \vec{B} - \\ &- \alpha k \, \frac{\omega_y^2 \omega_z^2}{\omega_{cy}^2 \omega_y^2 + \omega_{cz}^2 \omega_z^2 + \omega_y^2 \omega_z^2}\, n_y - \\ &- \alpha^2 \frac{m}{2\hbar^2} \left(N^2 \frac{\left(\omega_{cz}(-\xi)\right)^2}{\omega_{\tilde{y}}^2} + N^2 \xi^2 \frac{\left(\omega_{cz}(\xi^{-1})\right)^2}{\omega_{\tilde{z}}^2} \right) n_y^2 \ , \end{aligned} \tag{3.53}$$

where we have already used the short hand notation (3.58) which will be introduced in Section 3.4.2. The effective mass μ and the transformation variable ξ are given in (3.17) and (3.18) respectively. The term linear in α is, in analogy to the two-dimensional case, related to the direct term (3.45a) of the perturbative result that we obtained in Section 3.3.2. The quadratic term is a new feature and it is obvious that this one is more general than the corresponding term above since it takes care of the coordinate system rotation which depends on ξ.

② Finally, let us look at system ② and the corresponding Hamiltonian (3.50). The shifted ladder operators read

$$b'_{\tilde{y}} := b_{\tilde{y}} + \alpha \mathrm{i} N \sqrt{\frac{m}{2\hbar^3 \omega_{\tilde{y}}}}\, n_x \ ,$$
$$b'_{\tilde{z}} := b_{\tilde{z}} + \alpha N \xi \sqrt{\frac{m}{2\hbar^3 \omega_{\tilde{z}}}}\, n_x \ ,$$

and the Hamiltonian becomes

$$H^{②} = \hbar\omega_{\tilde{y}} \left(b'^{\dagger}_{\tilde{y}} b'_{\tilde{y}} + \frac{1}{2} \right) + \hbar\omega_{\tilde{z}} \left(b'^{\dagger}_{\tilde{z}} b'_{\tilde{z}} + \frac{1}{2} \right) + \frac{\hbar^2 k^2}{2\mu} + \frac{g}{2} \mu_{\mathrm{B}} \vec{n} \vec{B} - \alpha^2 \frac{m}{2\hbar^2} n_x^2 \ , \tag{3.54}$$

where μ and ξ are given in (3.26) and (3.27) respectively. In this system the in-plane field is parallel to the direction of transport (x-direction) and thus $n_y = 0$. An interesting outcome is that the term linear in the Bychkov-Rashba parameter disappears. This is in agreement with the fact that the matrix element H_{++} (3.45a) of the perturbative treatment in Sect. 3.3.2 vanishes as well. Moreover it is important to note that the quadratic term is independent of the rotation variable ξ, thus it is a fundamental property which does not change compared to the two-dimensional approximation. It is only dependent on the magnetic field in x-direction.

To get an intuitive feeling for these Hamiltonians and the effects of spin-orbit coupling, let us neglect terms of the order $O(\alpha^2 \frac{m}{\hbar^2})$ and look at the dispersion relation. $H^{\textcircled{2D}}$ (3.52) can then be written as

$$H^{\textcircled{2D}} \cong \hbar\Omega_{y,cz}\left(b'^{\dagger}_{y'} b'_{y'} + \frac{1}{2}\right) + \frac{\left(\hbar k - \alpha \frac{m}{\hbar} n_y\right)^2}{2\mu} + \frac{g}{2}\mu_{\mathrm{B}}\vec{n}\vec{B}\ , \tag{3.55}$$

whereas from (3.53) we get the Hamiltonian

$$H^{①} \cong \hbar\omega_{\tilde{y}}\left(b'^{\dagger}_{\tilde{y}} b'_{\tilde{y}} + \frac{1}{2}\right) + \hbar\omega_{\tilde{z}}\left(b'^{\dagger}_{\tilde{z}} b'_{\tilde{z}} + \frac{1}{2}\right) + \frac{\left(\hbar k - \alpha \frac{m}{\hbar}\,\zeta\, n_y\right)^2}{2\mu} + \frac{g}{2}\mu_{\mathrm{B}}\vec{n}\vec{B} \tag{3.56}$$

with

$$\zeta := \frac{\left(\omega_y^2 + \omega_{cz}^2\right)\omega_z^2}{\omega_{cy}^2\omega_y^2 + \omega_{cz}^2\omega_z^2 + \omega_y^2\omega_z^2}\ ,$$

and (3.54) of system ② becomes

$$H^{②} \cong \hbar\omega_{\tilde{y}}\left(b'^{\dagger}_{\tilde{y}} b'_{\tilde{y}} + \frac{1}{2}\right) + \hbar\omega_{\tilde{z}}\left(b'^{\dagger}_{\tilde{z}} b'_{\tilde{z}} + \frac{1}{2}\right) + \frac{\hbar^2 k^2}{2\mu} + \frac{g}{2}\mu_{\mathrm{B}}\vec{n}\vec{B}\ . \tag{3.57}$$

In a nutshell, we find that a magnetic field in y-direction shifts the dispersion relation parabolas of opposite spin orientation into different directions while a magnetic field in x-direction leaves the dispersion relation unchanged. This is sketched in Fig. 3.8. Note that it holds $\zeta \to 1$ for $\frac{\omega_y}{\omega_z} \ll \frac{\Omega_{y,cz}}{|\omega_{cy}|}$, which ensures and verifies that the kinetic parts of $H^{①}$ and $H^{\textcircled{2D}}$ coincide in the limit of an infinitely thin 2DES. In fact, for vanishing perpendicular field the condition simplifies to $\omega_{cy} \ll \omega_z$ and therefore we get $B_y \ll 4\,\mathrm{T}$ and $B_y \ll 70\,\mathrm{T}$ for an AlGaAs/GaAs/AlGaAs quantum well with the oscillator lengths $l = 12\,\mathrm{nm}$ and $l = 3\,\mathrm{nm}$ respectively.

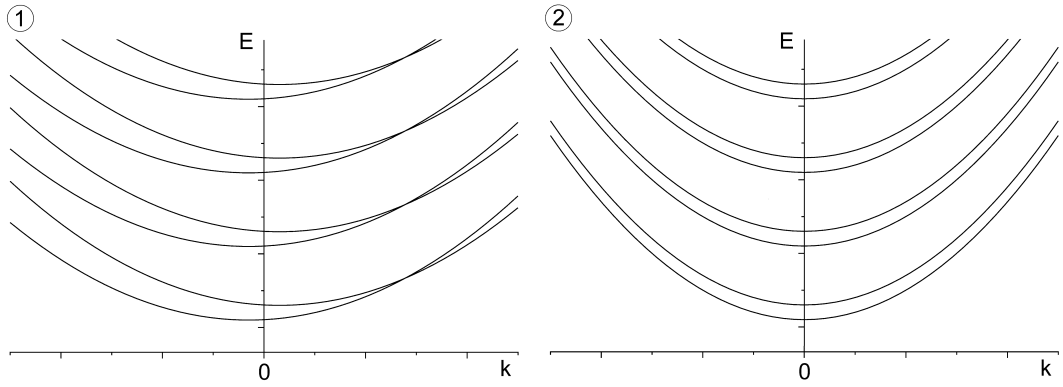

Figure 3.8: Schematic band structure for the lowest subband of the Hamiltonians $H^{①}$ (3.56) and $H^{②}$ (3.57) in arbitrary units. With respect to system ②, the $|+\rangle$ and $|-\rangle$ parabolas of system ① are shifted into opposite directions and flattened due to the larger effective mass μ. Note that for the region of the band crossing in system ① the description is incomplete since this approximation excludes explicitly the degenerate case. However, the horizontal shift was exaggerated for clarity and crossing would only occur for very large k-vectors.

3.4.2 Using the Spin Space Rotation

A complementary way to create an effective Hamiltonian, which takes care of spin-orbit coupling up to a desired order, is done by a unitary transformation which rotates locally the spin space [20]. In general, a spin space rotation of Θ around the unit vector $\hat{\Theta}$ is described by

$$U = \mathrm{e}^{-\frac{\mathrm{i}}{\hbar}\vec{\Theta}\vec{S}} ,$$

where the spin operator $\vec{S} = \frac{\hbar}{2}\vec{\sigma}$ is the generator of the rotation. In the present model systems the vector $\vec{\Theta}$ depends on both position and momentum operators, i.e. the local rotation is specified by a point in both real and momentum space. The resulting Hamiltonian is valid for arbitrarily strong magnetic fields and has no limitations on degenerate states. However, in order to solve these effective Hamiltonians one would need further approximations or numerical methods. Nevertheless they are useful to deduce important effects of SO coupling intuitively as we will see later.

The transformations for all three systems ㉔, ①, ② follow the same scheme which we introduce first. After that we derive the effective Hamiltonians for the specific systems.

Note that in this introductory part, we use hats to indicate operators for clarity, but we will resume to the stipulated notation afterwards. The basic idea is as follows:
For a Hamiltonian of the form

$$H = E\hat{b}^\dagger\hat{b} + \gamma\vec{\sigma}\vec{B} + \hat{M}\sigma_x + \hat{N}\sigma_y + L\sigma_y + C \ ,$$

where $\hat{b}^\dagger$, $\hat{b}$ are ladder operators, $\vec{B}$ is the magnetic field, σ_i is the i-th Pauli matrix, $\hat{M}$, $\hat{N}$ are functions of the ladder operators and E, γ, L, C are constants, one can think of a unitary transformation

$$U = \mathrm{e}^{\hat{\mathcal{R}}}$$

with an antihermitian $\hat{\mathcal{R}}$, i.e. $\hat{\mathcal{R}}^\dagger = -\hat{\mathcal{R}}$, which can be written as

$$\hat{\mathcal{R}} = \alpha\left(\hat{V}\sigma_x + \hat{W}\sigma_y\right) \ ,$$

where α is the Bychkov-Rashba parameter and $\hat{V}$, $\hat{W}$ are functions of the ladder operators, that can be expressed in a Taylor series

$$U = \mathrm{e}^{\hat{\mathcal{R}}} = 1 + \hat{\mathcal{R}} + O(\hat{\mathcal{R}}^2)$$

from what follows that

$$UHU^\dagger = H + \left[\hat{\mathcal{R}}, H\right] + O(\hat{\mathcal{R}}^2) \ .$$

Once we can find an $\hat{\mathcal{R}}$ which satisfies

$$\left[\hat{\mathcal{R}}, H\right] = -\hat{M}\sigma_x - \hat{N}\sigma_y + \hat{Q}\sigma_z + O(\hat{\mathcal{R}}^2) \ ,$$

with $\hat{Q} = \hat{Q}(\hat{b}^\dagger, \hat{b})$, we are left with a Hamiltonian of the form

$$\tilde{H} := UHU^\dagger = E\hat{b}^\dagger\hat{b} + \gamma\vec{\sigma}\vec{B} + \hat{Q}\sigma_z + L\sigma_y + C + O(\hat{\mathcal{R}}^2) \ ,$$

which can be written as

$$\tilde{H} \cong E\hat{b}^\dagger\hat{b} + \gamma\vec{\sigma}\vec{\tilde{B}} + C \ ,$$

where

$$\vec{\tilde{B}} := \begin{pmatrix} B_x \\ B_y + L \\ B_z + \hat{Q} \end{pmatrix} \ .$$

This is the framework that we will follow in the calculations of each system. In order to simplify the results appropriately, it proves useful to define the formal function $\omega_{cz} = \omega_{cz}(\xi)$ which reads

$$\omega_{cz}(\xi) := \omega_{cz} + \xi\omega_{cy} \ . \tag{3.58}$$

Particularly it holds $\omega_{cz}(0) = \omega_{cz}$ and we can use this as a generalization of the partial cyclotron frequency ω_{cz}. Then the transformations and resulting effective Hamiltonians of our model systems are given as follows:

(2D) We start with the two-dimensional approach which should already reveal the general behavior of a system with BR-SO coupling for an arbitrarily orientated magnetic field. But since it does not consider the third dimension, the method leads to a less accurate description of the effects. The Hamiltonian $H^{(2D)}$ (3.52) is transformed via

$$\tilde{H}^{(2D)} = U H^{(2D)} U^\dagger = \mathrm{e}^{\mathcal{R}} H^{(2D)} \mathrm{e}^{-\mathcal{R}} \,,$$

where

$$\mathcal{R} = \alpha \sqrt{\frac{m}{2\hbar^3 \Omega_{y,cz}}} \left[\frac{\Omega_{y,cz}^2 + \bar{g}\omega_{cz}^2}{\Omega_{y,cz}^2 - \bar{g}^2\omega_{cz}^2} \,\mathrm{i} \left(b_{y'}^\dagger + b_{y'} \right) \sigma_x + \frac{\Omega_{y,cz}\,(1+\bar{g})\,\omega_{cz}}{\Omega_{y,cz}^2 - \bar{g}^2\omega_{cz}^2} \left(b_{y'}^\dagger - b_{y'} \right) \sigma_y \right] .$$

The exponent consists of two parts: one proportional to $Y' \sigma_x$, the other $\propto P_{y'} \sigma_y$. With this choice of $\mathcal{R}$ and neglecting terms of the order $\mathcal{R}^2$, we can write the transformed Hamiltonian as

$$\tilde{H}^{(2D)} = \hbar\Omega_{y,cz} \left(b_{y'}^\dagger b_{y'} + \frac{1}{2} \right) + \frac{\hbar^2 k^2}{2\mu} + \frac{g}{2} \mu_\mathrm{B} \vec{\sigma} \vec{\tilde{B}} \tag{3.59a}$$

with

$$\vec{\tilde{B}} = \begin{pmatrix} B_x \\ B_y - \alpha k \dfrac{\omega_y^2}{\Omega_{y,cz}^2} \dfrac{2}{g\mu_\mathrm{B}} \\ B_z - \alpha \sqrt{\dfrac{2m}{\hbar^3 \Omega_{y,cz}}} \left(\mathfrak{B}^* b_{y'}^\dagger + \mathfrak{B} b_{y'} \right) \end{pmatrix} ,$$

where we defined

$$\mathfrak{B} := \frac{\left(\Omega_{y,cz}^2 + \bar{g}\omega_{cz}^2 \right) B_y - \mathrm{i}\Omega_{y,cz}\,(1+\bar{g})\,\omega_{cz} B_x}{\Omega_{y,cz}^2 - \bar{g}^2\omega_{cz}^2} \,.$$

The operator-dependent part of the generalized Zeeman term can also be incorporated into the harmonic oscillator. This leads to an equivalent form of the Hamiltonian which is given by

$$\tilde{H}^{(2D)} = \frac{\left(P_{y'} + \alpha \dfrac{\bar{g}e}{\hbar\Omega_{y,cz}} \mathrm{Im}(\mathfrak{B}) \sigma_z \right)^2}{2m} + \frac{1}{2} m \Omega_{y,cz}^2 \left(Y' - \alpha \frac{\bar{g}e}{m\hbar\Omega_{y,cz}^2} \mathrm{Re}(\mathfrak{B}) \sigma_z \right)^2 +$$

$$+\frac{\hbar^2k^2}{2\mu}+\frac{g}{2}\mu_{\mathrm{B}}\vec{\sigma}\begin{pmatrix} B_x \\ B_y-\alpha k\dfrac{\omega_y^2}{\Omega_{y,cz}^2}\dfrac{2}{g\mu_{\mathrm{B}}} \\ B_z \end{pmatrix}. \tag{3.59b}$$

We find a modification of the parabolas which is different for opposite spin orientations in both position and momentum space, the former proportional to B_y, the latter proportional to B_x. Note moreover that it holds $\mathfrak{B}|_{B_z=0}=B_y$, that is for vanishing perpendicular field the shift of the momentum operator disappears. In the remaining Zeeman term the effective field in y-direction becomes k-dependent whereas the magnetic field parallel to the quantum wire, B_x, remains the same for all configurations.

① To go beyond this, we start with system ① where the in-plane field is along the y-direction. The exponent of the momentum and position dependent spin rotation transforming Hamiltonian $H^{①}$ (3.49) is given by

$$\mathcal{R}=\alpha N\sqrt{\frac{m}{2\hbar^3\omega_{\tilde{y}}}}\left[\frac{\omega_{\tilde{y}}^2+\omega_{cz}(-\xi)\bar{g}\omega_{cz}}{\omega_{\tilde{y}}^2-\bar{g}^2\omega_{cz}^2}\mathrm{i}\left(b_{\tilde{y}}^\dagger+b_{\tilde{y}}\right)\sigma_x+\frac{\omega_{\tilde{y}}(\omega_{cz}(-\xi)+\bar{g}\omega_{cz})}{\omega_{\tilde{y}}^2-\bar{g}^2\omega_{cz}^2}\left(b_{\tilde{y}}^\dagger-b_{\tilde{y}}\right)\sigma_y\right]-$$
$$-\alpha N\xi\sqrt{\frac{m}{2\hbar^3\omega_{\tilde{z}}}}\left[\frac{\omega_{\tilde{z}}^2+\omega_{cz}(\xi^{-1})\bar{g}\omega_{cz}}{\omega_{\tilde{z}}^2-\bar{g}^2\omega_{cz}^2}\mathrm{i}\left(b_{\tilde{z}}^\dagger+b_{\tilde{z}}\right)\sigma_x+\frac{\omega_{\tilde{z}}\left(\omega_{cz}(\xi^{-1})+\bar{g}\omega_{cz}\right)}{\omega_{\tilde{z}}^2-\bar{g}^2\omega_{cz}^2}\left(b_{\tilde{z}}^\dagger-b_{\tilde{z}}\right)\sigma_y\right]$$

which resembles the two-dimensional case but taking the additional dimension and the weighting between these via the prefactors N and $-N\xi$ into account. The resulting Hamiltonian reads

$$\tilde{H}^{①}=\hbar\omega_{\tilde{y}}\left(b_{\tilde{y}}^\dagger b_{\tilde{y}}+\frac{1}{2}\right)+\hbar\omega_{\tilde{z}}\left(b_{\tilde{z}}^\dagger b_{\tilde{z}}+\frac{1}{2}\right)+\frac{\hbar^2k^2}{2\mu}+\frac{g}{2}\mu_{\mathrm{B}}\vec{\sigma}\vec{\tilde{B}} \tag{3.60a}$$

with

$$\vec{\tilde{B}}=\begin{pmatrix} 0 \\ \dfrac{\omega_{\tilde{y}}^2\omega_z^2}{\omega_{cy}^2\omega_{\tilde{y}}^2+\omega_{cz}^2\omega_z^2+\omega_{\tilde{y}}^2\omega_z^2}\dfrac{2}{g\mu_{\mathrm{B}}} \\ B_z-\alpha N\sqrt{\dfrac{2m}{\hbar^3\omega_{\tilde{y}}}}\left(\mathfrak{B}_{\tilde{y}}^*b_{\tilde{y}}^\dagger+\mathfrak{B}_{\tilde{y}}b_{\tilde{y}}\right)+\alpha N\xi\sqrt{\dfrac{2m}{\hbar^3\omega_{\tilde{z}}}}\left(\mathfrak{B}_{\tilde{z}}^*b_{\tilde{z}}^\dagger+\mathfrak{B}_{\tilde{z}}b_{\tilde{z}}\right) \end{pmatrix},$$

where we defined

$$\mathfrak{B}_{\tilde{y}}:=\frac{\omega_{\tilde{y}}^2+\omega_{cz}(-\xi)\bar{g}\omega_{cz}}{\omega_{\tilde{y}}^2-\bar{g}^2\omega_{cz}^2}B_y\in\mathbb{R},$$

$$\mathfrak{B}_{\tilde{z}}:=\frac{\omega_{\tilde{z}}^2+\omega_{cz}(\xi^{-1})\bar{g}\omega_{cz}}{\omega_{\tilde{z}}^2-\bar{g}^2\omega_{cz}^2}B_y\in\mathbb{R},$$

and can equivalently be written as

$$\begin{aligned}\tilde{H}^{①} = & \frac{P_{\tilde{y}}}{2m} + \frac{1}{2}m\omega_{\tilde{y}}^2\left(\tilde{Y} - \alpha N\frac{\bar{g}e}{m\hbar\omega_{\tilde{y}}^2}\mathfrak{B}_{\tilde{y}}\sigma_z\right)^2 + \\ & + \frac{P_{\tilde{z}}}{2m} + \frac{1}{2}m\omega_{\tilde{z}}^2\left(\tilde{Z} + \alpha N\xi\frac{\bar{g}e}{m\hbar\omega_{\tilde{z}}^2}\mathfrak{B}_{\tilde{z}}\sigma_z\right)^2 + \\ & + \frac{\hbar^2k^2}{2\mu} + \frac{g}{2}\mu_{\mathrm{B}}\vec{\sigma}\begin{pmatrix} 0 \\ B_y - \alpha k\dfrac{\omega_y^2\omega_z^2}{\omega_{cy}^2\omega_y^2 + \omega_{cz}^2\omega_z^2 + \omega_y^2\omega_z^2}\dfrac{2}{g\mu_{\mathrm{B}}} \\ B_z\end{pmatrix}.\end{aligned} \tag{3.60b}$$

Hence, both real space parabolas are shifted as a function of the magnetic field but opposite for different spin orientations. Moreover, in analogy to the previous case, it holds $\mathfrak{B}_{\tilde{y}}|_{B_z=0} = \mathfrak{B}_{\tilde{z}}|_{B_z=0} = B_y$ and we also get a k-dependent effective magnetic field in y-direction, but more general than in the two-dimensional approximation.

② The three-dimensional approach to the case of an in-plane field parallel to the x-axis, system ②, leads to the Hamiltonain $H^{②}$ (3.50). The spin space rotation is described by

$$\begin{aligned}\mathcal{R} = & \alpha N\sqrt{\frac{m}{2\hbar^3\omega_{\tilde{y}}}}\left[\frac{\omega_{\tilde{y}}^2 + \bar{g}\omega_{cz}^2}{\omega_{\tilde{y}}^2 - \bar{g}^2\omega_{cz}^2}\,\mathrm{i}\left(b_{\tilde{y}}^\dagger + b_{\tilde{y}}\right)\sigma_x + \frac{\omega_{\tilde{y}}\left(1+\bar{g}\right)\omega_{cz}}{\omega_{\tilde{y}}^2 - \bar{g}^2\omega_{cz}^2}\left(b_{\tilde{y}}^\dagger - b_{\tilde{y}}\right)\sigma_y\right] + \\ & + \alpha N\xi\sqrt{\frac{m}{2\hbar^3\omega_{\tilde{z}}}}\left[\frac{\omega_{\tilde{z}}^2 + \bar{g}\omega_{cz}^2}{\omega_{\tilde{z}}^2 - \bar{g}^2\omega_{cz}^2}\left(b_{\tilde{z}}^\dagger - b_{\tilde{z}}\right)\sigma_x - \frac{\omega_{\tilde{z}}\left(1+\bar{g}\right)\omega_{cz}}{\omega_{\tilde{z}}^2 - \bar{g}^2\omega_{cz}^2}\,\mathrm{i}\left(b_{\tilde{z}}^\dagger + b_{\tilde{z}}\right)\sigma_y\right]\end{aligned}$$

and the Hamiltonian after the transformation reads

$$\tilde{H}^{②} = \hbar\omega_{\tilde{y}}\left(b_{\tilde{y}}^\dagger b_{\tilde{y}} + \frac{1}{2}\right) + \hbar\omega_{\tilde{z}}\left(b_{\tilde{z}}^\dagger b_{\tilde{z}} + \frac{1}{2}\right) + \frac{\hbar^2k^2}{2\mu} + \frac{g}{2}\mu_{\mathrm{B}}\vec{\sigma}\vec{\tilde{B}} \tag{3.61a}$$

with

$$\vec{\tilde{B}} = \begin{pmatrix} B_x \\ -\alpha k\dfrac{\omega_y^2}{\omega_y^2 + \omega_{cz}^2}\dfrac{2}{g\mu_{\mathrm{B}}} \\ B_z - \alpha N\sqrt{\dfrac{2m}{\hbar^3\omega_{\tilde{y}}}}\left(\mathfrak{B}_{\tilde{y}}^* b_{\tilde{y}}^\dagger + \mathfrak{B}_{\tilde{y}} b_{\tilde{y}}\right) - \alpha N\xi\sqrt{\dfrac{2m}{\hbar^3\omega_{\tilde{z}}}}\left(\mathfrak{B}_{\tilde{z}}^* b_{\tilde{z}}^\dagger + \mathfrak{B}_{\tilde{z}} b_{\tilde{z}}\right)\end{pmatrix},$$

where we defined

$$\mathfrak{B}_{\tilde{y}} := \frac{-\mathrm{i}\omega_{\tilde{y}}\left(1+\bar{g}\right)\omega_{cz}B_x}{\omega_{\tilde{y}}^2 - \bar{g}^2\omega_{cz}^2} \notin \mathbb{R}\,,$$

$$\mathfrak{B}_{\tilde{z}} := \frac{\omega_{\tilde{z}}\,(1+\bar{g})\,\omega_{cz} B_x}{\omega_{\tilde{z}}^2 - \bar{g}^2\omega_{cz}^2} \in \mathbb{R}\ .$$

In the same spirit as above, we merge the operator-dependent Zeeman term into the oscillators

$$\begin{aligned}\tilde{H}^{②} =& \frac{\left(P_{\tilde{y}} + \alpha N \frac{\bar{g}e}{\hbar\omega_{\tilde{y}}} \operatorname{Im}(\mathfrak{B}_{\tilde{y}})\sigma_z\right)^2}{2m} + \frac{1}{2} m\omega_{\tilde{y}}^2 \tilde{Y}^2 + \\ &+ \frac{P_{\tilde{z}}^2}{2m_{\tilde{z}}} + \frac{1}{2} m_{\tilde{z}}\omega_{\tilde{z}}^2 \left(\tilde{Z} - \alpha N \xi \frac{\bar{g}e}{m\hbar\omega_z\omega_{\tilde{z}}} \mathfrak{B}_{\tilde{z}}\sigma_z\right)^2 + \\ &+ \frac{\hbar^2 k^2}{2\mu} + \frac{g}{2}\mu_{\mathrm{B}} \vec{\sigma} \begin{pmatrix} B_x \\ -\alpha k \frac{\omega_y^2}{\omega_y^2 + \omega_{cz}^2} \frac{2}{g\mu_{\mathrm{B}}} \\ B_z \end{pmatrix}\end{aligned} \tag{3.61b}$$

with $m_{\tilde{z}}$ defined in (3.30), and obtain that both the momentum operator $P_{\tilde{y}}$ and the position operator $\tilde{Z}$ are shifted. However, since these operators are linear combinations of the "real" position and momentum operators (comp. (3.28)), we cannot directly compare these shifts with the ones of ㉔ (3.59b). As argued in Section 3.2.4, the axes $\tilde{y}$ and $\tilde{z}$ span a coordinate system with a non-trivial real space representation, thus it is hard to interpret the shifts intuitively. Nevertheless, more important is that all shifts vanish for a pure in-plane field, i.e. $\vec{B} = B_x \hat{e}_x$, which is in contrast to system ① (comp. (3.60b)).

4 Anisotropies in Narrow Wires

At last we want to focus on narrow quantum wires ($\omega_y \neq 0$), where the system shows anisotropic behavior for an in-plane field perpendicular or parallel to the transport direction. For this setup we expect to observe a difference in the energies of the Landau levels, in the curvature of the dispersion relation, in the required magnetic field that is needed to make the spin-polarized, Zeeman split Landau levels overlap, in the energy contribution at the crossing due to BR-SOI, and to have an intrinsic SO-induced shift of the energy parabolas in the case of an in-plane field along the y-direction. In the following we will emphasize these anisotropies and give some food for thought how these can be measured.

4.1 Collecting Anisotropic Quantities

In order to stress the anisotropic behavior, let us define the quantity $\digamma$

$$\digamma := \begin{cases} +1 & \text{for system ①} \\ -1 & \text{for system ②} \end{cases} \tag{4.1}$$

which reflects the differences of system ① and system ② with a simple sign, and rewrite the variables with respect to $\digamma$.

The magneto-electric frequencies, given in (3.13), (3.15), then read

$$\begin{aligned} \omega_\pm^2 = \frac{1}{2}\Big[& \omega_y^2 + \omega_z^2 + \omega_{\text{cip}}^2 + \omega_{cz}^2 \pm \big[\omega_y^4 + \omega_z^4 + \omega_{\text{cip}}^4 + \omega_{cz}^4 + \\ & + 2\left(-\omega_y^2\omega_z^2 + \omega_y^2\omega_{cz}^2 + \omega_z^2\omega_{\text{cip}}^2 - \omega_z^2\omega_{cz}^2 + \omega_{\text{cip}}^2\omega_{cz}^2 - \digamma\,\omega_y^2\omega_{\text{cip}}^2\right)\big]^{\frac{1}{2}} \Big] \end{aligned} \tag{4.2}$$

where ω_{cip} is the partial cyclotron frequency of the corresponding in-plane field.

The effective mass μ (3.17), (3.26), whose inverse is proportional to the curvature of the dispersion relation, can be written as

$$\mu = m\left(1 + \frac{\omega_{cz}^2}{\omega_y^2} + \frac{\omega_{\mathrm{cip}}^2}{\omega_z^2}\,\frac{1+F}{2}\right) . \tag{4.3}$$

The condition for the in-plane magnetic field (3.43), which is needed to make the Zeeman split, spin-polarized Landau levels overlap, was presented in Chapter 3.3 for the limit $\omega_y \to 0$ and it was stated that this can be used as approximation for both system ① and ② of wide waveguides. The exact expression for a semiconductor system with $|g| < 2$ is somewhat more complicated. Neglecting the parabola shift due to SOI, it reads

$$\begin{aligned}\omega_{\mathrm{cip}}^2 = \frac{\omega_y^2+\omega_z^2}{2\left(\bar{g}^2-1\right)} - \omega_{cz}^2 - \frac{1}{4\left(\bar{g}^2-1\right)\bar{g}^2}\left(1+F\right)\omega_y^2 - \frac{1}{2\left(\bar{g}^2-1\right)}\Bigg[\left(\omega_y^2-\omega_z^2\right)^2 - \\ - 4\left(\bar{g}^2-1\right)\frac{\omega_{cz}^2\omega_z^2}{\bar{g}^2} + \frac{4}{\bar{g}^2}\omega_y^2\omega_z^2 - \frac{1}{\bar{g}^2}\left(\frac{\bar{g}^2-1}{\bar{g}^2}\omega_y^2 + \omega_z^2 - 8\left(\bar{g}^2-1\right)\omega_{cz}^2\right)\left(1+F\right)\omega_y^2\Bigg]^{\frac{1}{2}}\end{aligned} \tag{4.4}$$

where

$$\bar{g} := \frac{g}{2}\beta . \qquad \text{(same as (3.41))}$$

The formula expressing the energy correction $E_{n,k}^{1^{\mathrm{st}}}$ **at the crossing** is quite long and complicated, thus we stick to the forms given in Section 3.3.3.

The shift of the spin-polarized levels in k-space, which was derived in Section 3.4.1 using the high field approximation, can be described by a generalized wave number given by

$$\kappa := k - \alpha\zeta\frac{m}{\hbar^2}\frac{B_y}{B}\frac{1+F}{2} , \tag{4.5}$$

where

$$\zeta = \frac{\left(\omega_y^2+\omega_{cz}^2\right)\omega_z^2}{\omega_{cy}^2\omega_y^2 + \omega_{cz}^2\omega_z^2 + \omega_y^2\omega_z^2} .$$

With these definitions, the eigenvalues of both Hamiltonians (3.56), (3.57) read

$$E_{n,n'}(k) = \hbar\omega_-\left(n+\frac{1}{2}\right) + \hbar\omega_+\left(n'+\frac{1}{2}\right) + \frac{\hbar^2\kappa^2}{2\mu} + \frac{g}{2}\mu_{\mathrm{B}}\vec{n}\vec{B} , \tag{4.6}$$

where

$$\vec{n} = \pm \left(\frac{B_x}{B}, \frac{B_y}{B}, \frac{B_z}{B} \right) \ . \qquad \text{(comp. (3.51))}$$

4.2 Discussion

Finally we want to discuss the effects of in-plane magnetic fields, modeled by the DSA (Chap. 3), and, for narrow 2D quantum wires, the influence of the anisotropic quantities on transport experiments. For this purpose, we introduce in each part briefly the measurements and known results of systems without or with weak in-plane magnetic fields and conclude with perspectives on the alteration of the outcome in suggested setups where the DSA or even the anisotropies become important.

In the ballistic regime of a nanostructure, the conductance of a two-dimensional electron waveguide is given by[1]

$$G = \frac{e^2}{\pi\hbar} M \ , \tag{4.7}$$

where $M \in \mathbb{N}$ counts the (spin-degenerate) *transverse modes* below the Fermi energy, that is it gives the amount of occupied energy levels which contribute to transport. Without a magnetic field and for a fixed Fermi level, M depends on the width of the sample because this is what controls the spacings between the levels. Hence, changing the width also influences the conductance which reveals step-like behavior due to the discreteness of M (Fig. 4.1). This is fairly understood and has been proved by so-called *quantum point contact* (QPC) measurements [43, 44], where a lateral gate voltage perpendicular to a 2D quantum wire was used to tune the width of the conductor.
This theory can be extended by our work when adding an in-plane magnetic field to the QPC or, equivalently, to a narrow quantum wire. In the MEFs (4.2) the term proportional to Γ couples the width of the conductor with the strength of the in-plane magnetic field. For a vanishing perpendicular field, they read

$$\omega_\pm^2 = \frac{1}{2} \left[\omega_y^2 + \omega_z^2 + \omega_{\text{cip}}^2 \pm \sqrt{\omega_y^4 + \omega_z^4 + \omega_{\text{cip}}^4 + 2 \left(-\omega_y^2 \omega_z^2 + \omega_z^2 \omega_{\text{cip}}^2 - \Gamma \omega_y^2 \omega_{\text{cip}}^2 \right)} \right]$$

and if we assume that there is only one subband of the magneto-electric confinement ω_+ occupied, the effective width of the sample is only related to the frequency ω_-. Thus,

[1] In fact, G^{-1} is the *contact resistance* of a mesoscopic, ballistic waveguide sandwiched between two (infinitely) wide, '*reflectionless*' contacts in the *linear response* (or low bias) *regime*. For further details, see Ref. [4] or any other good book on mesoscopic transport theory.

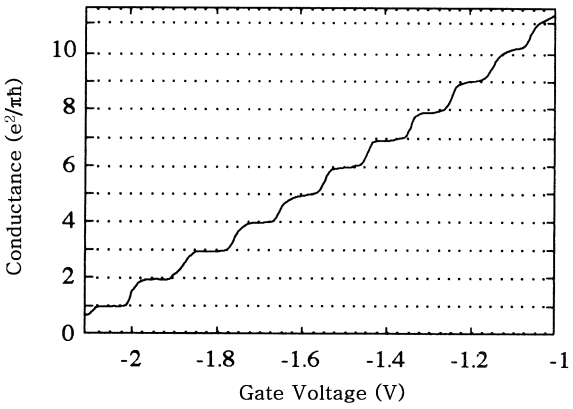

Figure 4.1: Conductance of a ballistic quantum point contact dependent on its width. Using the *split-gate configuration*, the gate voltage adjusts the effective width of the QPC which affects M. Therefore the conductance changes step-like according to (4.7). Reproduced from Ref. [4]. Original source: Ref. [43].

the number of occupied levels M is anisotropic in both the electrically controllable width concealed in ω_y and the applied magnetic field B_{ip}. A measurement of the conductance would reveal steps that are shifted with respect to the gate voltage for an in-plane magnetic field that is orientated perpendicular (system ①) or parallel (system ②) to the direction of transport. Moreover, note that due to the Zeeman splitting, additional conductance steps compared to ordinary QPC measurements should become visible since each spin-polarized level carries the conductance

$$G_{\uparrow\downarrow} = \frac{e^2}{2\pi\hbar} \,, \tag{4.8}$$

which is just half of the step height given in Fig. 4.1. We believe that these kinds of measurements on narrow quantum wires provide a feasible way to verify the theory and to explore the nature of the anisotropies in the experiment.

The situation changes fundamentally when applying a magnetic field perpendicular to the 2D conductor stripe [4, 10, 19]. The Lorentz force acts in the plane which leads to localized bulk states and extended edge states that can be explained semiclassically by circular orbits and *skipping orbits* respectively. In transport measurements it results in a linear increase of the resistance across the Hall bar at weak fields (regime of *low-field magnetoresistance*), Shubnikov-de Haas (SdH) oscillations of the longitudinal

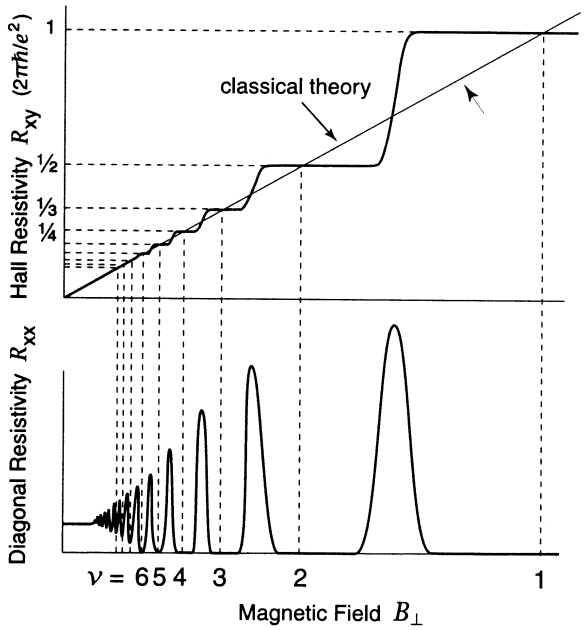

Figure 4.2: Schematic graph of transverse (top) and longitudinal (bottom) resistance of a Hall bar. One can easily distinguish the low field limit with linear behavior, the intermediate regime with SdH oscillations and the integer QHE for high magnetic fields. Note that the filling factors ν are integral where the Hall resistivity crosses the hypothetical, classical trajectory. Source: Ref. [10].

resistance in the intermediate regime (*high-field magnetoresistance*), and peaks of the longitudinal and steps of the transverse resistance for high magnetic fields (*integer quantum Hall effect* (integer QHE)).[2] This is sketched schematically in Fig. 4.2, where the *Hall plateaus* with their corresponding filling factors ν, which give the number of occupied, spin-resolved levels in the system,[3] are displayed. Note that in this graph the resistances are plotted with respect to the magnetic field strength. This is because the energy levels (of a wide Hall bar) are proportional to the cyclotron frequency ω_{cz} which is proportional to the perpendicular field and therefore, one can use B_z to make

[2]For even higher magnetic fields, one enters the regime of the *fractional quantum Hall effect* [10], which is a many-body effect and beyond the scope of this work.

[3]The filling factors possess strong similarity to the number of transverse modes M that we had before since one could argue $2M = \nu$ for complete filling of the Landau levels, which consist of two Zeeman split levels each. However, whereas M was defined to be natural, ν may be any positive number, thus it can also hold information about partial filling of the energy levels.

the levels pass through a quasichemical potential that is fixed during the measurement. For further details, we would like to refer to the literature, e.g. Ref. [4, 10, 19].
If we now consider a narrow Hall bar and an additional in-plane magnetic field, the Landau levels are determined by the anisotropic MEFs given by equation (4.2). Since the energy and energy spacings of the levels are determined by the anisotropic term $\hbar\omega_- \left(n + \frac{1}{2}\right)$, we expect the Hall plateaus and the conductance peaks in a graph similar to Fig. 4.2 to be shifted and also the width of and distance between them to change for a setup given by system ① and ② respectively. One would also expect to have increased frequencies of SdH oscillations which will be different for both orientations of the in-plane field, too. Moreover, note that the density of states changes as discussed in Chapter 2 according to (2.10) as well.
In the regime of low-field magnetoresistance, Drude's formula predicts for $\vec{B} = B\hat{e}_z$ a constant longitudinal resistivity of

$$\rho_{xx} = \sigma^{-1} = \frac{m}{e^2 n\tau}$$

whereas the transverse resistivity is linear in the perpendicular magnetic field

$$\rho_{yx} = -\rho_{xy} = \frac{B_z}{en}$$

what can also be read off qualitatively in Fig. 4.2. Here m is the bulk effective mass of the electron, n is the electron density and τ is the momentum relaxation time. In the *Drude model* [4] one can also include an arbitrarily orientated magnetic field and derive the resistivity tensor. It reads

$$\hat{\rho} = \sigma^{-1} \begin{pmatrix} 1 & -\mu_e B_z & \mu_e B_y \\ \mu_e B_z & 1 & -\mu_e B_x \\ -\mu_e B_y & \mu_e B_x & 1 \end{pmatrix} , \tag{4.9}$$

where $\sigma = en\mu_e$ is the conductivity and $\mu_e := \frac{e\tau}{m}$ the electron mobility. Setting the current density of the y- and z-direction to zero, one obtains

$$\text{System ①:} \quad \begin{pmatrix} E_x \\ E_y \\ E_z \end{pmatrix} = \sigma^{-1} \begin{pmatrix} 1 \\ \mu_e B_z \\ -\mu_e B_y \end{pmatrix} j_x ,$$

$$\text{System ②:} \quad \begin{pmatrix} E_x \\ E_y \\ E_z \end{pmatrix} = \sigma^{-1} \begin{pmatrix} 1 \\ \mu_e B_z \\ 0 \end{pmatrix} j_x .$$

Hence, in this model the longitudinal and transverse resistivity is isotropic and does not change due to the additional in-plane field. However, this model does not account

for any boundary conditions and we have shown that transport anisotropies occur only for narrow Hall bars with a non-negligible frequency ω_y. Taking into account the anisotropic effective mass μ (4.3) of the DSA and noting that the particle velocity is related to the slope of the dispersion relation via

$$v(k) = \frac{1}{\hbar}\frac{\partial E(k)}{\partial k} = \frac{\hbar k}{\mu} \ ,$$

we assume the in-plane field to have a direct influence on the resistance of a Hall bar in the low field regime below the SdH oscillations, i.e. the longitudinal resistivity is different for a field parallel or perpendicular to the direction of transport. This may be approximated by replacing the bulk electron mass in ρ_{xx} with μ.
We conclude that experimental analysis of narrow Hall bar resistivities could provide deeper insight into the effects of transverse magnetic fields and the involved anisotropies. These model systems could provide a basic framework for further investigations on transport properties of any laterally confined system with arbitrarily orientated magnetic field such as quantum dots or other complex structures.

A special situation occurs when an in-plane magnetic field is used to increase the Zeeman splitting such as the spin-polarized energy bands of neighboring Landau levels overlap (comp. Chap. 3.3). The condition (4.4) predicts that the required field is different for the contemplated systems ① and ②, thus it seems possible that this difference can be detected in associated experiments, so-called *coincidence measurements* [26, 49]. However, due to the strong dependence of (4.4) on the Landé factor and the bulk effective mass via the partial cyclotron frequencies, it is not obvious whether this discrepancy can really be measured since we do not have analytic formulas for these quantities, hence we cannot exactly state how these quantities behave in this limit (comp. p. 11). At least, it is challenging to give reliable, accurate predictions for the required in-plane magnetic fields, but they can be approximated using adequate values for g and m or using the bulk values as a first approach. Nevertheless, it turned out that the requirements for level coincidence may indeed be very different for both systems as we will see later (p. 79).
Assuming to be in the regime of coincidence, one can continue to argue that BR-SOI provides a non-negligible contribution to the eigenenergies of the system which was calculated by first order degenerate perturbation theory in Chapter 3.3 for the 2D-EMA and the DSA. This energy correction ($E^{1^{\text{st}}}_{n,k}$) leads to a repulsion of the bands which, however, vanishes if $\vec{B} = B\hat{e}_x$ (Fig. 4.3). Since the band anticrossing is proportional to the Bychkov-Rashba parameter α, one could use this effect to determine the spin-orbit

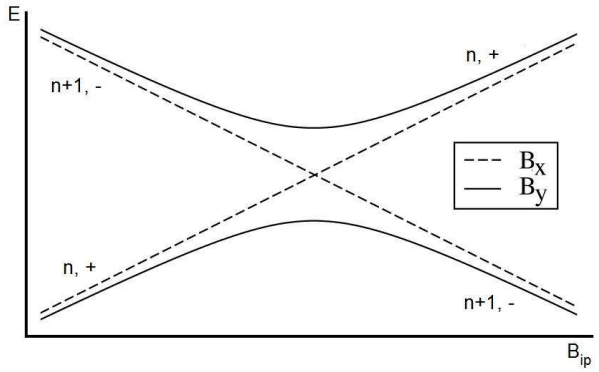

Figure 4.3: Schematic crossing of two spin-polarized energy levels due to an in-plane magnetic field for the case $B_z = 0$, $k = 0$. The field is directed in either y- or x-direction, which corresponds to system ① (solid lines) and ② (dashed lines) respectively. Anticrossing only occurs for $B_y \neq 0$.

coupling strength over a wide range of magnetic fields within the DSA by using the formulas given in Section 3.3.3. This could be done with QPC transport measurements or within the integer QHE.[4]

For $B_z = 0$ the conductance of a ballistic waveguide is given by (4.8) for each spin-polarized level, i.e. the number of occupied, spin-resolved transverse modes $M_s \in \mathbb{N}$ determines the resistance of the sample. This is sketched in Fig. 4.4, where the dispersion relation and the conductance in terms of M_s is plotted. Note that in this graph, the anisotropic Landau level energy as described above, was omitted for clarity, hence the subband steps are located at or around the same energy, which is, in fact, not true for narrow quantum wires. Nevertheless, we can see that the height of the smaller step (solid line) is given by the anticrossing, thus it is proportional to α and can be used to measure this quantity.

In the integer QHE, the longitudinal resistance is finite whenever the quasichemical potential is located at an energy level of the bulk system. In coincidence measurements with narrow Hall bars, the peaks will avoid to overlap due to the band anticrossing given by $2E^{1^{\text{st}}}_{n,k}$ which is anisotropic with respect to the in-plane field. Note that a

[4] For a system with both Bychkov-Rashba and Dresselhaus SOI (comp. Chap. 3.3) one can determine the relative strength, that is the ratio of the BR parameter α and the Dresselhaus parameter, usually denoted as β, using optical [15] or electrical [34, 35] techniques. In our case we can deduce the absolute strength of α for a given system electrically in materials with negligible or without SOI due to bulk inversion asymmetry.

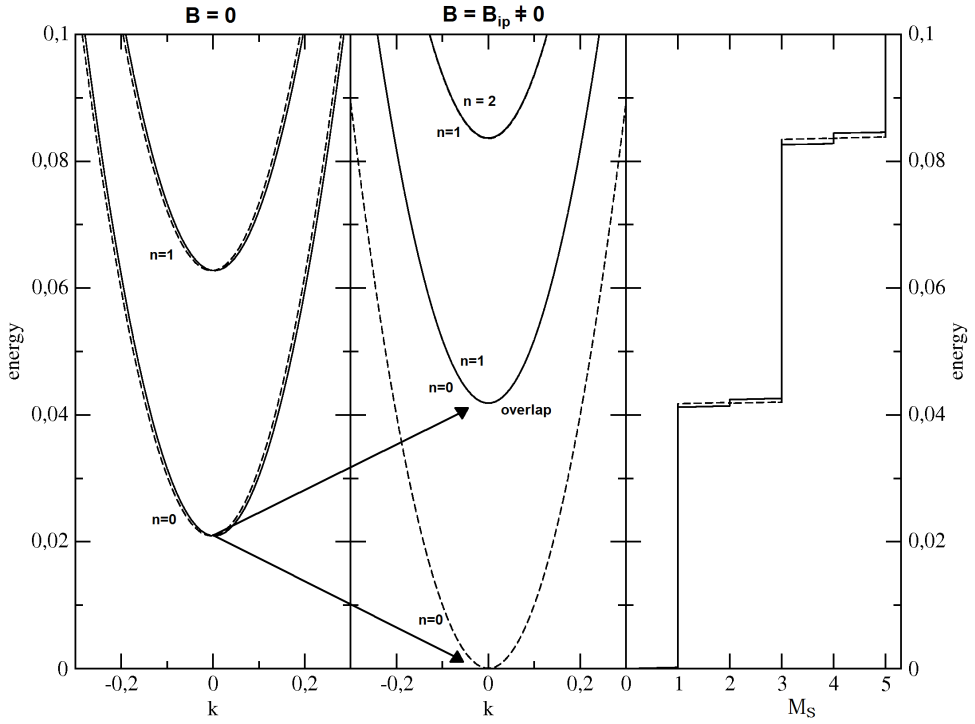

Figure 4.4: Dispersion relation for zero and non-zero in-plane field ($B_{\mathrm{ip}} = B_x$) of a narrow electron waveguide with $B_z = 0$ and number of occupied levels M_s in arbitrary units. The arrows emphasize the Zeeman splitting and the in-plane field in the second graph is chosen to be the way that $E^-_{n+1}(k) = E^+_n(k)$. The number of modes is shown for $B_{\mathrm{ip}} = B_x$ (dashed lines) and $B_{\mathrm{ip}} = B_y$ (solid lines).

crossing situation, as shown in Fig. 4.3, can only occur for $B_z = 0$, i.e. not in the QHE. This technique may be useful to confirm the anisotropies predicted by the DSA for narrow Hall bars, but it seems difficult to obtain an accurate value for α because of the many quantities that depend on the experimental parameter, the magnetic field, compared to an ordinary QHE measurement. Although the predicted anisotropies seem to explain the outcome of Ref. [26, 49], it lacks the important condition of a narrow Hall bar. In these experiments, the sample widths should be approximated with $\omega_y \to 0$, which means that any Bychkov-Rashba induced transport anisotropy disappears. Thus it may indeed be the formation of stripe phases as suggested by the authors, which drives the anisotropic resistance of these experiments. However, this is a many-body

effect and beyond the scope of this work.

What is a "narrow" quantum wire? In Chapter 2 we have specified the meaning of "weak in-plane field", that is we clarified the question for what magnetic field strengths the two-dimensional approximation (2.14) fails. A different task is to ask about the conditions for what the discussed anisotropies become visible. The answer has so far been given by the characteristic "narrow" which a quantum wire was supposed to be. However this expression needs to be specified in more detail. To face this question, we calculate the MEFs (4.2), the effective mass μ (4.3) and the energy contribution due to BR-SOI at the crossing of Zeeman split Landau levels $E_{n,k}^{1^{\text{st}}}$ (comp. Sect. 3.3.3) for some model systems.

Let us think of two realizations of a two-dimensional (Al)GaAs electron system: a quantum well (I) and a heterostructure (II). Both may be approximated with a harmonic potential to make sure that we can use the DSA. For the quantum well we use $\hbar\omega_z' = 7.24\,\text{meV}$ whereas $\hbar\omega_z'' = 126\,\text{meV}$ gives the confinement frequency of the heterostructure. This corresponds to oscillator lengths[5] of $l_z' = 12.5\,\text{nm}$ and $l_z'' = 3\,\text{nm}$ respectively. Moreover we use $m = 0.067\,m_\text{e}$ in all following calculations.
At first, we look at the anisotropy[6] of ω_- at a certain in-plane field ($B_z = 0$) for different widths of a quantum wire that is patterned on system I or II. Using equation (4.2) we obtain

- $\Delta E' = 0.1\,\text{meV}$ for system I with $l_y = 62.7\,\text{nm}$ at $B_\text{ip} = 5\,\text{T}$,
- $\Delta E' = 1\,\mu\text{eV}$ for system I with $l_y = 1\,\mu\text{m}$ at $B_\text{ip} = 25\,\text{T}$ and
- $\Delta E'' = 0.1\,\text{meV}$ for system II with $l_y = 20\,\text{nm}$ at $B_\text{ip} = 20\,\text{T}$

which verifies that for wide samples the anisotropy becomes very small even for large magnetic fields.
For the effective mass μ (4.3) of two model Hall bars with a perpendicular field of $B_z = 0.38\,\text{T}$ ($\hbar\omega_{cz} = 0.66\,\text{meV}$) we get

- $\mu' = \begin{cases} 7.6m\ (①) \\ 6.2m\ (②) \end{cases}$ for system I with $l_y = 62.7\,\text{nm}$ at $B_\text{ip} = 5\,\text{T}$ and

[5] The oscillator length, defined by $l := \sqrt{\frac{\hbar}{m\omega}}$ for a harmonic oscillator with frequency ω, is the standard deviation of the ground state. Hence, one may call $w = 2l$ the width of the potential.
[6] The anisotropy of a MEF for a given magnetic field is expressed by $\Delta E = \hbar\,|\omega_\pm^{①} - \omega_\pm^{②}|$.

- $\mu'' = \begin{cases} 1.13m \text{ (①)} \\ 1.06m \text{ (②)} \end{cases}$ for system II with $l_y = 20\,\text{nm}$ at $B_{\text{ip}} = 20\,\text{T}$.

Hence, both cases reveal anisotropic behavior even if it is strongly suppressed in the given instance of a heterostructure.
And at last we present some examples for the band anticrossing using the results derived in Section 3.3.3. We have shown above that the Landau levels overlap for an in-plane field parallel to the direction of transport (②) if the perpendicular field vanishes (Fig. 4.3). Thus we focus first on this situation but give also an example in the quantum Hall regime afterwards. The anisotropy[7] of the anticrossing for $B_z = 0$ is only determined by the energy gap of system ① since $E_{0,0}^{②,1^{\text{st}}} = 0$. Note that the due to the condition (4.4), the required in-plane fields differ from system ① to system ② as well. We have

- $\Delta E' = 0.016\,\text{meV}$ for system I with $l_y = 62.7\,\text{nm}$ at $B_{\text{ip}}^{①} = 13.2\,\text{T}$ / $B_{\text{ip}}^{②} = 2.6\,\text{T}$,
- $\Delta E' = 1\,\mu\text{eV}$ for system I with $l_y = 1\,\mu\text{m}$ at $B_{\text{ip}}^{①} = 12\,\text{mT}$ / $B_{\text{ip}}^{②} = 12\,\text{mT}$ and
- $\Delta E'' = 0.05\,\text{meV}$ for system II with $l_y = 20\,\text{nm}$ at $B_{\text{ip}}^{①} = 115\,\text{T}$ / $B_{\text{ip}}^{②} = 28\,\text{T}$.

It seems that a heterostructure system is useless to discover anisotropies in QPC measurements due to the high required fields. We find that for system I and sample widths of some tens of nanometer, the difference in the required magnetic field becomes very strong, whereas the anisotropy of the anticrossing remains small. If we switch on a perpendicular magnetic field $B_z = 3.05\,\text{T}$ ($\omega_{cz} = 5.27\,\text{meV}$), we get

- $\Delta E'' = 0.5\,\mu\text{eV}$ for system I with $l_y = 62.7\,\text{nm}$ at $B_{\text{ip}}^{①} = 31.9\,\text{T}$ / $B_{\text{ip}}^{②} = 30.6\,\text{T}$, where $2\left|E_{0,0}^{①,1^{\text{st}}}\right| = 25.1\,\mu\text{eV}$ and $2\left|E_{0,0}^{②,1^{\text{st}}}\right| = 24.6\,\mu\text{eV}$.

Note that these energies were calculated with the Bychkov-Rashba parameter $\alpha = 6.9 \cdot 10^{-13}\,\text{eVm}^{-1}$ [51], which was assumed to be fixed for all situations.

[7] The anisotropy of the anticrossing is given by the expression $\Delta E = 2\left|\left|E_{0,0}^{①,1^{\text{st}}}\right| - \left|E_{0,0}^{②,1^{\text{st}}}\right|\right|$.

5 Summary and Outlook

The knowledge of the orbital effects of transverse magnetic fields in low-dimensional systems proved useful for a quantitative description of physical properties in the regime of large fields. The meaning of "large" was specified in Chapter 2 (p. 11) within a comparison of the oscillator length of the perpendicular, electrostatic confinement and the magnetic length, which can be identified with the classical cyclotron radius. In the same chapter we also presented a short survey of the *effective mass approximation* [3, 4, 45] and pointed out the problems of a purely two-dimensional description. In fact, we calculated with the help of a simple model [17], which assumed an infinite two-dimensional electron gas and a purely in-plane magnetic field, that the field caused a diamagnetic shift of the eigenenergies and a spatial shift of the states, which alter the effective mass and the Landé factor (g-factor) due to non-parabolicity and wall penetration [6, 7, 8, 16, 23, 29, 38, 39, 45, 48]. Moreover, the effective mass perpendicular to the field, m_y (2.8), certainly changed the effective width of a confined system. It is obvious that a generalization of this first approach was needed to describe an experimental setup such as given in Ref. [26, 49] with lateral field strengths up to 30 T in order to gain an accuracy of the model which was necessary to reconstruct the results theoretically.

In Chapter 3 we developed and discussed the diamagnetic shift approximation, i.e. a model where all electrostatic confinements were assumed to be harmonic, which fully accounted for orbital effects of a magnetic field whose in-plane orientation was perpendicular (system ①) or parallel (system ②) (comp. p. 18) to a quantum wire or Hall bar. Therefore we calculated in Chapter 3.1 with the help of the *invariant eigen-operator method* [14, 22] the eigenenergies of both cases and compared the limits of the results with the *integer Quantum Hall effect* [4, 10, 17, 19] and with the model system of Chapter 2 [17], which was an infinite two-dimensional electron gas in a pure in-plane field. We finished this part with an example calculation of the level coincidence, a situation where the lateral field was used to increase the Zeeman splitting until the spin-polarized bands of neighboring Landau levels coincided, which was based on the

sample of Ref. [26] and we verified that an overlap of two spin-polarized energy levels was possible in the regime that had been used in this experiment. Chapter 3.2 dealt with the explicit transformations which were used to decouple the systems ① and ②. These brought insight into the actual orbital effects and we found that in the Landau gauge the magnetic field perpendicular to the quantum wire could be fully resolved in a shifted, rotated and rescaled electrostatic confinement whereas a lateral magnetic field parallel to the current caused additional dynamics which was more difficult to map in real space. However, in the latter case classical trajectories revealed skipping orbit like behavior in an effective confinement which was shifted to the edges of the sample but stayed in the plane, i.e. was not tilted as in system ②. After that, we investigated in Chapter 3.3 the impact of the *Bychkov-Rashba spin-orbit interaction* [12, 18, 45, 51] in order to gain more precise results as for the two-dimensional approximation for the corrections at the level coincidence, the *spin hot spots* [11]. It turned out that even if spin-orbit coupling failed to explain the anisotropic transport of the experiments in Ref. [26, 49] due to the large widths of their samples, the diamagnetic shift approximation predicted similar anisotropies in narrow waveguides which could possibly be detected experimentally and could be used to deduce the *Bychkov-Rashba parameter* α [12, 45, 51] at large magnetic fields. An approximated Hamiltonian for the limit of high magnetic fields and weak spin-orbit coupling, and an effective Hamiltonian created by a unitary transformation which caused a rotation in spin space, were derived in Chapter 3.4 for both system ① and ② and also for the two-dimensional effective mass approximation for comparison. These forms were useful to get an intuitive access to the influence of spin-orbit coupling on a quantum wire system.

Chapter 4 was dedicated to the anisotropies of narrow quantum wires which could be of special interest for future experiments on small nanostructures in high magnetic fields. We discussed different experimental setups and the expected anisotropic influence of Bychkov-Rashba interaction on these systems. We concluded this chapter with quantitative calculations for some examples of narrow conductors and predicted the outcome of corresponding measurements.

To put it in a nutshell, we have seen that for low-dimensional systems with high in-plane fields the orbital effects should not be excluded from an adequate description of the important physics and the diamagnetic shift approximation is a first step into the right direction. However, replacing all confinements with a harmonic potential yields the limitation of this formalism. Moreover, new materials and more advanced techniques increase the available maximum strength of stable magnetic fields for experiments, thus

it is obvious that further improvements of this approximation are necessary and also the need for a more sophisticated description is present.

For the future it may be reasonable to perform a systematic, numerical investigation of transport in a quantum wire to compare quantitatively the diamagnetic shift approximation with the two-dimensional effective mass Hamiltonian in the regime of large transverse magnetic fields. This would yield a desirable extension to and verification of the discussion of Chapter 4. An obvious enhancement of the diamagnetic shift approximation would be given by the incorporation of *Dresselhaus spin-orbit interaction* [12, 18, 45, 51]. This effect is important because many of the experiments on low-dimensional systems are based on semiconductors with bulk inversion asymmetry. Moreover it is essential for spin transport, especially for calculations of spin relaxation rates in electron waveguides that lack bulk inversion symmetry. Following the methods of this thesis, it also seems feasible to derive a diamagnetic shift approximation for quantum dots which would be valuable to lower the discrepancy between theoretical and experimental results of physical properties at high in-plane fields such as the spin relaxation rates of Ref. [40]. An improved handling of the orbital effects, especially the influence on spin-orbit interaction in general, may be derived from the $\vec{k} \cdot \vec{p}$ theory (*envelope function approximation*) [12, 45], which is also a desirable, though challenging project for the future.

A Useful Transformations

Archetype 1

Consider a Hamilton operator of the type

$$H = \frac{P_x^2}{2m} + \frac{1}{2}m\Omega_x^2 X^2 + \frac{P_y^2}{2m} + \frac{1}{2}m\Omega_y^2 Y^2 + \gamma XY \ ,$$

where γ is a real parameter. The system can be decoupled into two independent harmonic oscillators by choosing the transformation[1]

$$X = N(\tilde{X} + \xi\tilde{Y}) \qquad , \qquad Y = N(-\xi\tilde{X} + \tilde{Y}) \ ,$$

where

$$N = \frac{1}{\sqrt{1+\xi^2}} \qquad \text{and} \qquad \xi = \frac{m(\Omega_x^2 - \Omega_y^2)}{2\gamma} \pm \sqrt{1 + \left(\frac{m(\Omega_x^2 - \Omega_y^2)}{2\gamma}\right)^2} \ .$$

Of course the momentum operators have to be rotated in the same way. They read

$$P_x = N(P_{\tilde{x}} + \xi P_{\tilde{y}}) \qquad , \qquad P_y = N(-\xi P_{\tilde{x}} + P_{\tilde{y}}) \ .$$

The sign within ξ can be chosen ad libitum.[2] Note that $\xi > 0$ or $\xi < 0$ for $+$ or $-$ respectively.
With these conditions one can easily prove the identity

$$P_x^2 + P_y^2 = P_{\tilde{x}}^2 + P_{\tilde{y}}^2$$

[1] In fact this is a rotation of the coordinate system by $\theta = \arctan(-\xi)$. It follows that $\theta \in]0, \frac{\pi}{2}[$ for $\xi < 0$ and $\theta \in]-\frac{\pi}{2}, 0[$ for $\xi > 0$ where we have $\xi \gtrless 0$ for $\pm$ within ξ respectively. The inverse transformation is given by $\tilde{X} = N(X - \xi Y)$, $\tilde{Y} = N(\xi X + Y)$ and $P_{\tilde{x}} = N(P_x - \xi P_y)$, $P_{\tilde{y}} = N(\xi P_x + P_y)$.

[2] In this work, whenever this sign needs to be specified, the minus is used.

and one obtains

$$H = \frac{1}{2m}(P_{\tilde{x}}^2+P_{\tilde{y}}^2)+\frac{1}{2}m(\Omega_x^2+\xi^2\Omega_y^2)N^2\tilde{X}^2-\gamma\xi N^2\tilde{X}^2+\frac{1}{2}m(\xi^2\Omega_x^2+\Omega_y^2)N^2\tilde{Y}^2+\gamma\xi N^2\tilde{Y}^2 =$$

$$= \frac{P_{\tilde{x}}^2}{2m}+\frac{1}{2}m \underbrace{N^2\left(\Omega_x^2+\xi^2\Omega_y^2-\frac{2\gamma\xi}{m}\right)}_{=:\omega_{\tilde{x}}^2} \tilde{X}^2 + \frac{P_{\tilde{y}}^2}{2m}+\frac{1}{2}m \underbrace{N^2\left(\xi^2\Omega_x^2+\Omega_y^2+\frac{2\gamma\xi}{m}\right)}_{=:\omega_{\tilde{y}}^2} \tilde{Y}^2 =$$

$$= \frac{P_{\tilde{x}}^2}{2m}+\frac{1}{2}m\omega_{\tilde{x}}^2\tilde{X}^2 + \frac{P_{\tilde{y}}^2}{2m}+\frac{1}{2}m\omega_{\tilde{y}}^2\tilde{Y}^2 \ .$$

Thus in the new coordinates H is separable and the solution reads $\Psi_{n,n'}(\tilde{x},\tilde{y}) = \phi_n^{\omega_{\tilde{x}}}(\tilde{x})\phi_{n'}^{\omega_{\tilde{y}}}(\tilde{y})$ where $\phi^{\omega_{\tilde{x}}}$ and $\phi^{\omega_{\tilde{y}}}$ solve the harmonic oscillator equations of $\tilde{x}$ and $\tilde{y}$ respectively. The eigenvalues of the system are given by

$$E(n,n') = \hbar\omega_{\tilde{x}}(n+\frac{1}{2})+\hbar\omega_{\tilde{y}}(n'+\frac{1}{2}) \ .$$

Archetype 2

Consider a more general Hamiltonian of the form

$$H = \frac{P_x^2}{2m}+aX^2+\alpha X+\frac{P_y^2}{2m}+bY^2+\beta Y+\gamma XY \ ,$$

where $a, b, \alpha, \beta, \gamma$ are real parameters. We split the linear terms into two parts each and write $\alpha = \alpha_1 + \alpha_2$ and $\beta = \beta_1 + \beta_2$. The transformation is defined as follows

$$X = X' - \frac{\alpha_1}{2a} \quad , \quad Y = Y' - \frac{\beta_1}{2b} \ ,$$

where

$$\alpha_1 = \frac{2a(2\alpha b-\gamma\beta)}{4ab-\gamma^2} \quad , \quad \alpha_2 = \frac{\gamma(2\beta a-\gamma\alpha)}{4ab-\gamma^2} \ ,$$

$$\beta_1 = \frac{2b(2\beta a-\gamma\alpha)}{4ab-\gamma^2} \quad , \quad \beta_2 = \frac{\gamma(2\alpha b-\gamma\beta)}{4ab-\gamma^2} \ .$$

The inverse transformation is trivial and the momentum operators do not change due to the translation in real space. The Hamiltonian in the new coordinates now reads

$$H = \frac{P_{x'}^2}{2m}+aX'^2+\frac{P_{y'}^2}{2m}+bY'^2+\gamma X'Y'+\frac{\alpha\beta\gamma-a\beta^2-b\alpha^2}{4ab-\gamma^2} \ .$$

Up to a constant term, this is the Hamiltonian given in archetype 1 which can be solved as described there.

Archetype 3

A Hamiltonian of the type

$$H = \frac{P_x^2}{2m} + \alpha P_x + \frac{1}{2}m\omega_x^2 X^2 + \frac{P_y^2}{2m} + bY^2 + \beta Y + \gamma Y P_x \ ,$$

where α, b, β, γ are real parameters, is somewhat more difficult to separate. If we want to use archetype 2, we need to think of a substitution which creates an effective momentum operator $\bar{X}$ from the position operator X and an effective position operator $\bar{P}_x$ from the momentum operator P_x. As we will show below, this substitution is straightforward and well-defined up to a sign, which can be chosen ad libitum.
In order to derive the effective momentum and position operators, we start with a model Hamiltonian, the simple harmonic oscillator in one dimension. The Hamiltonian reads

$$H_{\mathrm{SHO}} = \frac{P^2}{2m} + \frac{1}{2}m\omega^2 R^2 \ ,$$

with the momentum operator P and the position operator R. The Hamiltonian can be rewritten as

$$H_{\mathrm{SHO}} = \frac{(m\omega R)^2}{2m} + \frac{1}{2}m\omega^2 \left(\frac{P}{m\omega}\right)^2 \equiv \frac{\bar{R}^2}{2m} + \frac{1}{2}m\omega^2 \bar{P}^2 \ ,$$

where we defined the operators $\bar{R}^2$ and $\bar{P}^2$, hence we know $\bar{R}$ and $\bar{P}$ up to the sign. So far it seems that we can choose the sign of $\bar{R}$ and $\bar{P}$ independently. However this is not true since in order to have proper effective momentum and position operators they must satisfy the commutation relation such as $[R, P] = \mathrm{i}\hbar I$. Thus we have

$$\mathrm{i}\hbar I \stackrel{!}{=} \left[\bar{P}, \bar{R}\right] = \left[\begin{smallmatrix}+\\-\\-\end{smallmatrix}\frac{P}{m\omega}, \begin{smallmatrix}+\\-\\+\end{smallmatrix} m\omega R\right] = \begin{smallmatrix}+\\+\\-\end{smallmatrix} PR \begin{smallmatrix}-\\+\\+\end{smallmatrix} RP = \begin{smallmatrix}-\\+\\+\end{smallmatrix} [R, P] = \begin{smallmatrix}-\\+\\+\end{smallmatrix} \mathrm{i}\hbar I \stackrel{!}{=} \mathrm{i}\hbar I \ ,$$

which shows that the signs of $\bar{R}$ and $\bar{P}$ must be opposite. Finally we are left with two equivalent representations of the effective momentum and position operators:

$$\bar{R} = \mp m\omega R \quad , \quad \bar{P} = \pm \frac{P}{m\omega} \ .$$

In the same way we can express the x-coordinate of the Hamiltonian H in terms of effective momentum and position operators. It reads

$$H = \frac{\bar{X}^2}{2m} + \bar{a}\bar{P}_x^2 + \bar{\alpha}\bar{P}_x + \frac{P_y^2}{2m} + bY^2 + \beta Y + \bar{\gamma} Y \bar{P}_x \ ,$$

where we defined $\bar{a} := \frac{1}{2}m\omega_x^2$, $\bar{\alpha} := \pm m\omega_x\alpha$ and $\bar{\gamma} := \pm m\omega_x\gamma$. Note that the sign is given by the choice of $\bar{P}_x$. This Hamiltonian now satisfies the requirements for the usage within archetype 2.

B Useful Identities

Throughout the thesis we introduce many different forms of and links between the important functions that characterize system ① and ②. Beyond the formulas already given in Chapter 3, it proves useful to know about the following identities, which can be derived from the quantities defined in Chapter 3.2. Note, however, that these equations only hold for the sign convention of ξ established in Section 3.2.3, which was used during the whole work.

For the MEFs of both systems we can write:

①

$$\begin{aligned}\omega_{-}^{①} &= \sqrt{\frac{1}{1+\xi'^{-2}}\,\Omega_{z,cy}^2 + \frac{1}{1+\xi'^{2}}\,\Omega_{y,cz}^2 - 2\omega_{cy}\omega_{cz}\frac{1}{\xi'+\xi'^{-1}}}\ ,\\ \omega_{+}^{①} &= \sqrt{\frac{1}{1+\xi'^{2}}\,\Omega_{z,cy}^2 + \frac{1}{1+\xi'^{-2}}\,\Omega_{y,cz}^2 + 2\omega_{cy}\omega_{cz}\frac{1}{\xi'+\xi'^{-1}}}\ ,\end{aligned} \tag{B.1a}$$

$$\text{with}\quad \xi' = \begin{cases}\xi_+ & \text{if}\quad \operatorname{sign}(\omega_{cy}\omega_{cz}) = +1\\ \xi_- & \text{if}\quad \operatorname{sign}(\omega_{cy}\omega_{cz}) = -1\end{cases}\ , \tag{B.1b}$$

where

$$\xi_\pm = \Xi \pm \sqrt{1+\Xi^2} \qquad \text{with} \qquad \Xi = \frac{\Omega_{y,cz}^2 - \Omega_{z,cy}^2}{2\,\omega_{cy}\,\omega_{cz}}\ . \qquad \text{(comp. (3.18))}$$

This form is equivalent to the equations (3.13), (3.22), (3.33) and (3.34).

②

$$\begin{aligned}\omega_{-}^{②} &= \sqrt{\frac{1}{1+\xi'^{-2}}\,\omega_z^2 + \frac{1}{1+\xi'^{2}}\,\Omega_{y,cx,cz}^2 + 2\omega_{cx}\omega_z\frac{1}{\xi'+\xi'^{-1}}}\ ,\\ \omega_{+}^{②} &= \sqrt{\frac{1}{1+\xi'^{2}}\,\omega_z^2 + \frac{1}{1+\xi'^{-2}}\,\Omega_{y,cx,cz}^2 - 2\omega_{cx}\omega_z\frac{1}{\xi'+\xi'^{-1}}}\ ,\end{aligned} \tag{B.2a}$$

$$\text{with}\quad \xi' = \begin{cases}\xi_- & \text{if}\quad \operatorname{sign}(\omega_{cx}) = +1\\ \xi_+ & \text{if}\quad \operatorname{sign}(\omega_{cx}) = -1\end{cases}\ , \tag{B.2b}$$

where

$$\xi_{\pm} = \Xi \pm \sqrt{1+\Xi^2} \qquad \text{with} \qquad \Xi = -\frac{\Omega_{y,cx,cz}^2 - \omega_z^2}{2\,\omega_{cx}\,\omega_z}\,, \qquad \text{(comp. (3.27))}$$

which is equivalent to (3.15), (3.32), (3.35) and (3.36).

The transform variable ξ' (B.1b), (B.2b) also fulfills the following identities:

①

$$\xi'_{①} = \frac{\omega_+^{①2} - \omega_{cy}^2 - \omega_z^2}{\omega_{cy}\,\omega_{cz}} \quad , \quad \frac{1}{1+\xi'^2_{①}} = \frac{\omega_-^{①2} - \omega_{cy}^2 - \omega_z^2}{\omega_-^{①2} - \omega_+^{①2}}\,,$$
$$\xi'^{-1}_{①} = -\frac{\omega_-^{①2} - \omega_{cy}^2 - \omega_z^2}{\omega_{cy}\,\omega_{cz}} \quad , \quad \frac{1}{1+\xi'^{-2}_{①}} = -\frac{\omega_+^{①2} - \omega_{cy}^2 - \omega_z^2}{\omega_-^{①2} - \omega_+^{①2}}\,.$$

②

$$\xi'_{②} = \frac{\omega_-^{②2} - \omega_y^2 - \omega_{cx}^2 - \omega_{cz}^2}{\omega_{cx}\,\omega_z} \quad , \quad \frac{1}{1+\xi'^2_{②}} = \frac{\omega_+^{②2} - \omega_y^2 - \omega_{cx}^2 - \omega_{cz}^2}{\omega_+^{②2} - \omega_-^{②2}}\,,$$
$$\xi'^{-1}_{②} = -\frac{\omega_+^{②2} - \omega_y^2 - \omega_{cx}^2 - \omega_{cz}^2}{\omega_{cx}\,\omega_z} \quad , \quad \frac{1}{1+\xi'^{-2}_{②}} = -\frac{\omega_-^{②2} - \omega_y^2 - \omega_{cx}^2 - \omega_{cz}^2}{\omega_+^{②2} - \omega_-^{②2}}\,.$$

Note that here we used explicitly a subscript to emphasize that ξ' is indeed different for both systems. For the rest of the work, it has been suppressed for clarity.

For $\omega_y = 0$, one can also show that it holds

$$\xi'_{①} = \frac{\omega_{cz}\xi'_{②} - \omega_{\mathrm{cip}} - \omega_z\xi'_{②}}{\omega_{cz} - \omega_z + \omega_{\mathrm{cip}}\xi'_{②}} \quad , \quad \xi'_{②} = -\frac{\omega_{cz}\xi'_{①} + \omega_{\mathrm{cip}} + \omega_z\xi'_{①}}{\omega_{cz} + \omega_z - \omega_{\mathrm{cip}}\xi'_{①}}\,,$$

and

$$\frac{1}{1+\xi'^2_{①}}\left[\left(\omega_{cz} - \xi'_{①}\omega_{\mathrm{cip}}\right)\frac{B_z}{B} + \omega_-\right]^2 = \frac{1}{1+\xi'^2_{②}}\left[\omega_{cz} + \omega_-\frac{B_z}{B}\right]\,.$$

The latter is the reason for the isotropy described in Section 3.3.3.

Bibliography

[1] Ashcroft, N. W., and N. D. Mermin, 1976, *Solid State Physics* (Saunders, New York).

[2] Bernardes, E. S., J. Schliemann, J. C. Egues, and D. Loss, Spin-orbit interaction in symmetric wells and cycloidal orbits without magnetic fields, 2007, Phys. Rev. Lett. **66**, 076603.

[3] Bruus, H., and K. Flensberg, 2004, *Many-Body Quantum Theory in Condensed Matter Physics: An Introduction* (Oxford University Press, Oxford).

[4] Datta, S., 1995, *Electronic Transport in Mesoscopic Systems* (Cambridge University Press, Cambridge).

[5] Demler, E., D.-W. Wang, S. Das Sarma, and B. I. Halperin, Quantum Hall stripe phases at integer filling factors, 2003, Solid State Commun. **123**, 243.

[6] de Dios-Leyva, M., N. Porras-Montenegro, H. S. Brandi, and L. E. Oliveira, Electron g-Factor and Cyclotron Effective Mass in Semiconductor Quantum Wells Under Growth-Direction Applied Magnetic Fields, 2005, Braz. J. Phys. **36**, 854.

[7] de Dios-Leyva, M., E. Reyes-Gómez, C. A. Perdomo-Leiva, and L. E. Oliveira, Effects of non-parabolicity and in-plane magnetic fields on the cyclotron effective mass and $g_{\perp}$-factor in GaAs-(Ga,Al)As quantum wells, 2006, Phys. Rev. B **73**, 085316.

[8] de Dios-Leyva, M., N. Porras-Montenegro, H. S. Brandi, L. E. Oliveira, Cyclotron effective mass and Landé g factor in GaAs-$Ga_{1-x}Al_xAs$ quantum wells under growth-direction applied magnetic fields, 2006, J. Appl. Phys. **99**, 104303.

[9] Emery, V. J., E. Fradkin, S. A. Kivelson, and T. C. Lubensky, Quantum Theory of the Smectic Metal State in Stripe Phases, 2000, Phys. Rev. Lett. **85**, 2160.

[10] Ezawa, Z. F., 2008, *Quantum Hall Effects: Field Theoretical Approach and Related Topics*, Second Edition (World Scientific Pub Co, Singapore).

[11] Fabian, J., and S. Das Sarma, Spin Relaxation of Conduction Electrons in Polyvalent Metals: Theory and a Realistic Calculation, 1998, Phys. Rev. Lett. **81**, 5624.

[12] Fabian, J., A. Matos-Abiague, C. Ertler, P. Stano, and I. Žutić, Semiconductor Spintronics, 2007, Acta Phys. Slov. **57**, 565.

[13] Fal'ko V. I., B. L. Altshuler, O. Tsyplyatev, Anisotropy of spin splitting and spin relaxation in lateral quantum dots, 2005, arXiv:cond-mat/0501046v1.

[14] Fan, H.-Y., C. Li, Invariant 'eigen-operator' of the square of Schrödinger operator for deriving energy-level gap, 2004, Phys. Lett. A **321**, 75.

[15] Ganichev, S. D., V. V. Bel'kov, L. E. Golub, E. L. Ivchenko, P. Schneider, S. Giglberger, J. Eroms, J. De Boeck, G. Borghs, W. Wegscheider, D. Weiss, and W. Prettl, Experimental Separation of Rashba and Dresselhaus Spin Splittings in Semiconductor Quantum Wells, 2004, Phys. Rev. Lett. **92**, 256601.

[16] Hannak, R. M., M. Oestreich, A. P. Heberle, and W. W. Rühle, Electron g Factor in Quantum Wells Determined by Spin Quantum Beats, 1994, Sol. Stat. Comm. **93**, 313.

[17] Heinzel, T., 2007, *Mesoscopic Electronics in Solid State Nanostructures* (Wiley-VCH, Berlin).

[18] Kavokin, K. V., and M. E. Portnoi, Spin-orbit terms in multi-subband electron systems: a bridge between bulk and two-dimensional Hamiltonians, 2008, arXiv:cond-mat/0310318v2.

[19] von Klitzing, K., G. Dorda, and M. Pepper, New Method for High-Accuracy Determination of the Fine-Structure Constant Based on Quantized Hall Resistance, 1980, Phys. Rev. Lett. **45**, 494.

[20] Könemann, J., R. J. Haug, D. K. Maude, V. I. Fal'ko, and B. L. Altshuler, Spin-Orbit Coupling and Anisotropy of Spin Splitting in Quantum Dots, 2005, Phys. Rev. Lett. **94**, 226404.

[21] Laughlin, R. B., Anomalous Quantum Hall Effect: An Incompressible Quantum Fluid with Fractionally Charged Excitations, 1983, Phys. Rev. Lett. **50**, 1395.

[22] Liu, Y.-M., Y.-H. Ji, The Invariant Eigen-Operator Method for Hamiltonians with Coordinates-Coordinates Coupling Terms, 2009, Int. J. Theor. Phys. **48** 1500.

[23] Lommer, G., F. Malcher, and U. Rößler, Reduced g factor of subband Landau levels in AlGaAs/GaAs heterostructures, 1985, Phys. Rev. B **32**, 6965.

[24] Moroz, A. V., C. H. W. Barnes, Effect of the spin-orbit interaction on the band structure and conductance of quasi-one-dimensional systems, 1999, Phys. Rev. B **60**, 14272.

[25] Pala, M. G., M. Governale, U. Zülicke, and G. Iannaccone, Rashba spin precession in quantum Hall edge channels, 2004, cond-mat/0409580.

[26] Pan, W., H. L. Störmer, D. C. Tsui, L. N. Pfeiffer, K. W. Baldwin, and K. W. West, Highly anisotropic transport in the integer quantum Hall effect, 2001, Phys. Rev. B **64**, 121305.

[27] Papa, E., J. Schliemann, A. H. MacDonald, and M. P. A. Fisher, Quantum theory of bilayer quantum Hall smectics, 2003, Phys. Rev. B **67**, 115330.

[28] Raith, M., M. Wimmer, and J. Fabian, Spin orbit interaction in 2D electron gases with small in-plane magnetic fields, 2008, unpublished.

[29] Reyes-Gómez, E., C. A. Perdomo Leiva, L. E. Oliveira, and M. de Dios-Leyva, Effects of In-Plane Magnetic Fields on the Electron Cyclotron Effective Mass and Landé Factor in GaAs-(Ga,Al)As Quantum Wells, 2005, Braz. J. Phys. **36**, 858.

[30] Reynoso, A., G. Usaj, M. J. Sanchez, and C. A. Balseiro, Theory of Edge States in Systems with Rashba Spin-Orbit Coupling, 2004, arXiv:cond-mat/0407138.

[31] Robinett, R. W., 2006, *Quantum Mechanics*, Classical Results, Modern Systems, and Visualized Examples, Second Edition (Oxford University Press, New York).

[32] Sakurai, J. J., 1994, *Modern Quantum Mechanics*, Revised Edition, (Addison-Wesley).

[33] Salis, G., B. Ruhstaller, K. Ensslin, K. Campman, K. Maranowski, and A. C. Gossard, Subband densities in quantum wells under in-plane magnetic fields, 1998, Phys. Rev. B **58**, 1436.

[34] Scheid, M., M. Kohda, Y. Kunihashi, K. Richter, and J. Nitta, All-Electrical Detection of the Relative Strength of Rashba and Dresselhaus Spin-Orbit Interaction in Quantum Wires, 2008, Phys. Rev. Lett. **101**, 266401.

[35] Scheid, M., İ. Adagideli, J. Nitta, and K. Richter, Anisotropic universal conductance fluctuations in disordered quantum wires with Rashba and Dresselhaus spin–orbit interaction and an applied in-plane magnetic field, 2009, Semicond. Sci. Technol. **24**, 064005.

[36] Schliemann, J., Cyclotron motion and magnetic focusing in semiconductor quantum wells with spin-orbit coupling, 2008, Phys. Rev. B **77**, 125303.

[37] Serra, L., D. Sanchez, and R. Lopez, Rashba interaction in quantum wires with in-plane magnetic fields, 2005, arXiv:cond-mat/0504578v2.

[38] Snelling, M. J., G. P. Flinn, A. S. Plaut, R. T. Harley, A. C. Tropper, R. Eccleston, and C. C. Phillips, Magnetic g factor of electrons in GaAs/$Al_xGa_{1-x}As$ quantum wells, 1991a, Phys. Rev. B **44**, 11345.

[39] Snelling, M. J., E. Blackwood, C. J. McDonagh, R. T. Harley, and C. T. B. Foxon, Exciton, heavy-hole, and electron g factors in type-I GaAs/$Al_xGa_{1-x}As$ quantum wells, 1991b, Phys. Rev. B **45**, 3922.

[40] Stano, P., and J. Fabian, Theory of phonon-induced spin relaxation in laterally coupled quantum dots, 2006, cond-mat/0512713.

[41] Trushin, M., and J. Schliemann, Anisotropic current-induced spin accumulation in the two-dimensional electron gas with spin-orbit coupling, 2007, Phys. Rev. B **75**, 155323.

[42] Tsui, D. C., H. L. Störmer, and A. C. Gossard, Two-Dimensional Magnetotransport in the Extreme Quantum Limit, 1982, Phys. Rev. Lett. **48**, 1559.

[43] van Wees, B. J., H. van Houten, C. W. J. Beenakker, J. G. Williamson, L. P. Kouwenhoven, D. van der Marel, and C. T. Foxon, Quantized conductance of point contacts in a two-dimensional electron gas, 1988, Phys. Rev. Lett. **60**, 848.

[44] Wharam D. A., T. J. Thornton, R. Newbury, M. Pepper, H. Ahmed, J. E. F. Frost, D. G. Hasko, D. C. Peacock, D. A. Ritchie, and G. A. C. Jones, One-dimensional transport and the quantisation of the ballistic resistance, 1988, J. Phys. C: Solid State Phys. **21**, L209.

[45] Winkler, R., 2003, *Spin-orbit coupling effects in two-dimensional electron and hole systems* (Springer, Berlin).

[46] Winkler, R., U. Zülicke, and J. Bolte, Oscillatory multiband dynamics of free particles: The ubiquity of *zitterbewegung* effects, 2007, Phys. Rev. B **75**, 205314.

[47] Yu, P. Y., and M. Cardona, 2005, *Fundamentals of Semiconductors*, 3rd Ed. (Springer, Berlin).

[48] Yugova, I. A., A. Greilich, D. R. Yakovlev, A. A. Kiselev, M. Bayer, V. V. Petrov, Yu. K. Dolgikh, D. Reuter, and A. D. Wieck, Universal behavior of the electron g-factor in GaAs/AlGaAs quantum wells, 2008, physics/0610216v1.

[49] Zeitler, U., H. W. Schumacher, A. G. M. Jansen, and R. J. Haug, Magnetoresistance Anisotropy in Si/SiGe in Tilted Magnetic Fields: Experimental Evidence for a Stripe-Phase Formation, 2001, Phys. Rev. Lett. **86**, 866.

[50] Zülicke, U., J. Bolte, R. Winkler, Magnetic focusing of charge carriers from spin-split bands: semiclassics of a Zitterbewegung effect, 2007, New J. Phys. **9**, 355.

[51] Žutić, I., J. Fabian, and S. Das Sarma, Spintronics: Fundamentals and applications, 2004, Rev. Mod. Phys. **76**, 323.

Acknowledgment

Special thanks go to my supervisor, Prof. Dr. Jaroslav Fabian, who has always found some minutes to discuss results and concepts even if he did not have any. He has supported me with valuable advice and inspired me in all phases of the thesis development.
I would also like to thank the members of the Spintronics Research Group, namely Samvel Badalyan, Fabio Baruffa, Christian Ertler, Martin Gmitra, Sergej Konschuh, Alex Matos-Abiague, Benedikt Scharf, and Marko Turek who provided me with food for thought in group seminars and personal conversations. Thanks to my old schoolmate and fellow student Michael Jobst for refreshing my motivation continuously during the whole studies. And last but not least, many thanks to my parents Jutta and Gerhard Raith and my sister Sabine for all their support.

E R K L Ä R U N G

Hiermit erkläre ich, dass die Diplomarbeit selbstständig angefertigt und keine Hilfsmittel außer den in der Arbeit angegebenen benutzt habe.

Regensburg, den 24. Juni 2009